Computer simulation of arterial blood flow under external acceleration

by

Douglas A. Cornet

A Thesis Submitted to the
Graduate Faculty in Partial Fulfillment of the
Requirements for the Degree of
MASTER OF SCIENCE

Major: Biomedical Engineering

Iowa State University
Ames, Iowa
1991

TABLE OF CONTENTS

LIST OF TABLES

LIST OF FIGURES

NOMENCLATURE

a	cross-sectional area
A_o	cross-sectional area at reference pressure
A_s	cross-sectional lumen area in stenosis
b_x	body-force vector component in axial direction
c_v	viscous term coefficient in wall shearing stress equation
c_u	inertial term coefficient in wall shear stress equation
C	arterial compliance
C_o'	modified linear compliance coefficient
C_1'	modified non-linear compliance coefficient
C_T	volume compliance of terminal impedance
D	arterial diameter
G	gravitational acceleration
K_t	turbulence coefficient in stenosis equation
K_u	unsteady flow coefficient in stenosis equation
K_v	viscous coefficient in stenosis equation
L	segment length
L_s	stenosis length
P, p	instantaneous pressure

$\bar{P}, \bar{p}$	mean pressure
q	instantaneous flow
$\bar{q}$	mean flow
R	segment radius
R_1	proximal resistance of terminal impedance (small vessel term)
R_2	distal resistance of terminal impedance (arterioles and capillaries)
R_T	total resistance of terminal impedance
t	time
x	segment axial coordinate and body ventral coordinate
z	body sagittal coordinate
α	dimensionless frequency (Wormersley parameter)
Δt	time increment
λ	dimensionless velocity profile coefficient
μ	fluid dynamic viscosity
ν	fluid kinematic viscosity
ρ	fluid density
ω	basic circular frequency of a pulse

Subscripts:

a	arterial
v	venous

CHAPTER 1. INTRODUCTION

> Ce n'est pas la résistance de la matière qui sera la limite des performances aérobatiques de l'oiseau artificiel, mais bien la résistance physiologique de l'homme, qui en est le cerveau.[1]
>
> -Louis Blériot

During World War I, the study of gravitational loss of consciousness (G-LOC) was born. In 1918, Henry Head reported on a test pilot that had blacked out after pulling +4.5 Gs in his Sopwith Triplane (Voge, 1980). In an attempt to prevent further episodes, researchers at that time primarily concerned themselves with physiological compensation of acceleration stress. The anti-gravitational suit (G-suit) was created to directly oppose the downward movement of blood under external acceleration by forcing blood that pooled in the lower extremities back into the thoracic cavity. This was accomplished by the pilot wearing a pair of trousers that inflated when he experienced $+G_z$ (head-to-foot) acceleration.

Modern high-performance aircraft are capable of high speed, altitude, turn rates, and G-loading. For example, at Mach 2 (twice the speed of sound), a General Dy-

[1] "It is not the resistance of matter which limits the aerobatic performance of the artificial bird, but the physiologic resistance of man, who is the bird's brain." From Schubert, 1935 (Gaur, 1961a).

namics F-16 Fighting Falcon can bank 83.6° and turn 180° in just over 16 seconds. As shown in Figure 1.1 centripetal acceleration on the airframe is *nine* times that of gravity. In other words, the pilot weighs nine times that which he weighed standing on the surface of the earth.

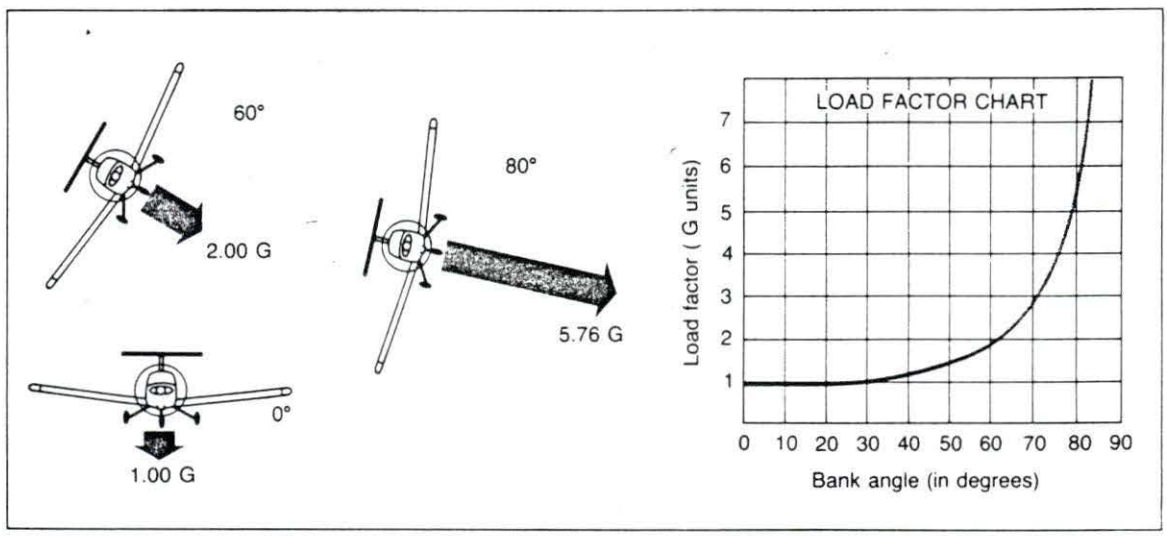

Figure 1.1: Turn forces versus bank angle (Glaeser et al., 1985)

Traditionally, the loading of an airframe is stated in multiples of gravitational force called G-forces or Gs. By this convention, positive acceleration (in excess of 1G) is when an airframe is accelerated upward and negative acceleration when an airframe is accelerated downward, as shown in Figure 1.2. The gravitational load acts in the opposite direction; a positive acceleration as shown in Figure 1.2 creates a positive G-load in the opposite direction.

The acceleration due to earth's gravitational field acts in the positive direction as well, creating a gravitational force (load) towards the center of the earth. An object resting on the surface of the earth does not fall to the center of the earth but is supported by the ground which, in effect, accelerates the object in the $+G_z$

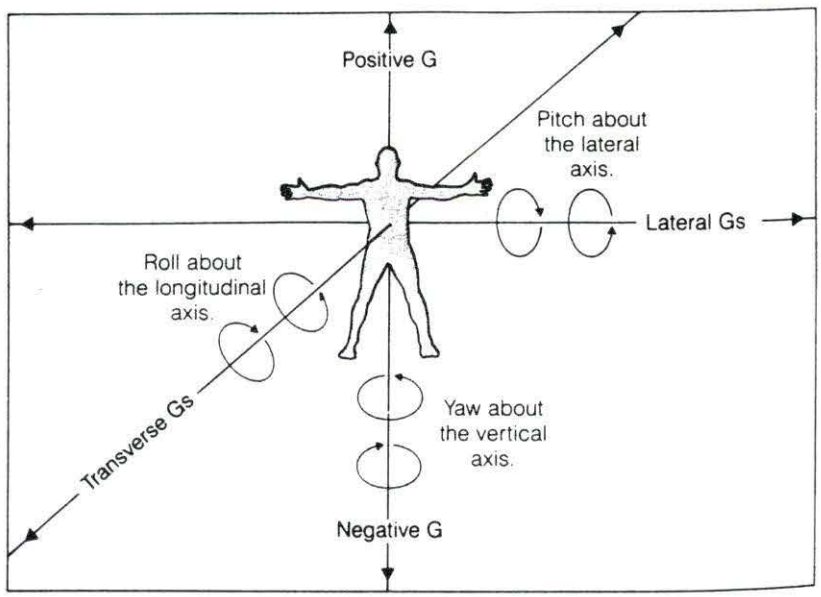

Figure 1.2: Aircraft and pilot coordinate frame (Glaeser et al., 1985)

direction. This load is, by definition, $+1$ G_z.

During positive acceleration, hydrostatic pressure is increased in the arteries, hampering cerebral circulation. Blood pools in the lower extremities as shown in Figure 1.3. If induced hydrostatic pressure becomes greater than head-level arterial blood pressure, cerebral flow ceases and a loss of consciousness results.

Gravitational loss of consciousness, or G-LOC, is one of the leading causes of pilot fatality and loss of aircraft. At Mach 2, an aircraft travels over 2000 feet per second. If a pilot is unconscious for only 24 seconds, (a conservative time) she will regain control of the aircraft 10 miles away from where she blacked out.

Recent military research has emphasized new techniques and devices to increase a pilot's tolerance to gravitational stress, both in magnitude and duration of the acceleration. Improved G- suits, supinating seats, positive breathing apparatus, and

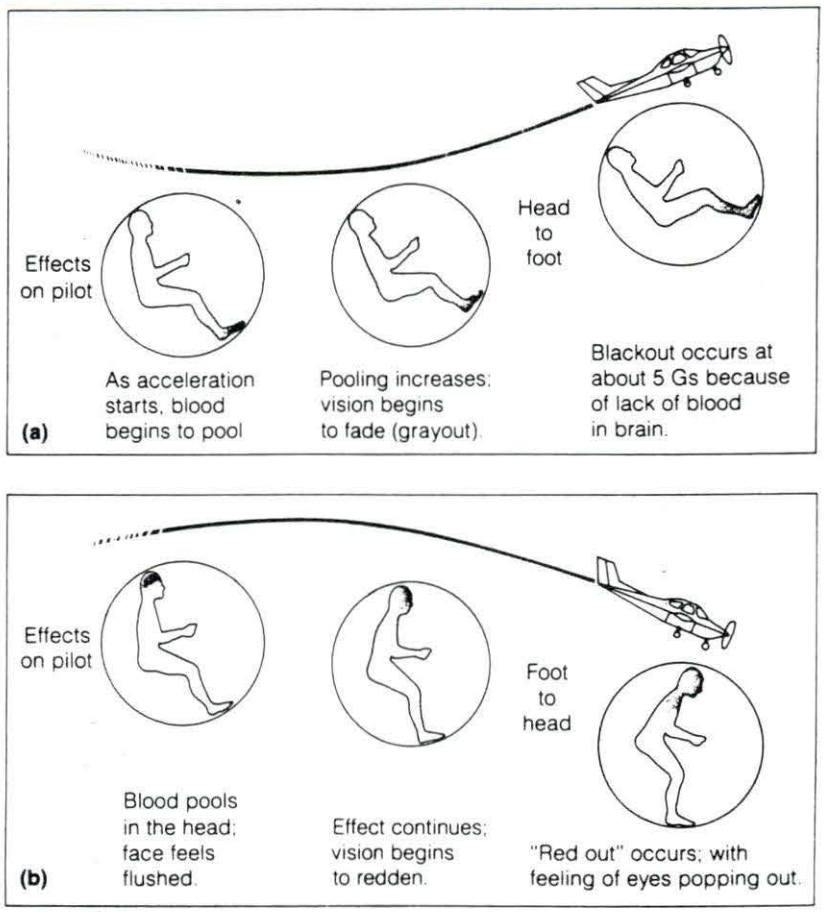

Figure 1.3: Effects of sustained G-forces (Glaeser et al., 1985)

straining techiniques such as the Valsalva and M-1 maneuvers are techniques used in modern fighter aircraft. As aircraft become faster and more maneuverable, such as the YF-22 Advanced Tactical Fighter proposed by Lockheed and General Dynamics, new techniques and/or expansion of the existing techniques will be required. Only a thorough understanding of the effect of acceleration on the cardiovascular system will allow the development of new techniques and devices.

Although most research has been empirical centrifuge studies to determine qual-

itative pressure and flow endpoints of a pilot's consciousness, computer models are being developed to study the hemodynamics of $+G_z$ acceleration. The present study integrates the findings of acceleration physiologists into a previously developed computer model of the human arterial system. The several purposes of this study are:

- Integrate $+G_z$ acceleration physiological data found in literature into an arterial flow computer simulation.
- Evaluate the sensitivity of the model to various physiological parameters.
- Investigate the manner in which the human body compensates for $+G_z$ acceleration loads.
- Compare simulated $+0$ G_z (supine) and $+1$ G_z (standing) models with experimental data found in literature.
- Compare high-G_z (greater than $+1$ G_z) models with human centrifuge data found in literature.
- Investigate ways to model an anti-G suit and compare models with human centrifuge data.
- Determine the effect of stenoses on blood flow under external acceleration.
- Recommend changes to be made in the computer model to better simulate $+G_z$ acceleration. Also recommend additional centrifuge studies to qualitativly determine several physiological parameters that are needed for the computer models.

CHAPTER 2. LITERATURE REVIEW

Positive acceleration (headwards) of a human increases hydrostatic pressures within the arterial tree as the apparent weight of every part of the person increases proportionally with the magnitude of the acceleration. Conversely, acceleration downwards (footwards) decreases hydrostatic pressures and apparent weight. Positive upwards acceleration ($+G_z$) crushes a pilot into his seat while a negative upwards acceleration ($-G_z$) pushes a pilot off his seat and into his harness. A $+1$ G_z acceleration is that which is felt while standing on the earth's surface at sea-level. Figure 2.1 is a nomogram relating aircraft velocity, turn rate, and G-forces developed.

Gravitational Loss of Consciousness

High sustained $+G_z$ acceleration (HSG) is defined as $+6$ G_z or higher acceleration for 15 seconds or longer at maximum G (Burton et al., 1974). HSG drops head-level blood pressure sufficiently to cause a loss of consciousness (G-LOC) in the unprotected, relaxed pilot. G-suits, straining maneuvers, and pilot conditioning can raise a pilots tolerance to G-LOC (G-TOL).

Symptoms prior to G-LOC may include (in order): fatigue, perspiration, cough (especially if the pilot is breathing a high oxygen mixture), a feeling of warmth, calf pain, tingling in the extremities and face, and Peripheral Light Loss (PLL); also

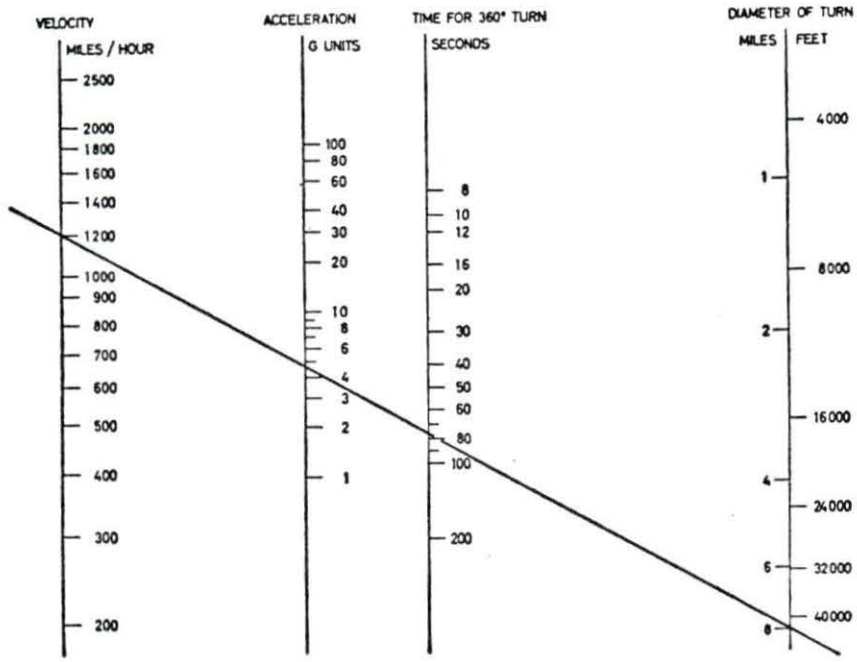

Figure 2.1: Turn rate, velocity, and G-force nomogram (Gaur, 1961b)

called tunnel-vision or grayout (Burton et al., 1974; Gauer, 1961[a]; Gilles, 1965; Gillingham, 1988; Glaister, 1990; Krutz et al., 1973; Sandler et al., 1977; Voge, 1980; Whinnery, 1988). PLL begins as the retinal beds become starved for oxygen due to impaired cerebral circulation. Tunnel-vision becomes more pronounced with $+G_z$ duration of up to 5 seconds or an increase in $+G_z$. PLL progresses until LOMA (Limitation of Ocular Mobility under Acceleration), loss of hearing and/or Central Light Loss (CLL), also called blackout, occur. Shortly following LOMA and CLL is G-LOC. During HSG, G-LOC follows CLL by 4–5 seconds (Glaister, 1990).

There are two types of G-LOC (Type I and Type II). Type I G-LOC is a period of short duration unconsciousness without any convulsions. Type II is unconsciousness of longer duration accompanied by flailing convulsions (Whinnery, 1988).

The USAF and Navy, concerned with maintaining pilot safety, focus their research efforts to determine man's G-TOL and finding ways to improve it. As aircraft turn rates continue to improve, finding more effective methods of raising G-TOL becomes paramount. Most research conducted by the United States Air Force School of Aerospace Medicine (USAFSAM) and the Naval Air Development Center (NADC) includes centrifuge experiments on man and animals to determine how long a pilot can maintain consciousness. These same studies have also yielded data on how long a pilot remains incapable of controlling his aircraft after G-LOC (Whinnery, 1988). Table 2.1 shows the results of the USAF SAM and NADC studies on incapacitation times. ROR stands for Rapid Onset Run, meaning a high rate of turn and G-force development. ROR is frequently encountered in fighter aircraft. GOR stands for Gradual Onset Run meaning a slow, gradual G-force development, usually of low magnitude. GOR is encountered in the Space Shuttle during its reentry. Incapacitation times are listed in seconds. Two forms of incapacitation were found: unconsciousness (absolute incapacitation) followed by a period of disorientation and confusion (relative incapacitation).

Table 2.1: USAF SAM G-LOC incapacitation times (Whinnery, 1988)

Group	N	Incapacitation(s)		
		Absolute	Relative	Total
All	55	16	15	31
GOR	34	19	16	35
ROR	21	12	12	24
Type I G-LOC	38	15	13	28
Type II G-LOC	17	20	17	37

Physiological Response to $+G_z$ Acceleration

As hydrostatic pressures increase with $+G_z$ acceleration, blood tends to pool at the feet, reducing head-level blood pressure without any change in ventricular pressure. The heart must develop a higher output pressure to maintain cerebral pressure against the hydrostatic gradient. Figure 2.2 dramatically shows the hydrostatic effect on a seated pilot at $+1$ G_z and at $+6$ G_z. Without any other changes in the arterial circulation, man would lose consciousness at $+5$ G_z (Burton et al., 1974). However, many physiologic changes occur, both adverse and beneficial, to change the G-LOC point of the unprotected man.

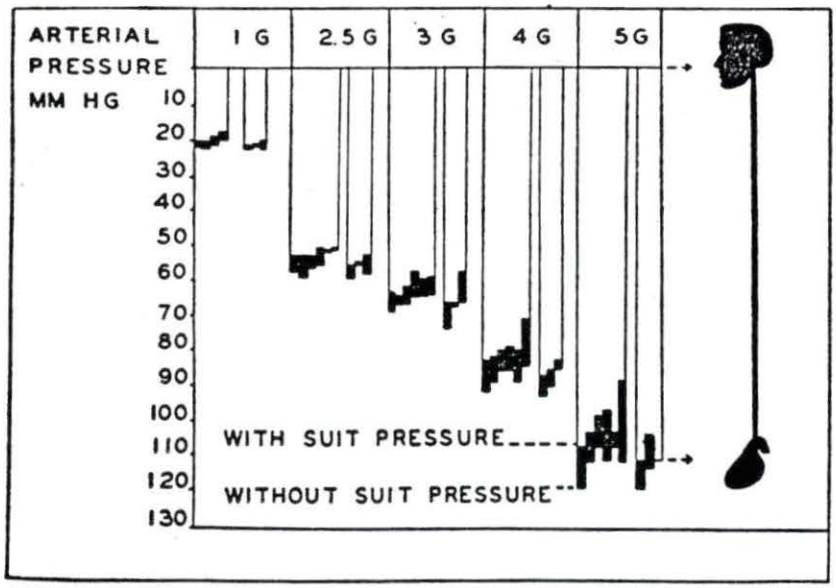

Figure 2.2: Hydrostatic column effect during $+G_z$ acceleration (Gaur, 1961a)

During HSG, blood pools in the lower extremities, reducing cardiac output. Heart rate and total peripheral resistance rise to try to raise cerebral blood pressure. Lower body arterial pressures increase. Cerebral blood pressure, venous return, ven-

tricular volume, central blood vessel diameter, and arterial pO_2 start to fall. Cerebral peripheral resistance falls to improve cerebral circulation. A complete description of these HSG effects and the body's compensatory mechanisms follows.

Systemic circulation

In 1886, Wagner introduced the Hydrostatic Indifference Point (HIP): a natural reference point for measuring changes in hydrostatic pressure. The pressure at this point is constant and not a function of position or G acceleration (Gaur, 1961a; Glaister, 1990). The HIP for the human body arterial system is located at about the level of the aortic valve. Figure 2.3 shows the HIP in a seated man as a function of $+G_z$. It can be seen that the eye-level mean arterial blood pressure in an unprotected man will drop to zero mm Hg at just over $+5$ G_z. This is slightly lower than Burton's observation of $+6$ G_z.

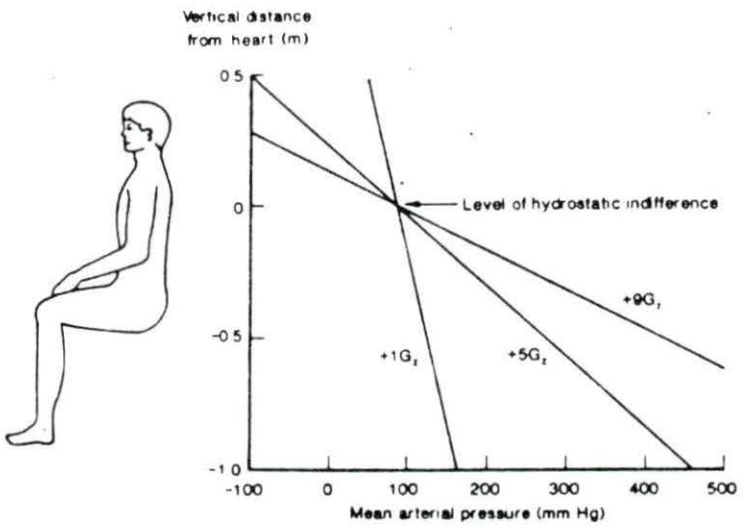

Figure 2.3: Effect of $+G_z$ induced hydrostatic pressure gradients on mean arterial blood pressure in a seated man (Glaister, 1990)

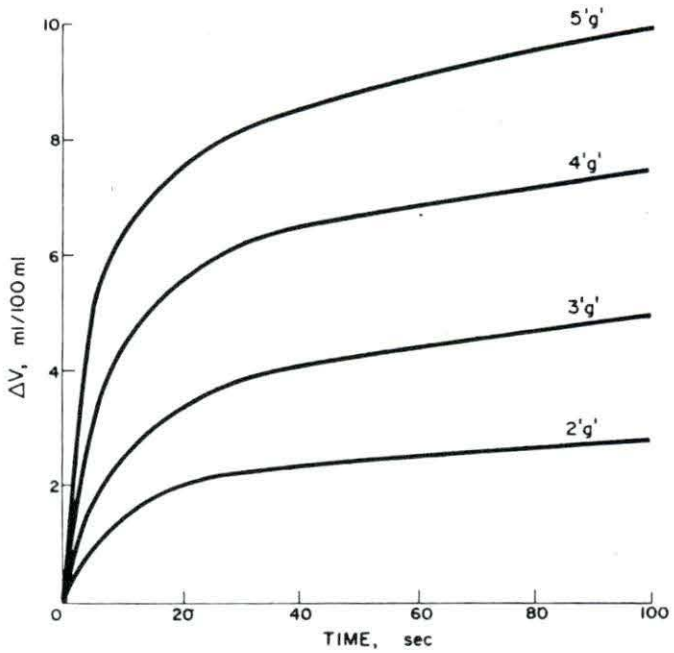

Figure 2.4: Change in calf volume with $+G_z$ (Howard, 1965)

Although this hydrostatic pressure drop occurs instantaneously with the onset of $+G_z$, compensatory mechanisms are delayed in reacting since blood does not shift instantaneously. Blood pools in the capacitance vessels (veins) in the lower body, especially the legs. These vessels distend rapidly at first but take time to reach equilibrium. Figure 2.4 shows the changes in calf volume as a function of time and $+G_z$. Pooling of blood in the lower venous system effectively reduces circulating blood volume (hypovolemia), causing a reduction in cardiac output and a subsequent further loss in cerebral blood pressure (Erickson, 1976; Ganong, 1989; Gaur and Salzman, 1961; Howard, 1965; Glaister, 1990). From this plot, one can see how fast blood is effectively lost from the circulation and the time frame involved in loss of cerebral circulation.

Hypotension and hypovolemia trigger secretion on arginine vasopressin (an antidiuretic) by the posterior pituitary gland (Ganong, 1989). These hormones may not counteract fluid loss in acute $+G_z$ exposure, but may increase G tolerance with repeated exposures (Glaister, 1990).

Positive G_z forces compress the heart muscle along its longitudinal axis, reducing ventricular volume (stroke volume) and further reducing cardiac output (Erickson, 1976; Burton et al., 1974). Leverett et al. (1975) found a drop in contractility (dP/dt) of the left ventricle in dogs during centrifuge experiments.

Located in the walls of the aortic arch and the carotid sinus are stretch receptors known as baroreceptors. Stretch receptors are very sensitive to changes in arterial blood pressure. Under normal arterial pressure (nominally 100 mm Hg), these baroreceptors send impulses to the brain at a basal frequency. These impulses inhibit discharge of vasoconstrictive neurons and excite the cardiac vagus nerve, which affects a drop in heart rate (bradycardia). Any reduction in arterial pressure lowers the firing frequency of baroreceptor cells causing less inhibition of sympathetic neurons that increase heart rate (tachycardia) and less excitation of neurons that produce bradycardia. Stimulation of the vagus nerve lowers heart rate. The reflex reduction in inhibition (relative increase in stimulation) of the sympathetic adrenergic efferents (vasoconstrictive nerves) stimulates the vasomotor center of the brain (VMC) and increases heart rate and contractility (Figure 2.5). These factors lead to a rise in arterial flow and systolic pressure (Chien, 1985; Forster and Whinnery, 1988; Ganong, 1989; Gaur and Salzman, 1961; Glaister, 1990; Voge, 1980).

Occasionally, a drop in heart rate occurs just at $+G_z$ onset and precedes the baroreflex tachycardia by 5 seconds. Peterson et al. (1975) and Erickson et al.

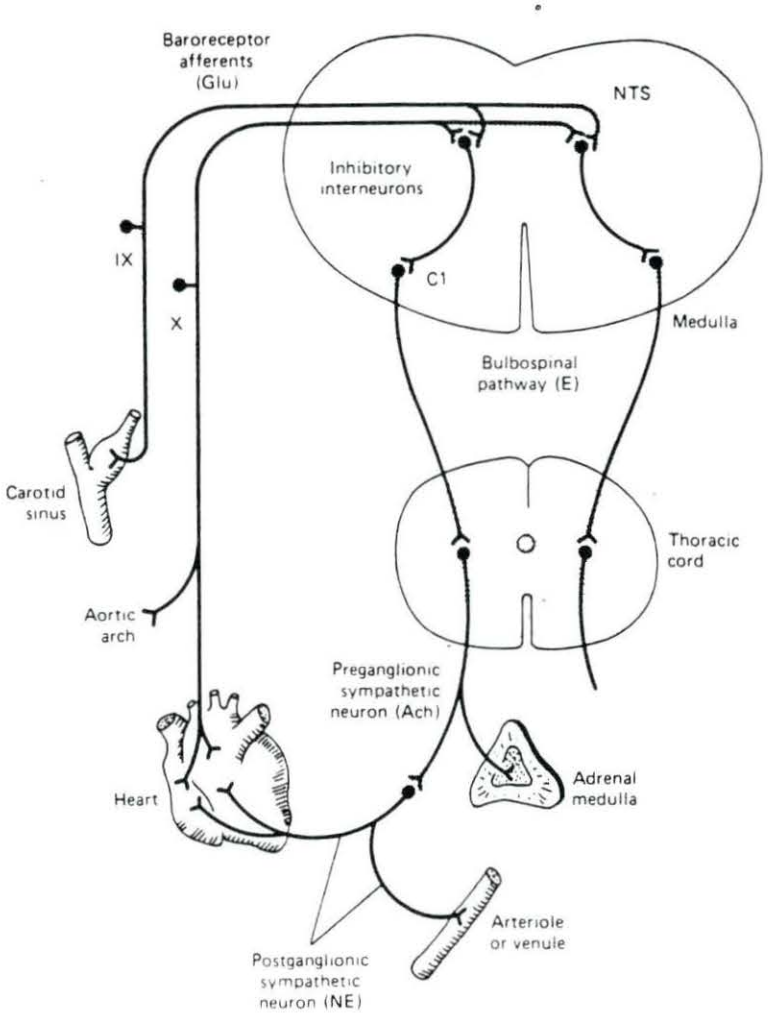

Figure 2.5: Neural pathways for regulating systemic blood pressure (Ganong, 1989)

(1976) both observed this phenomenon in canine centrifuge studies. Two possible explanations have been offered by Erickson et al. and Glaister (1990). Glaister notes that the carotid sinus is located at a lower hydrostatic pressure point than the aortic arch during $+G_z$. At +9 G_z, the pressure difference between these two baroreceptor sites could be as much as 100 mm Hg. Immediately following $+G_z$ onset, the carotid sinus stretch receptor senses the pressure drop and would stimulate the VMC. The aortic arch stretch receptors, however, would not see a hydrostatic change, being near the HIP, nor would they see a pressure change due to a blood volume loss this soon and would act to counteract the stimulation of the VMC. No change in blood pressure would occur.

Erickson's centrifuge experiments (1976) involved cineradiographic (X-ray motion pictures) studies which revealed a marked diameter reduction and elongation in the blood vessels central to the heart. This mechanical stretching of the artery triggers the stretch receptors in the aortic arch to increase their discharge frequency which stimulates the cardiac vagus nerve and produces what Leverett calls "high G bradycardia," (Burton et al., 1974). The carotid sinus receptors and cerebral ischemia would eventually (about 5 seconds post-G onset) sense the blood pressure drop and trigger the VMC, increasing heart rate and contractility. This suggests why this bradycardia is never seen at or beyond maximum G. Dogs who did not exhibit this behavior tended to develop higher cerebral pressures at +Gz and compensated better (Erickson, 1976).

When heart rate changes, the period of the cardiac cycle as a whole does not just shorten but the periods of systole and diastole shorten at differennt rates. Duration of diastole decreases much faster than the duration of systole. Cardiac muscle can

repolarize faster, if needed, as it does in an increased heart rate. For example, duration of systole decreases from 270 ms at a heart rate of 75 bpm to 160 ms at a heart rate of 200 bpm — a 41% drop. Diastolic duration, however, drops from 530 ms to 140 ms for heart rates of 75 bpm and 200 bpm, respectively — a 63% drop (Ganong, 1989).

Another function of the baroreceptor's relative stimulation of the sympathetic nervous system is the increase of peripheral resistance (Ganong, 1989; Glaister, 1990). Peripheral resistance is a measure of the pressure drop across a blood vessel or capillary bed for a given flow rate. For any vascular bed, peripheral resistance (PR) is measured by:

$$PR = \bar{q}\,(MABP - MVP) \tag{2.1}$$

where MABP = mean arterial blood pressure, MVP = mean venous blood pressure, and $\bar{q}$ = mean flow.

Pressure drop is greatest across the arterioles (Figure 2.6), up to 60% of the total 100 mm Hg drop that normally occurs in the human arterial tree (Caro, 1978; McDonald, 1974; Milnor, 1982). In studies of hypertensive and hypotensive cats, Fung (1984) found that the pressure drop across the arterioles varied most with variations in central arterial pressure. He concluded that the arterioles function to maintain a constant capillary pressure. The control mechanism is believed to be primarily the contraction and dilatation of the metarterioles and precapillary sphincters as shown in Figure 2.7 (Ganong, 1989; Martini, 1989).

Baroreflex relative stimulation of the sympathetics effect a release of vasoactive catecholamines (hormones) by the adrenal medulla into the circulation. Among these are epinephrine (adrenaline) and norepinephrine (noradrenaline) (Ganong, 1989; Glais-

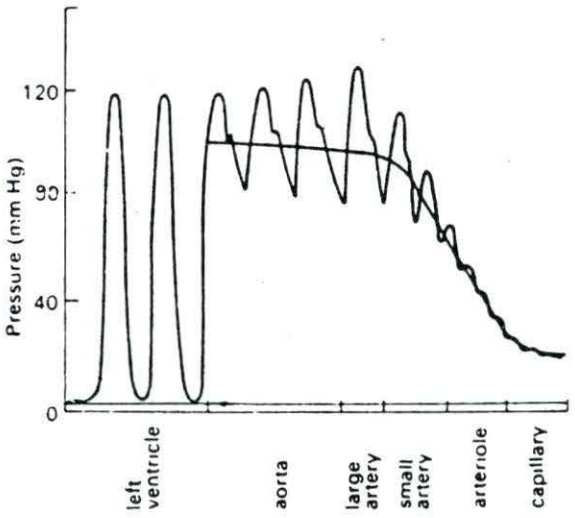

Figure 2.6: Pressure drops in arterial circulation (Caro et al., 1978)

ter, 1990). Norepinephrine (NEph) and epinephrine (Eph) increase heart rate and contractility. NEph produces vasoconstriction in most organs and muscles. Eph, however, causes skeletal muscle vessels to dilate and thus lower peripheral resistance (Ganong, 1989). Since human centrifuge studies have shown that peripheral resistance does increase, one could conclude that Eph is not secreted by the adrenal medulla in great amounts. One explanation for the higher than normal levels of Eph in the blood is leakage from sympathetic synapses that utilize Eph (Glaister, 1990). Such neurons are found in the inhibitory pathway of the baroreceptors (Figure 2.5).

Peripheral resistance rise as a function of G_z up to 1 G but has been found to rise linearly with G_z after 1 G as shown in Figure 2.8 (Howard, 1965).

An increase peripheral resistance raises central arterial pressure at the expense of blood flow to the dependant vascular beds. Glaister (1990) and Erickson et al. (1976) found that a generalized vasoconstriction does not occur. Rather, they found that, in dogs, arterial flow to the gut fell 33% at +4.2 G_z but coronary flow remained

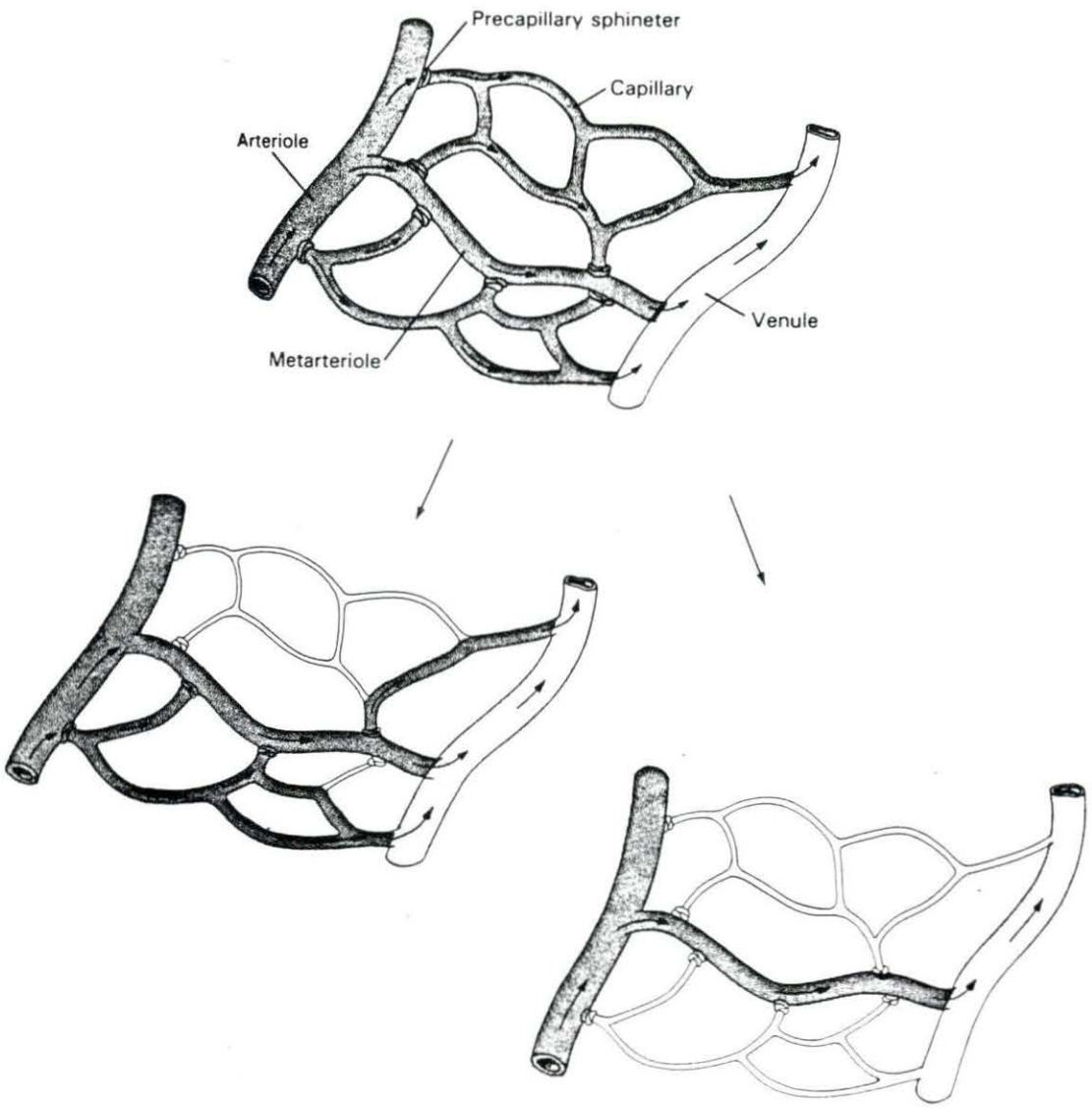

Figure 2.7: Function of the precapillary sphincter (Martini, 1989)

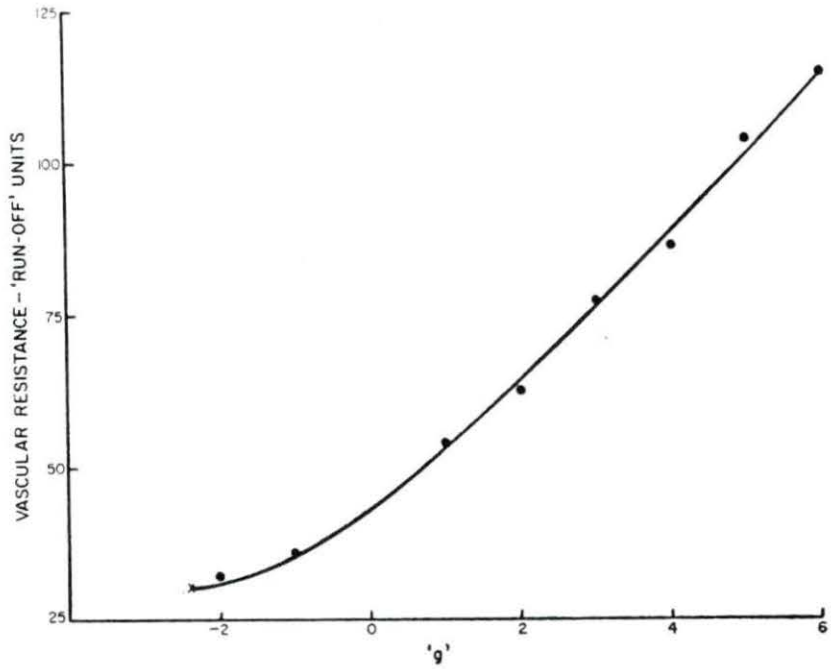

Figure 2.8: Total peripheral resistance versus $+G_z$ (Howard, 1965)

unchanged or even increased. Total cardiac output was down 54%, but 33% of the cardiac output went to the myocardium. However, even coronary circulation may be compromised at higher $+G_z$ levels.

Cerebral circulation, the improvement of which is the entire purpose for increasing central arterial pressure, is not inhibited by any systemic vasoconstriction. In fact, cerebral blood vessels dilate to improve cerebral flow.

Cerebral circulation

During acceleration, Peripheral Light Loss (PLL), or tunnel vision, occurs when systolic arterial blood pressure at eye-level falls to approximately 50 mm Hg. Central Light Loss (CLL), or blackout, occurs at the cessation of retinal flow. Blood can

no longer perfuse the retina when the mean eye-level blood pressure is less than 20 mm Hg (Burton et al., 1974; Burns et al., 1986; Glaister, 1990; Krutz et al., 1973; Leverett et al., 1973).

Researchers in the 1950s and 1960s concluded that retinal flow ceases at 20 mm Hg because the intraocular pressure of 20–25 mm Hg set up an occlusive pressure gradient. However, transcutaneous Doppler ultrasound studies have shown that flow in the superficial temporal artery stops at an arterial mean pressure of 20 mm Hg. This suggests flow cessation occurs at the critical closing pressure of the artery rather than because of an occlusive pressure gradient in the capillary bed.

The superficial temporal artery is frequently used in $+G_z$ physiology research because it is close to the skin and flow is easily measured by ultrasound. It is at eye-level and therefore has the same hydrostatic pressures as the eye. Flow cessation in this artery coincides with PLL, and flow cessation always precedes G-LOC by 2–20 seconds under constant and increasing $+G_z$ (Sandler et al., 1977).

The response of the cerebral vascular bed to variations in arterial pressure maintains a constant cerebral blood flow. Similar to systemic capillary regulation, dilatation of the cerebral vessels occurs during hypotension and constriction during hypertension. Figure 2.9 shows cerebral blood flow (CBF) versus mean arterial blood pressure (MABP). At $+1$ G_z, constant flow is maintained over an arterial pressure range of 50–144 mm Hg (Chien, 1985; McCulloch, 1988). Below 50 mm Hg, cerebral blood flow falls in direct proportion to drops in perfusion pressure (difference between arterial pressure and venous pressure). Decreasing cerebral blood flow increases the partial pressure of CO_2 (pCO_2) in the brain and reducing its pO_2. An increase in pCO_2 in the brain triggers this reflex cerebral vasodilation and increases absorbance

of O_2 per unit volume of blood (Ganong, 1989).

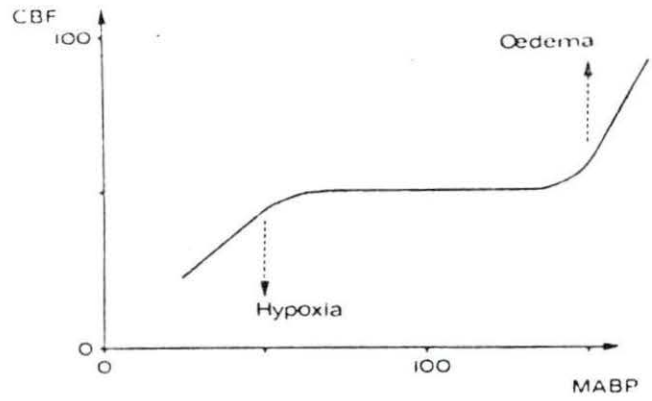

Figure 2.9: Cerebral blood flow versus mean arterial blood pressure (McCulloch, 1988)

In studies of humans in hypotension induced by hemorrhage (assumed to be at $+0$ G_z), unconsciousness occurs at a head-level mean arterial pressure of 50 mm Hg (Glaister, 1990). However, during high-G acceleration, perfusion pressure is maintained below 50 mm Hg. What allows a pilot to retain consciousness down to a mean pressure of 20 mm Hg is attributed to venous drainage. During $+G_z$ acceleration, jugular pressure at the base of the skull drops 5-8 mm Hg to subatmospheric, which maintains perfusion pressure and, in effect, siphons blood from the brain despite the fact that the vein has already collapsed. Cerebral vascular resistance drops further because the decreased venous blood and cerebrospinal fluid pressures reduces peripheral pressure on the cerebral vessels (Chien, 1985; Ganong, 1989; Glaister 1990).

Blood flow to the brain will eventually stop if the gravitational acceleration is great enough, despite the autoregulatory mechanisms of the cerebral vasculature. Every $+1$ G_z increase in acceleration drops the head level blood pressure 20–25 mm

Hg (Burns et al., 1986).

Figure 2.10 shows a typical data set for a human centrifuge experiment using Doppler ultrasound (Sandler et al., 1977). During $+G_z$ acceleration, eye-level blood pressure drops, allowing retrograde flow in the temporal artery. Flow ceases when the pressure drops even further. CLL will occur 5–7 seconds after flow cessation (Glaister, 1990; Krutz et al., 1973; Sandler et al., 1977).

Improving G-TOL

Seatback Angles Presently, there are three methods of increasing G-TOL, the first being the reclining (supinating) seat. As a pilot's head is lowered or his or her hips and legs raised (Figure 2.11), the hydrostatic difference between the heart and head decreases. Most aircraft seatback angles are in the 13°–15° from vertical range except the F-16 (30°) and the YF-22 ATF (rumored to be greater than 30° and variable). Burns (1988) found no significant changes in G-TOL until the seatback angle increased beyond 30°. At angles from 45° to 55°, G-TOL increased by 0.063 G/degree. A 0.146 G/degree G-TOL increase was observed for seatback angles between 65° and 75°.

G-TOL will decrease as seatback angles are increased from 0° (upright) to around 15°-17°. In addition to the average 28–30 cm heart-to-head hydrostatic column (Glaister, 1990; O'Bryan, 1991), there is an 8–9 cm eye-to-brain hydrostatic column in the +x (ventral) direction. The resultant hydrostatic column, about 31 cm, lies 15°–17° ventral from vertical (heart-to-eye). With a seatback angle of 15°–17°, this resultant column, greater in length than the anatomical heart-to-head distance, is brought in line with the $+G_z$ acceleration vector. As seatback angles increase to

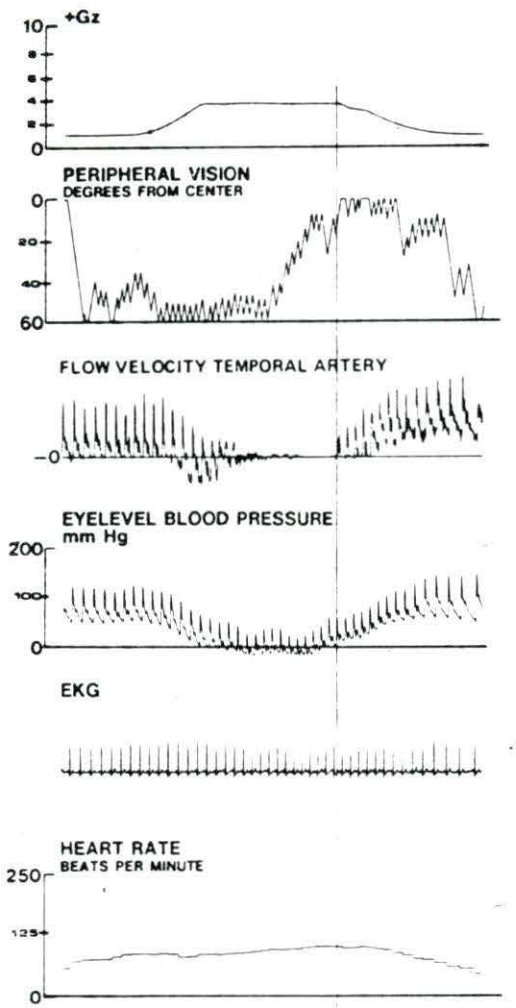

Figure 2.10: Temporal flow velocity, eye-level blood pressure, and $+G_z$ acceleration versus time (Sandler et al., 1977)

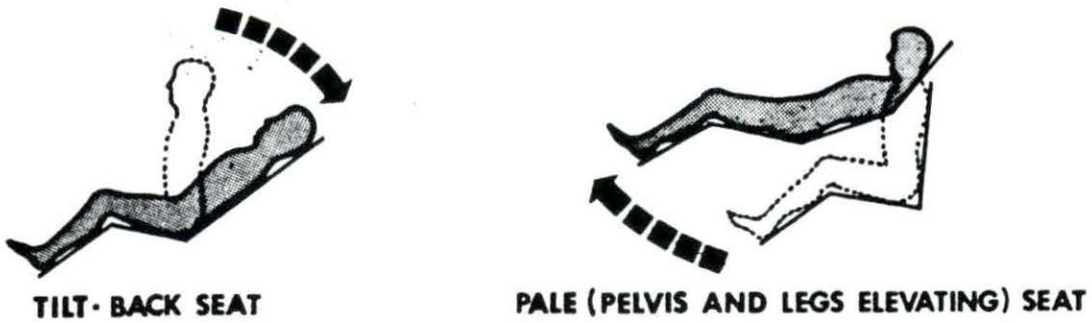

Figure 2.11: Head-tilt and PALE seats (Burton et al., 1974)

around 30°, the hydrostatic column in line with the G_z vector is the same length as that of sitting upright. G-protection will only occur with seatback angles of greater than 30°. Seatback angles greater than 75° do not afford any additional G-TOL since the eye-to-brain column in line with the G_z vector will be greater than the heart-to-head column at this point (Burns, 1988). Table 2.2 shows various seatback angles and the protection they provide.

Problems occur with having large seatback angles. Reduced visibility aft and below the aircraft prohibit the pilot from functioning properly. G-LOC becomes a possibility during $+G_x$ accelerations such as takeoffs and landings. Positioning of flight controls and instruments becomes difficult to place and not obstruct vision and emergency egress (ejection). For adequate forward visibility, the pilot's head must remain upright during flight, reducing G-TOL, and, as the body becomes increasingly supine, headrest angles become large. Large headrest angles are uncomfortable and

Table 2.2: Effect of seat back angle on G-TOL (Burton, 1974)

Subjects	Relaxed G tolerance					
	13°	30°	45°	55°	65°	75°
1	4.0	4.0	---	5.3	6.2	8.0
2	4.4	4.0	4.8	5.0	7.4	8.5
3	3.5	3.7	4.3	5.5	6.3	7.0
4	3.5	3.5	4.2	4.9	5.9	7.3
5	3.5	3.5	4.3	4.9	7.0	10.0
6	4.9	4.5	4.5	5.0	7.5	8.0
7	4.0	4.3	4.8	5.2	6.1	7.0
Mean	3.97	3.93	4.48[a]	5.11[b]	6.48[c]	7.97[c]
±Std. error	0.20	0.15	0.11	0.09	0.24	0.40

Significantly different from values at 13°:
a = $P < .05$; b = $P < .005$; c = $P < .001$.

could prove to be hazardous.

Increasing intrathoracic pressure Anti-G Straining Maneuvers (AGSM) and Positive Pressure Breathing (PPB) are two methods used to increase intrathoracic pressure. AGSM such as the Valsalva (L-1) and the Modified Valsalva or Mueller (M-1) increase thoracic pressure by forced expiration against a closed or partially closed glottis, respectively. PPB raises intrathoracic pressure by forced ventilation at 35 mm Hg pressure. An increase in intrathoracic pressure, used in conjunction with an anti-G suit, force blood from the thoracic cavity into the head and raise head-level blood pressure. Total increase in G-TOL is about 0.5 to 1.0 G. In theory, G-TOL could increase by 2.0 Gs with PPB at 70 mm Hg pressure (Burns et al. 1986; Burns, 1988, Shubrooks and Leverett, 1973).

Anti-G suits Today's G-suit is a garment that applies external counterpressure to a pilot's legs and abdomen to counteract the effects of $+G_z$ acceleration. Originally designed to combat venous pooling, the G-suit has been found to help counteract the primary cause of G-LOC — the drop in arterial pressure (Wood, 1987).

Ideally, a G-suit would apply counterpressure to the legs, abdomen, and arms to temporarily occlude arterial flow during $+G_z$ stress. Such suits were tested prior to WW II. Pilots refused to wear them because they were very uncomfortable even though they provided and additional +3 Gs of protection.

The G-suits used during WW II were a close fitting pair of trousers containing five inter-connected bladders: two calf, two thigh, and one abdominal. These bladders begin to inflate at $+2$ G_z and continue to inflate at 1.5 psi/G (78 mm Hg/G) to a maximum of 10.5 psi (545 mm Hg) (Burton et al., 1974). While these suits do not generate counterpressures high enough to occlude femoral arterial flow, the pressures developed increase femoral flow and can occlude flow in some vascular beds and therefore increase peripheral resistance. Other effects are a reduction of venous pooling, a reduction of the heart-to-head hydrostatic column somewhat by raising the diaphragm, and promotion of venous return by increasing the abdominal venous pressure to central venous pressure gradient. The G-TOL increase of these suits are about 1.9 G, 75% of which is being provided by the abdominal bladder. (Burns et al., 1986).

Experiments conducted by Gray et al. (1969) and Seaworth et al. (1985) agree with Burns that G-suits combat venous pooling and promote venous return by raising venous pressure in the legs and abdomen. From experiments conducted on stand-

ing men wearing G-suits, they observed a drop in peripheral resistance upon G-suit inflation. Arterial pressure increased upon inflation and flow diminished. By Equation 2.1, this is a net drop in peripheral resistance.

The G-suits used today are nearly identical to the WW II versions except that in modern suits, the coverage is not as complete. There are cutouts in the suit for pilot comfort. The standard USAF CSU-12/P cutaway suit, shown in Figure 2.12, provides an increased G-TOL of only 1.0 G (Figure 2.13). The suit was designed to counteract the G-forces generated by aircraft such as the P-51 Mustang and the P-47 Thunderbolt, not the high-Gs generated by modern fighter aircraft. Yet it is the most widely used G-suit in the world (Wood, 1987).

Figure 2.12: The USAF CSU–12/P five bladder G-suit (Burton et al., 1974)

New G-suits being developed by the USAF are complete skeleton suits: arms,

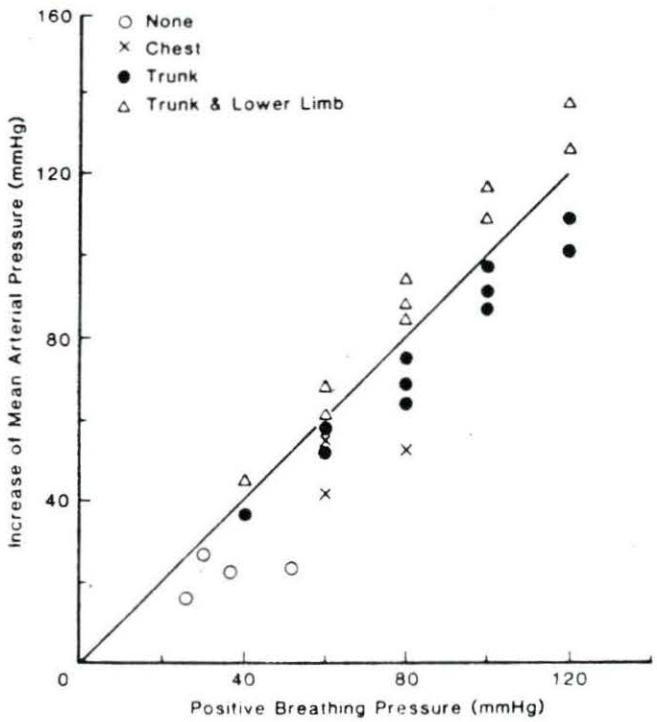

Figure 2.13: Mean arterial blood pressure versus positive pressure breathing and G-suits (Glaister, 1990)

legs and abdominal bladders. They also have faster responding control mechanisms (Burton, 1988; O'Bryon, 1991; Wood, 1990). Moore et al. (1988) have been developing a G-suit that superimposes a pulsatile pressure waveform over the standard inflation pressure. The periodic waveform is synchronized with the heart rate. Both computer simulations and centifuge tests show that this suit can provide an additional 0.6 G over the standard USAF CSU-12/P G-suit.

Stenoses

Arterial stenosis are caused by atherosclerotic plaques built up on the arterial wall. As they develop in size, they begin to project into the lumen of the artery, narrowing the diameter. Flow accelerates and may become turbulent through the stenosis. Distal capillary beds can respond to a growing stenosis by decreasing their resistance in order to maintain perfusion (Stergiopulos, 1987). When the occlusion becomes 80–90% of the cross-sectional area (critical stenosis), flow diminishes rapidly as the distal beds cannot compensate any further.

Pressure drops across a stenosis are measureable but because of the complexity of the turbulence present and non- linear terms appearing as a function of geometry, analytical methods have failed to completely model flow behavior.

Young and Tsai (1973a,b) studied hydraulic models of stenoses with steady and pulsating flows. They found an empirical relationship between the pressure drop and flow as

$$\Delta p(t) = \frac{K_v\,\mu}{D}\,q(t) + \frac{K_t\,\rho}{2\,A_o^2}\left[\frac{A_o}{A_s} - 1\right]\,q^2(t) + K_u\,\rho\,L_s\,\frac{dq(t)}{dt} \qquad (2.2)$$

where

A_o	=	non-occluded cross-sectional area
A_s	=	minimum cross-sectional area inside stenosis
D	=	diameter of non-occluded tube
K_v	=	empirical viscous coefficient
K_t	=	empirical turbulence coefficient
K_u	=	empirical unsteady coefficient

q	=	instantaneous flow in the unoccluded tube
μ	=	fluid viscosity
ρ	=	fluid density

Seeley and Young (1976) found that for varying geometries of blunt-ended stenoses, two empirical coefficients, K_t and K_u, depended little on geometry and could be approximated as constants, $K_t = 1.52$ and $K_u = 1.2$. The third term, K_v, was found to be a function of geometry by the relationship

$$K_v = 32 \frac{0.83\, L_s + 1.64\, D_s}{D} \left(\frac{A_o}{A_1} \right) \tag{2.3}$$

Complete treatment of the empirical studies is given by Young (1979).

CHAPTER 3. THE COMPUTER MODEL

The computer model used in this study was developed by Nikolaos Stergiopulos at Iowa State University. A complete derivation of the governing equations and boundary conditions can be found in his Ph.D. dissertation (1990) and by other related works by Porenta (1986), Rooz (1982), Young (1979), Young and Tsai (1973a,b), and Young et al. (1981). A brief synopsis of the model is given in this chapter.

The following derivation is based on the following assumptions:

- Arteries are modelled as linear, slightly tapered, straight tubes with circular cross sections.
- Arterial walls are incompressible, thin, and distensible. Their material properties assumed homogenous over the length of the segment.
- Segments are constrained in the longitudinal direction.
- Blood is considered an incompressible, homogenous, isotropic, Newtonian fluid.
- Flow is laminar, except possibly near localized constrictions; axisymmetric, and without secondary flows.
- Pressure is radially constant.

While these assumptions may not hold for all arterial flow cases, they have been proven to be reasonably valid for most studies and tend to give good approximations (Stergiopulos, 1990).

Mathematical Model

Governing equations

The mathematical model is based on the integral momentum approach. Assuming axial symmetry and no seepage, the continuity equation can be integrated to yield

$$\frac{\partial A}{\partial t} + \frac{\partial q}{\partial x} = 0 \tag{3.1}$$

Similarly, the momentum equation becomes

$$\frac{\partial q}{\partial t} + \frac{\partial}{\partial x}\left(\lambda \frac{q^2}{A}\right) = -\frac{A}{\rho}\frac{\partial p}{\partial x} + \frac{2\pi R \tau_w}{\rho} + A b_x \tag{3.2}$$

where $\left(\lambda \frac{q^2}{A}\right)$ is the convective acceleration, τ_w is the wall shear, and Ab_x is the external body force term.

The momentum flux coefficient, λ , is a function of the cross-sectional velocity profile. $\lambda = 1.0$ for a flat velocity profile and $\lambda = 4/3$ for a parabolic profile. For arterial flow in major arteries, λ can be reasonably approximated at 1.0.

Shear stress, τ_w, is approximated by

$$\tau_w = -\frac{\rho}{2\pi R}\left[\frac{8 C_v \pi \mu}{\rho A} q + (C_u - 1)\frac{\partial q}{\partial t}\right] \tag{3.3}$$

as developed by Young and Tsai (1973b), where C_v and C_u are functions of the Wormersly parameter, $\alpha = R\sqrt{\frac{\omega}{\nu}}$, where ω is the pulse frequency and ν is the kinematic viscosity. For simple harmonic flow in a straight, rigid tube, Young and Tsai found values for C_v and C_u as plotted in Figure 3.1.

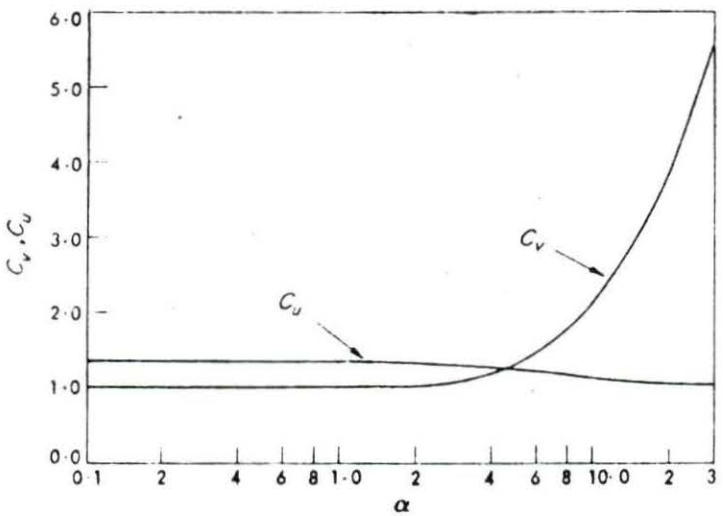

Figure 3.1: Coefficients of wall shearing stress for simple harmonic flow in a straight, rigid tube (Young and Tsai, 1973b)

A non-linear pressure-area relationship is modelled by

$$A(x) = A_O(x)\left[1 + C'_O(p - p_O) + C'_1(p - p_O)^2\right] \qquad (3.4)$$

where C'_O and C'_1 depend on the properties of the artery. Many different p-A relationships can be simulated using this non-linear form by judicious selection of C'_O and C'_1. For this study, a logarithmic p-A relationship is used. Raines et al. (1974) proposed the following logarithmic pressure relationship:

$$A(p,x) = A(p_O,x)\left[1 + K\ ln\frac{p}{p_O}\right] \tag{3.5}$$

By series expansion of Equation 3.5, C_o' and C_1' can be evaluated as

$$C_o' = \frac{K}{p_O} \tag{3.6}$$

$$C_1' = \frac{-K}{2p_O^2} \tag{3.7}$$

Boundary conditions

For the proximal boundary condition, a pressure or flow input waveform is prescribed at the root of the ascending aorta. For this study, a proximal flow condition is prescribed because of the availability of stroke volume data. Waveforms are approximated by a mean flow term and ten Fourier harmonics. The flow waveform for a heart rate of 60 bpm in the supine condition ($+0\ G_z$) is shown in Table 3.1.

It was intended to use the same Fourier coefficients to simulate the higher heart rates experienced in $+G_z$ acceleration. From the mathematical standpoint, changing the frequency of the arguments in the Fourier expansion is all that would be necessary. However, from a physiological standpoint, the entire waveform does not change with frequency. As heart rate increases, the systolic wavefrom remains essentially intact while the diastolic waveform is drastically altered. The basal Fourier coefficients must be modified to reflect the new waveform at different heart rates.

For small arteries and microcirculation, a lumped-parameter impedance distal boundary condition is used at each of the terminal vessels to take into account the resistances and capacitances of the vessels distal to the terminal point.

Table 3.1: Fourier coefficients for the proximal flow waveform

Harmonic	Cosine term $(\frac{m^3}{s})$	Sine term $(\frac{m^3}{s})$
0	0.86393E-4	0.00000E+0
1	-0.88455E-4	0.13368E-3
2	-0.52515E-4	-0.12280E-3
3	0.86471E-4	0.22459E-4
4	-0.26395E-4	0.22693E-4
5	-0.12987E-4	0.22398E-5
6	0.20133E-5	-0.22315E-4
7	0.70896E-5	0.10065E-4
8	0.32577E-5	-0.21066E-5
9	-0.56573E-5	0.90633E-5
10	-0.19302E-5	-0.85422E-5

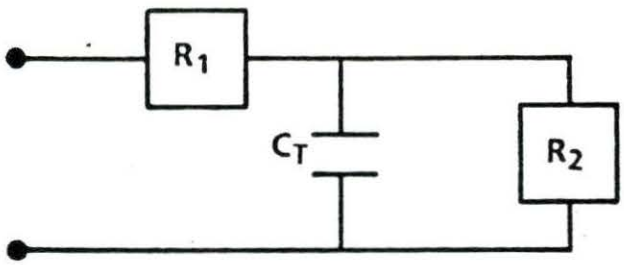

Figure 3.2: Modified windkessel model (Stergiopulos, 1990)

A modified windkessel model (Figure 3.2) is used for terminal impedances which relates pressure and flow by

$$\frac{\partial q}{\partial t} = \frac{1}{R_1}\frac{\partial p}{\partial t} + \frac{p}{R_1 R_2 C_T} - \left[1 + \frac{R_1}{R_2}\right]\frac{q}{R_1 C_T} \tag{3.8}$$

Total peripheral resistance for any vascular bed, R_T, is the sum of R_1 and R_2 for that bed.

Complicated flow patterns at branches and bifurcations are ignored by the model.

The simplifying boundary condition is merely that pressures remain constant and flows are conserved across a branch or bifurcation.

Stenosis

Arterial stenoses (Figure 3.3) create a pressure drop that is empirically predicted by the equation developed by Young and Tsai (1973b)

$$\Delta p(t) = \frac{4\,K_v\,\mu}{\pi D^3}\,q(t) + \frac{K_t\,\rho}{2\,A_o^2}\left[\frac{A_o}{A_s} - 1\right]\,q^2(t) + \frac{K_u\,\rho\,L_s}{A_o}\,\frac{dq(t)}{dt} \tag{3.9}$$

where

$$K_v = 32\,\frac{0.83\,L_s + 1.64\,D_s}{D}\left(\frac{A_o}{A_1}\right) \tag{3.10}$$

and $K_t = 1.52$, and $K_u = 1.2$.

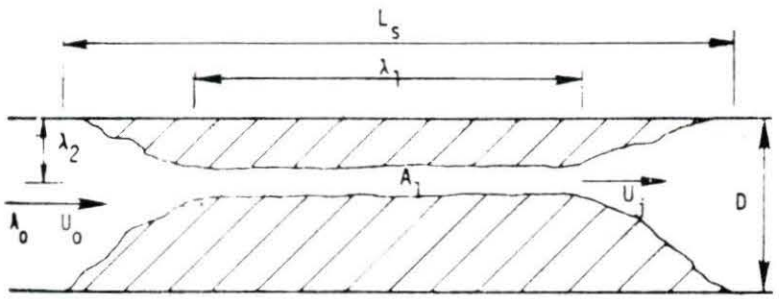

Figure 3.3: Geometry of an arterial stenosis (Young, 1979)

Acceleration

External acceleration is defined by the model as the dot product of the external body force vector and the segment position vector (a vector from the root of the ascending aorta to the arterial segment under consideration). For convenience, acceleration loads are input as multiples of gravity, or Gs. Axial components of acceleration are the momentum equation body force term.

Physiological Model

The model is an arterial tree with fifty-five arterial segments in 239 nodes. The first segment is the root of the ascending aorta at the aortic valve. Terminal segments are at the level of the tibial, radial, carotid, renal, and mesenteric arteries. Vasculature in the hands, feet, thoracic cavity, abdominal cavity and cranium as well as the coronary arteries are not modelled.

The model is a two dimensional projection of a 3-D arterial tree. The "person" is represented in a flat (supine or standing) position with the arms and legs out and flat as shown in Figure 3.4. Each of the segments is straight with a circular, but slightly tapering, cross-section.

Segment geometrical data (length, mean radius, and orientation, presented in Table 3.2, is adapted from Sud and Sekhon (1986). Estimation of the physiological parameters of volume compliance, terminal resistance, and terminal capacitance are given complete treatment in Stergiopulos (1990). Table 3.3 shows terminal impedances.

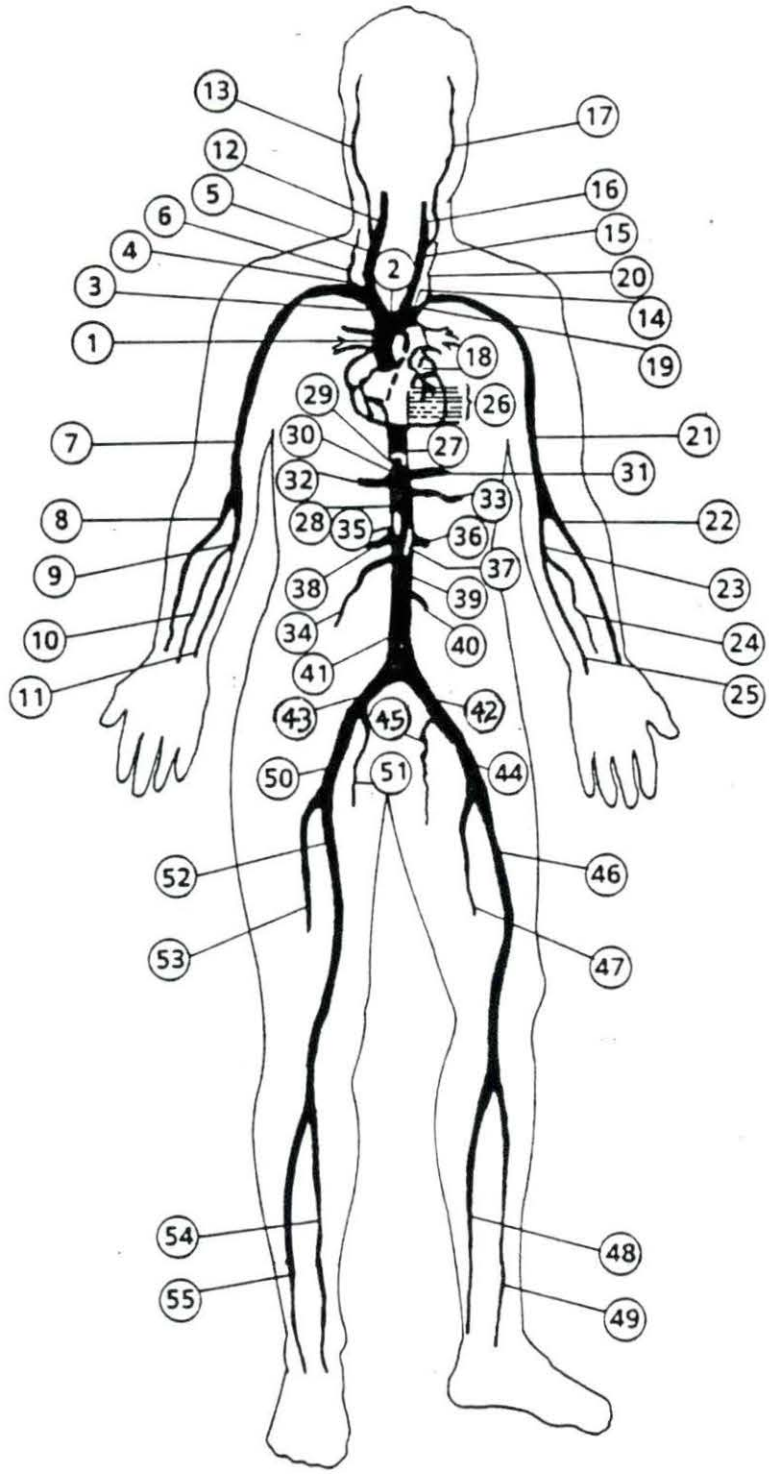

Figure 3.4: Geometric model (Stergiopulos, 1990)

Table 3.2: Arterial geometric data (Stergiopulos, 1990)

Seg.	Name	Length (cm)	Prox. R (cm)	Distal R (cm)	Angle (deg)	Vol. compliance ($10^{-6}\frac{cm^5}{dyne}$)
1	Ascending Aorta	4.0	1.470	1.440	90	104.400
2	Aortic Arch A	2.0	1.120	1.120	0	29.600
3	Innominate	3.4	0.620	0.620	135	13.500
4	R. Subclavian A	3.4	0.423	0.423	180	5.600
5	R. Carotid	17.7	0.370	0.370	90	21.360
6	R. Vertebral	14.8	0.188	0.183	120	1.682
7	R. Subclavian B	42.2	0.403	0.236	240	33.870
8	R. Radial	23.5	0.174	0.142	240	1.877
9	R. Ulnar A	6.7	0.215	0.215	240	1.110
10	R. Interosseous	7.9	0.091	0.091	240	0.090
11	R. Ulnar B	17.1	0.203	0.183	240	2.210
12	R. Internal Carotid	17.7	0.177	0.083	90	0.943
13	R. External Carotid	17.7	0.177	0.083	135	0.943
14	Aortic Arch B	3.9	1.070	1.070	0	52.100
15	L. Carotid	20.8	0.370	0.370	60	25.100
16	L. Internal Carotid	17.7	0.177	0.083	90	0.943
17	L. External Carotid	17.7	0.177	0.083	45	0.943
18	Thoracic Aorta A	5.2	0.999	0.999	270	59.700
19	L. Subclavian A	3.4	0.423	0.423	45	5.600
20	L. Vertebral	14.8	0.188	0.183	60	1.682
21	L. Subclavian B	42.2	0.403	0.236	300	33.870
22	L. Radial	23.5	0.174	0.142	300	1.877
23	L. Ulnar A	6.7	0.215	0.215	300	1.110
24	L. Interosseous	7.9	0.091	0.091	300	0.090
25	L. Ulnar B	17.1	0.203	0.183	300	2.210
26	Intercostals	8.0	0.200	0.150	0	3.000
27	Thoracic Aorta B	10.4	0.675	0.645	270	47.600
28	Abdominal Aorta A	5.3	0.610	0.610	270	20.400
29	Celiac A	1.0	0.390	0.390	0	1.360
30	Celiac B	1.0	0.200	0.200	0	1.000
31	Hepatic	6.6	0.220	0.220	315	2.300
32	Gastric	7.1	0.180	0.180	450	1.510
33	Splenic	6.3	0.275	0.275	0	3.740
34	Superior Mesenteric	5.9	0.435	0.435	225	10.400

Table 3.2 (Continued)

Seg.	Name	Length (cm)	Prox. R (cm)	Distal R (cm)	Angle (deg)	Vol. compliance ($10^{-6}\frac{cm^5}{dyne}$)
35	Abdominal Aorta B	1.0	0.600	0.600	270	4.000
36	L. Renal	3.2	0.260	0.260	0	1.670
37	Abdominal Aorta C	1.0	0.590	0.590	270	3.800
38	R. Renal	3.2	0.260	0.260	0	1.670
39	Abdominal Aorta D	10.6	0.580	0.548	270	33.900
40	Inferior Mesenteric	5.0	0.160	0.160	270	0.792
41	Abdominal Aorta E	1.0	0.520	0.520	270	3.500
42	L. Common Iliac	5.8	0.386	0.350	225	4.580
43	R. Common Iliac	5.8	0.386	0.350	225	4.580
44	L. External Iliac	14.4	0.320	0.270	315	15.620
45	L. Internal Iliac	5.0	0.200	0.200	270	3.300
46	L. Femoral	44.3	0.259	0.190	270	13.640
47	L. Deep Femoral	12.6	0.255	0.186	315	1.130
48	L. Posterior Tibial	32.1	0.247	0.141	270	2.206
49	L. Anterior Tibial	34.3	0.130	0.130	270	0.842
50	R. External Iliac	14.4	0.320	0.270	225	15.620
51	R. Internal Iliac	5.0	0.200	0.200	270	3.300
52	R. Femoral	44.3	0.259	0.190	270	13.640
53	R. Deep Femoral	12.6	0.255	0.186	225	1.130
54	R. Posterior Tibial	32.1	0.247	0.141	270	2.206
55	R. Anterior Tibial	34.3	0.130	0.130	270	0.842

Table 3.3: Terminal impedance data (Stergiopulos, 1990)

Segment	Total Resistance $(\frac{N-s}{m^5})$	Terminal Compliance $(\frac{m^5}{N})$
6	0.60100E+10	0.30955E-10
8	0.52800E+10	0.35235E-10
10	0.84300E+11	0.22069E-11
11	0.52800E+10	0.35235E-10
12	0.13900E+11	0.13384E-10
13	0.13900E+11	0.13384E-10
16	0.13900E+11	0.13384E-10
17	0.13900E+11	0.13384E-10
20	0.60100E+10	0.30955E-10
22	0.52800E+10	0.35235E-10
24	0.84300E+11	0.22069E-11
25	0.52800E+10	0.35235E-10
26	0.13900E+10	0.13384E-09
31	0.36300E+10	0.51251E-10
32	0.54100E+10	0.34389E-10
33	0.23200E+10	0.80191E-10
34	0.93000E+09	0.20005E-09
36	0.11300E+10	0.16164E-09
38	0.11300E+10	0.16464E-09
40	0.68800E+10	0.27041E-10
45	0.79360E+10	0.23443E-10
47	0.47700E+10	0.39003E-10
48	0.47700E+10	0.39003E-10
49	0.55900E+10	0.33281E-10
51	0.79360E+10	0.23443E-10
53	0.47700E+10	0.39003E-10
54	0.47700E+10	0.39003E-10
55	0.55900E+10	0.33281E-10

Centrifuge experimental data

Since the model does not include physiological control mechanisms, the appropriate mechanisms compensating for $+G_z$ acceleration must be supplied externally. Human centrifuge data have been compiled to be used in the model as an input parameter file. Acceleration physiologists frequently discuss four major physiological changes during $+G_z$ acceleration: stroke volume, cardiac output, heart rate, and peripheral resistance.

Cardiac output is a function of stroke volume and heart rate (CO = SV * HR) and is therefore not an independent parameter. Stroke volume is not a compensatory mechanism but is a indicator of venous pooling. By Starling's Law of the Heart, the less venous return, the less stroke volume. If the model included a venous system and a heart, stroke volume would be represented in the governing equations. Here, it is a measure of the predicted venous dynamics of the human circulatory system.

This study only examines the steady-state of the arterial system after the onset of $+G_z$ acceleration. Physiological responses to $+G_z$ acceleration tend to vary with the rate of $+G_z$ onset. For figher aircrew, rapid onset of $+G_z$ acceleration is of prime concern. For this study, only ROR (Rapid Onset Run) data are used, rather than GOR (Gradual Onset Run) data. The reasons as to why the physiological control mechanisms differ from ROR to GOR are beyond the scope of this study.

Human data compiled from Wood (1987), Howard (1965), and Ganong (1989) are shown in Table 3.4. Supine ($+0$ G_z) data used by Stergiopulos (1990) in the original model (Appendix) will be considered accurate for the Standard Man. All centrifuge data in the form of percentage change from supine will be referenced to this data set.

Table 3.4: Human physiological response to $+G_z$ acceleration in literature

$+G_z$	Stergiopulos	Ganong	Wood	Howard	Gotshall
Heart rate, bpm					
0	60	-	-	-	69
1	-	75[a]	90[b]	84[b]	-
2	-	-	95[a]	107[b]	-
3	-	-	112[a]	126[b]	-
4	-	-	127[a]	133[b]	-
Cardiac output ($m\ell s$)					
0	5184	-	-	-	6200
1	-	3888[a]	-	3888[a]	4500
2	-	-	3616[a]	-	-
3	-	-	3188[a]	-	-
4	-	-	3033[a]	-	-
Stroke vol., ($m\ell$)					
0	86.393	-	-	-	-
1	-	51.836[a]	-	-	46.65[a]
2	-	-	39.4[a]	-	-
3	-	-	32.66[a]	32.83[a]	-
4	-	-	26.44[a]	-	-
Peripheral Resistance					
0	Baseline	-	-	-	-
1	-	+25%	-	+25%	+54%
2	-	-	+17%[c] (+46%)	+50%	-
3	-	-	+41%[c] (+76%)	+80%	-
4	-	-	+59%[c] (+99%)	+109%	-

[a] Data listed as percent change from +0 G_z or +1 G_z. Numbers listed are taken from average values of +0 G_z or +1 G_z.

[b] GOR data. Not used for ROR calculations.

[c] From +1 G_z baseline.

Gotshall et al. (1991) published a paper at the conclusion of this study on gender-based physiological responses to $+G_z$ acceleration. An average was taken between the sexes and is presented in Table 3.4. This data set is not used in the determination of the Standard Man but is used for comparison.

Many other authors present human arterial data but only three were found that present all four of the desired parameters in one paper. Discrepancies in the parameters can be caused by simply using a different centrifuge. The shorter the centrifuge radius, the greater the head-to-foot acceleration gradient in the test subject. For example, subject 1 in centrifuge A may show far different test results than subject 2 in centrifuge B, despite the fact both centrifuges were run at the same $+G_z$ acceleration (Voge, 1980).

For comparison, canine and miniature swine ROR data are presented in Table 3.5. Standing human data during anti-G suit inflation found in Gray et al. (1969) and Seaworth et al. (1985) are shown in Table 3.6. Again, the data presented is after all physiologic control mechanisms are fully developed and steady-state is achieved.

Data from all applicable sources are averaged to form the Standard Man shown in Table 3.7. Because averaging of cardiac output, stroke volume and heart rate changed the final relationship between stroke volume and heart rate, cardiac output does not equal the product of stroke volume and heart rate in the Standard Man as it does for each individual author. Table 3.7 shows the cardiac output as determined by the product of stroke volume and heart rate as well as the percentage difference between the averaged cardiac output and the calculated cardiac output. Standard Man data will be used in the input parameter file for a $+G_z$ acceleration model. By comparing the model results with experimental measurements, the validity of the

Table 3.5: Animal physiological response to $+G_z$ acceleration

Species (Author)	n	$+G_z$	Superficial Temporal $\bar{P}$, (mm Hg)	Max. Heart Rate (bpm)	Min. Ascending Aortic $\bar{P}$ $\bar{P}$, (mm Hg)	Terminal Resistance (% fr. +0 G_z)
Canine						
(Erickson)	14	0[a]	-	180	180/150	-
		2.5	-	250	150/25	-
		2.8	-	-	100/75	-
		3.5	-	110	75/0	-
(Peterson)	8	0[a]	90–105	125	124	Base
		1	-	-	-	+40%
		2	90	110	121	+82%
		3	85	85	82	+96%
		4	80	60	62	+92%
		5	-	-	-	+129%
Mini. Swine						
(Burns)	9	0[a]	116–136	110	-	-
		3	17.2	215.4	-	-
		5	-21.9	221.0	-	-
		7	-89.9	215.4	-	-

[a] 0 G_z data refers to +1 G_x data.

model can be examined.

Numerical Solution

Each arterial segment is discretized into finite lengths. The governing equations used for the numerical solution are transformations of the differential equations (Equations 3.1– 3.4) to algebraic equations with approximations of the partial derivatives with finite difference equations. A complete description of the discretization and numerical solution is given in Stergiopulos (1990).

The program estimates initial pressures and flows throughout the entire model

Table 3.6: Human response to $+G_z$ acceleration while wearing anti-G suits

(All values	Gray et al.	Seaworth et al.		
are % change from	45s infl. 40° from vert. tilt	1 min infl. Standing		
zero inflation)	1.5 psi	2 psi	4 psi	6 psi
Heart rate	-12	+1	-10	-3
Cardiac output	+28	+32	+33	+35
Stroke volume	-	+23	+46	+35
Periph. resistance	-	-18	-19	-16
Mean arterial BP	-	+9	+16	+18

Table 3.7: The Standard Man in $+G_z$ acceleration

	$+0\ G_z$	$+1\ G_z$	$+2\ G_z$	$+3\ G_z$	$+4\ G_z$
Heart rate, bpm	60	75	92	112	129
Cardiac output, $m\ell$/min	5184	3888	3616	3188	3033
Stroke volume, $m\ell$	86.393	51.836	39.4	32.66	26.44
Periph. Resistance, % change from $+0\ G_z$	-	25	50	80	109
Calculated cardiac output (HR x SV), $m\ell$/min	5184	3888	3624	3658	3410
Percent change of calc. cardiac output from avg. cardiac output values	0	0	0.2	14.7	12.5

for the first calculated waveform. In the absence of external body forces, the modelled pressure and flow waveforms converge to a solution in two cycles. Transient waveforms exist in the first cycle, however. These are estimation errors of the program and are eliminated in the next cycle. However, in the presence of external accelerations or narrow stenoses, convergence is not reached for four to five cycles.

The finite difference scheme is programmed in Microsoft FORTRAN as well as standard FORTRAN-77. The complete Microsoft code, called PQYPLOT, is listed in the Appendix.

PQYPLOT uses an input data file, listed in the Appendix, for all arterial geometry, terminal impedances, Fourier coefficients, and mechanical properties of the system. For an increase in heart rate, the new frequency is part of the input file. PQYPLOT changes the period of the input boundary condition as a whole. Since the cardiac cycle waveform changes completely for changes in heart rate (Ganong, 1989), the Fourier coefficients must be modified.

The program FLOW, also listed in the Appendix, modifies the basal Fourier coefficients to fit a the new cardiac cycle as shown in Ganong (1989). FLOW calculates the new Fourier coefficients for the new period of the input boundary condition. Intended for eventual incorporation into PQYPLOT as a subroutine, FLOW presently is a separate program that rewrites the Fourier coefficients in the input data file. PQYPLOT, however, will reduce the period of this new waveform as it increases its heart rate. Rather than rewrite PQYPLOT, FLOW compensates for this by expanding the new waveform to fit a period of 1 second, the basal period in PQYPLOT. PQYPLOT then shrinks the waveform to the new period. Figure 3.5 shows a heart rate of 120 beats per minute after being processed by FLOW prior to being processed

by PQYPLOT and the final input flow waveform after processing by PQYPLOT.

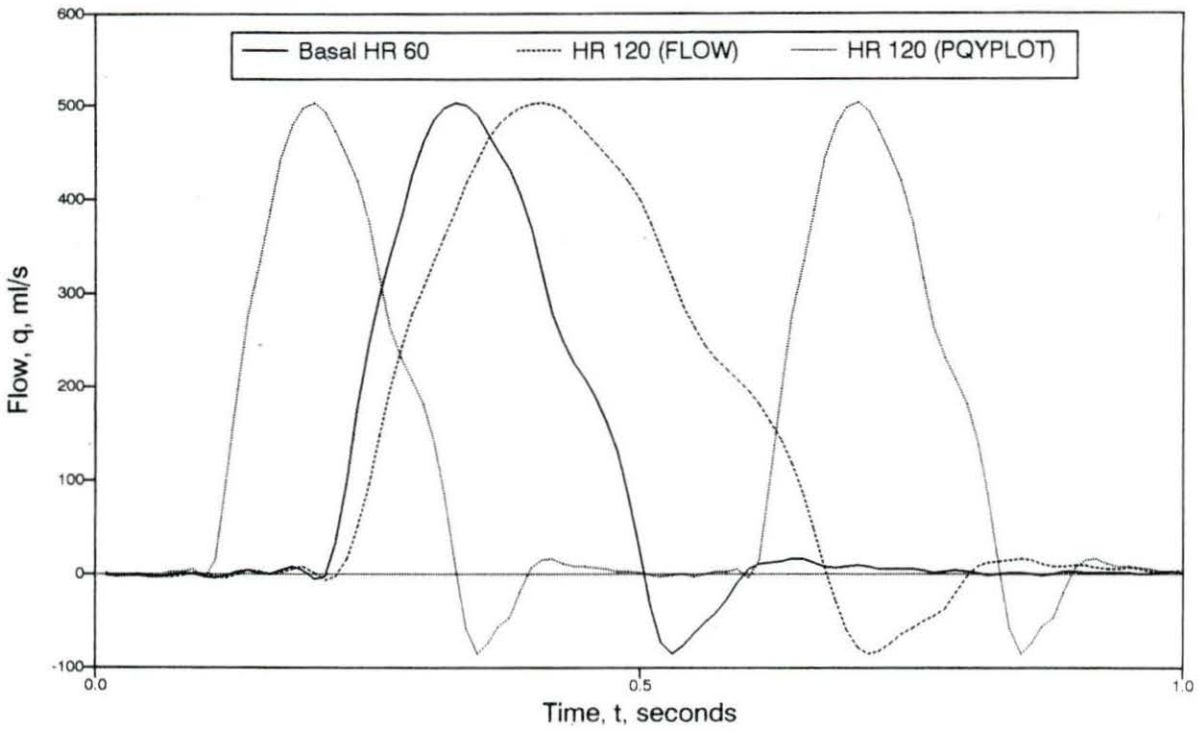

Figure 3.5: Outputs of the initial boundary flow condition FLOW and PQYPLOT for a heart rate of 120 bpm

The Microsoft programs were run on a Gateway 386–33 MH_z microcomputer with a 387 math co-processor. Run times in PQYPLOT for a time step of $\Delta t = 0.001$ seconds were 20 seconds per cycle. The FORTRAN-77 code was run on a DEC 3100 in a UNIX workstation environment. Run times for the same time step were 6.4 seconds per cycle including network transmission delays.

Compensatory Mechanisms

Physiological compensatory mechanisms are time dependent. While the model solves the governing equations while marching through time, the solution is not time dependent. The model, as it stands, can simulate $+G_z$ acceleration for the steady-state condition after any compensatory mechanisms have been fully developed. This steady-state usually occurs in the body 5–8 seconds after the G-loading has begun.

Compensatory mechanisms are not automatically accounted for in the model. Steady-state compensation is accomplished by changing the model input file parameters such as heart rate, peripheral resistance, and stroke volume to reflect such compensation.

The model is an arterial system without venous or cardiac dynamics. To simulate venous pooling and impaired venous return, the observable changes in stroke volume and cardiac output resulting from the venous dynamics are made part of the input flow condition. While not a complete description of the dynamics of the problem, general trends of physiological compensatory mechanisms can be studied.

CHAPTER 4. SENSITIVITY TO INPUT PARAMETERS

The response of the model to changes in the input parameters is of particular interest. If called upon to make a change in the system to maintain homeostasis, it is expected that the human body will use the mechanism that requires the least amount of deviation from its present state to elicit the required systemic change.

The control case established to which changes are compared is taken to be the supine ($+0$ G_z) case as done by Stergiopulos (1990). Stergiopulos showed that the convective acceleration term of the momentum equation had little impact on pressures and flows so it is ignored in this study. This control case is listed in the Appendix as the sample input data file CONTROL 0. All sensitivity studies are referenced to this run.

Two points of interest in the system were identified in order to observe the effects of $+G_z$ acceleration. The commonly observed artery for eye-level blood pressure is the temporal artery. Anatomically, the temporal artery is one of the two terminating branches of the external carotid artery. In the model, the temporal artery and its sister branch are represented by the one external carotid artery extended to the top of the head. Observations are made at the eye-level node (#74) of segment #17 (left external carotid)as shown in Figure 3.4. For the second point of interest, the left femoral artery at about knee level (node #183 in segment #46) is used. Lower

peripheral responses to $+G_z$ acceleration as well as the effect of G-suits on the lower extremites can be observed here.

The femoral arteries are located far from the heart and are symmetric branches from the midsaggital aortic trunk. Little differences in pressure or flow can be seen betweeen the left and right femoral arteries. The carotid arteries, however, branch non-symmetrically from two different vessels close to the heart. The right carotid, branching from the innominate and closer to the heart than the left, should have observable differences in pressure and flow from the left carotid which branches from the aortic arch. Differences should not be significant because the two arteries are nearly symmetric from the base of the neck cranially, but are worth investigating. Literature implies this viewpoint in that the left or right external carotids are rarely distinguished.

Some carotid artery results from the model are shown in Figures 4.1 and 4.2. Pressures and flows for the right and left external carotid arteries taken at eye-level (Node #56 in segment #13 and node #74 in segment #17, respectively) are plotted. No significant deviation in the waveforms is observed. Mean pressures and flows between the two arteries are within 0.1%. Higher mean pressure and flow are observed in the right external carotid. For further simulations, the left external carotid is arbitrarily chosen to be representative of head-level pressures and flows.

Heart Rate and Cardiac Output

Using the supine control case values (CONTROL 0) for terminal impedances and stroke volumes, heart rates of 60, 90, and 120 beats per minute are simulated. Input flow Fourier coefficients are modifed with FLOW prior to the execution of

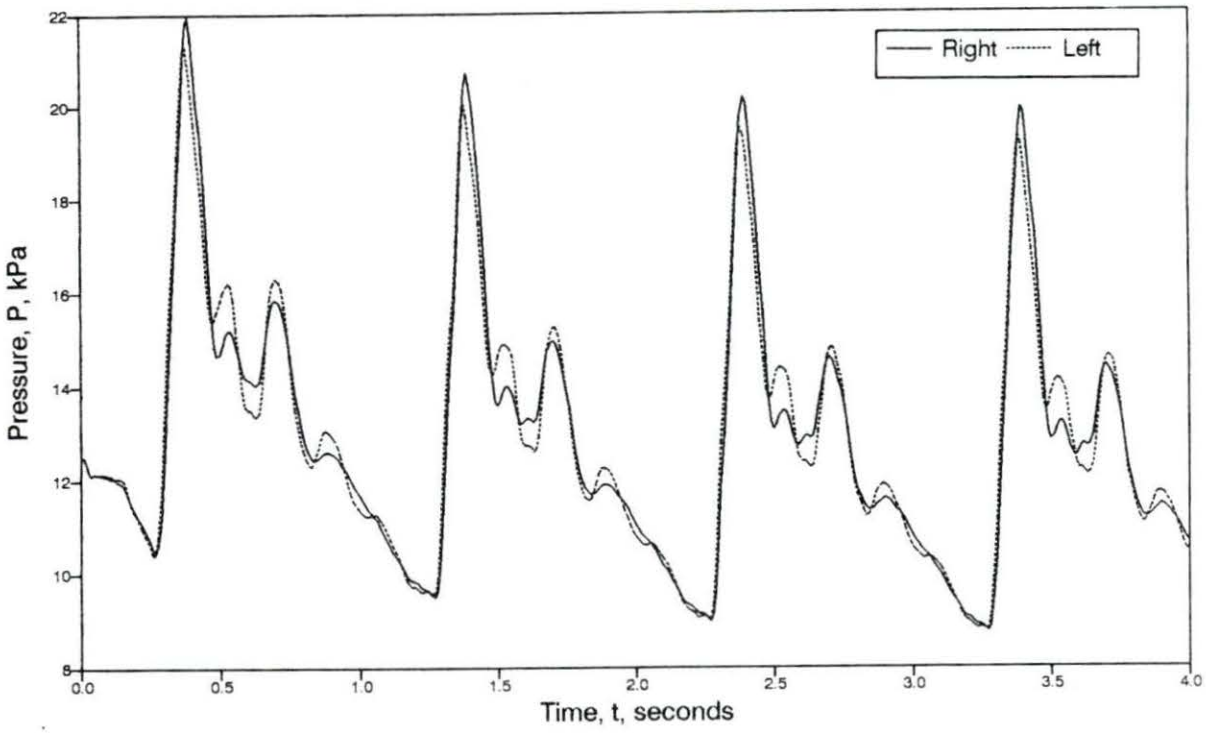

Figure 4.1: Pressure waveforms in the R. and L. external carotid arteries

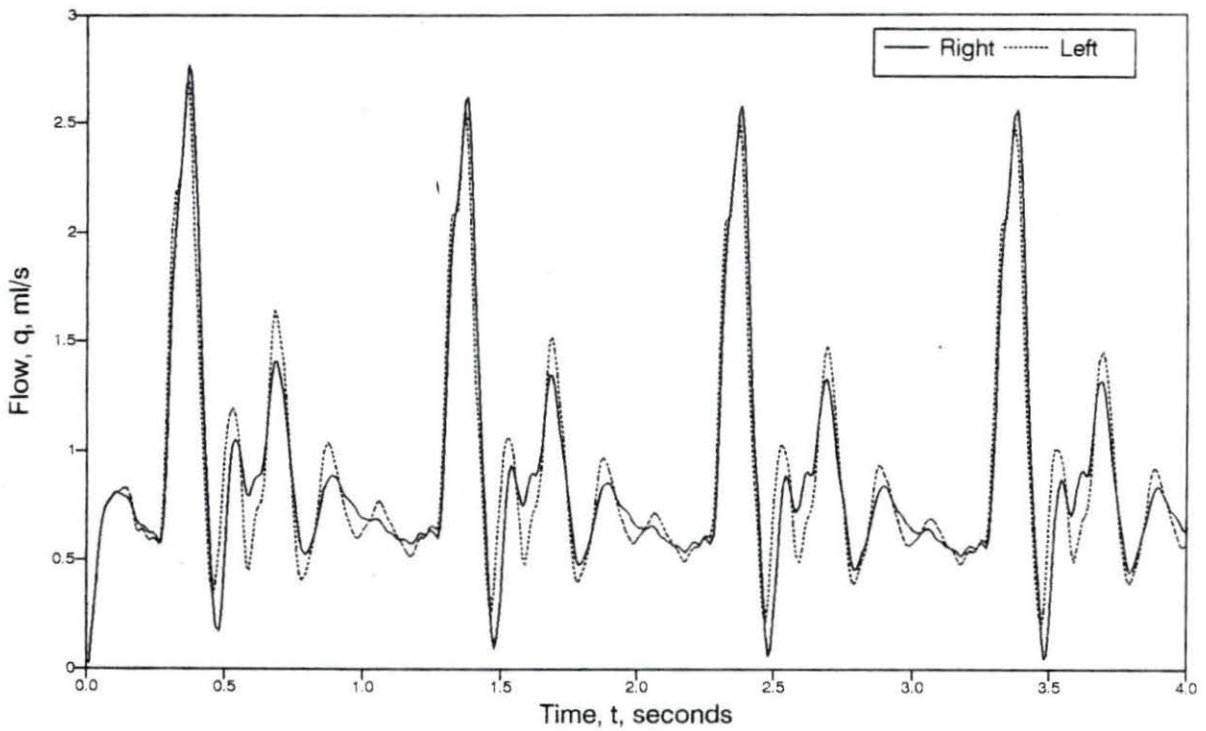

Figure 4.2: Flow waveforms in the R. and L. external carotid arteries

PQYPLOT. Figures 4.3 and 4.4 show the pressures and flows at the root of the ascending aorta (proximal boundary condition). The plot of flow rate versus time (Figure 4.4) shows how FLOW changes the frequency of the heart rate while the systolic flow pulse remains essentially invariant. Note that as heart rate increases, mean pressure in Figure 4.3 increases since more blood flow per unit time through a constant cross-sectional area will, by Poiseuille's Law, cause a pressure increase.

Figures 4.5 through 4.8 show the effects of increased heart rate on the external carotid and femoral arteries. Mean pressures and flows, shown in Table 4.1, increase both on a per unit time and per beat basis.

Table 4.1: Mean pressures and flows in the L. external carotid and femoral arteries with varying heart rate

(2 Cycle avg.)	L. Ext. Carotid		Femoral	
Heart Rate, bpm	$\bar{P}$, kPa (mm Hg)	$\bar{q}$, $m\ell/s$	$\bar{P}$, kPa	$\bar{q}$, $m\ell/s$
60	12.93 (97)	0.895	11.77	3.968
90	16.09 (121)	1.120	14.44	4.905
120	18.91 (142)	1.314	16.79	5.664

A change in heart rate changes cardiac output. Another way to change cardiac input is to change ventricular stroke volume (the amount of blood ejected from the left ventricle per beat).

Stroke volume can be modelled as a per beat mean flow. To change stroke volume, FLOW must recalculate the proximal Fourier coefficients for the new mean flow. Merely changing the mean flow term in the Fourier coefficients without changing the harmonic terms, shifts the entire waveform up or down, causing a positive or negative arterial flow through the aortic valve during diastole. For $+G_z$ applications, FLOW reduces the stroke volume to simulate the reduction in venous return. The

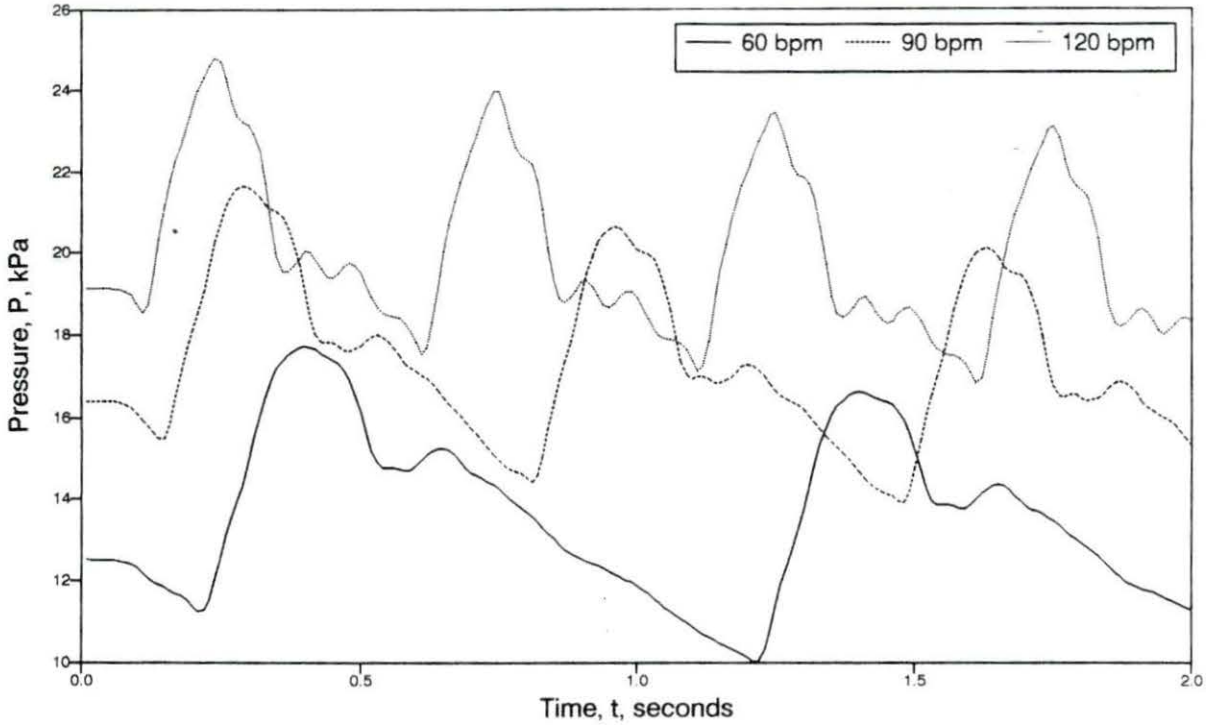

Figure 4.3: Pressure waveform in the ascending aorta

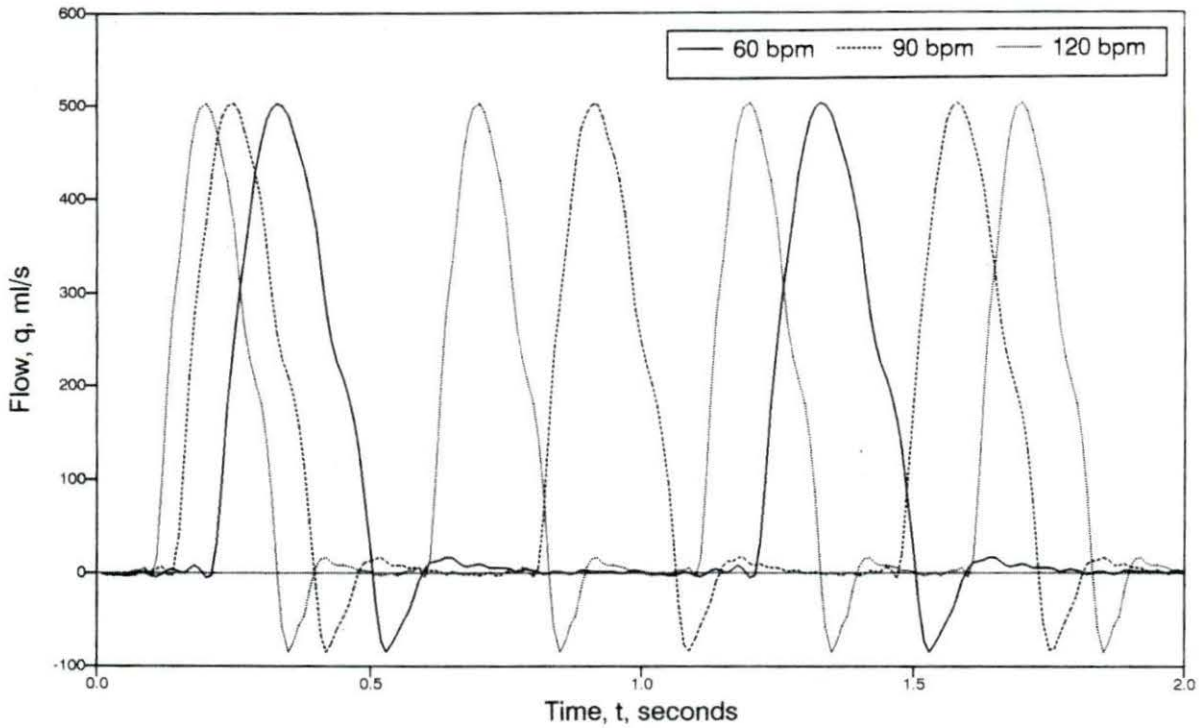

Figure 4.4: Proximal flow condition in the ascending aorta

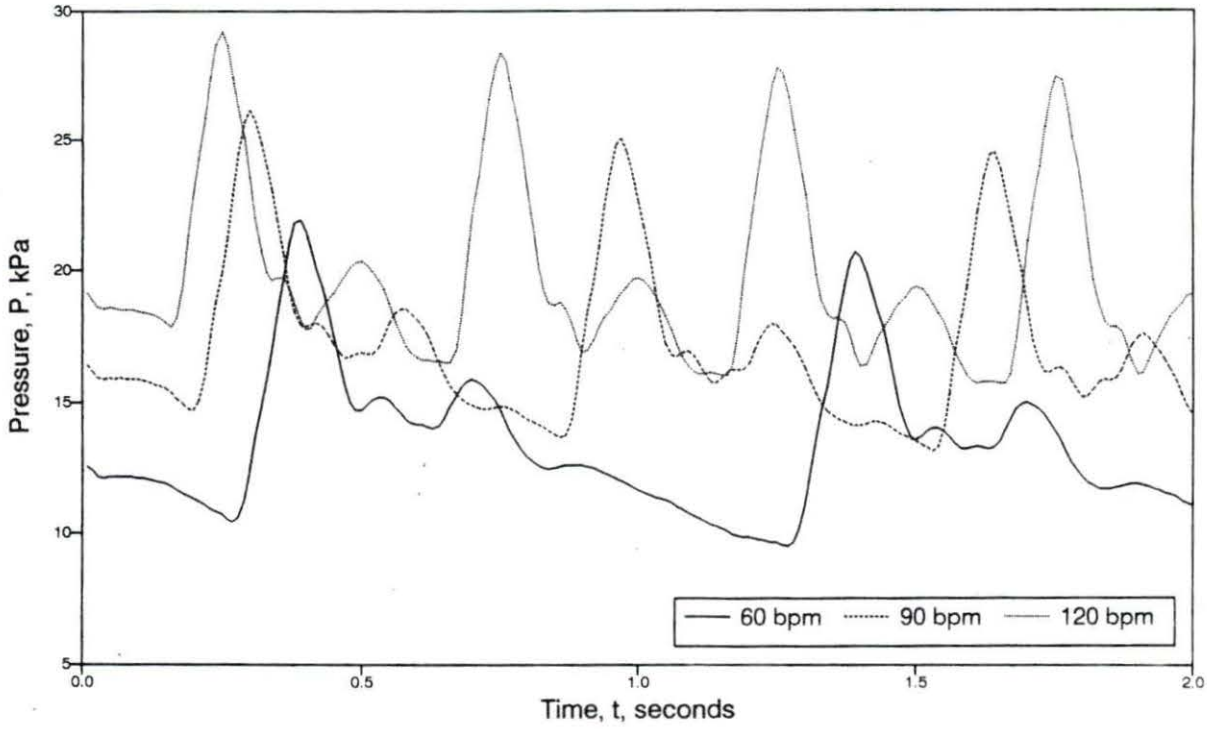

Figure 4.5: Pressure sensitivity to heart rate in the L. external carotid artery

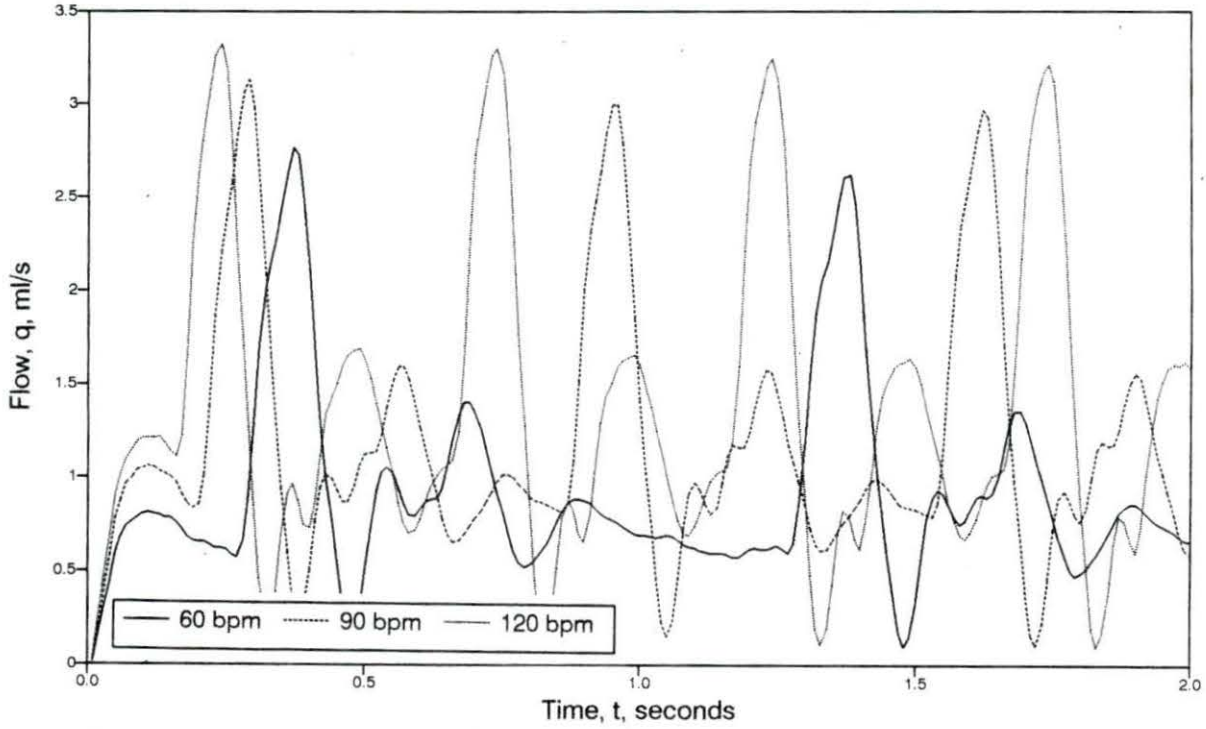

Figure 4.6: Flow sensitivity to heart rate in the L. external carotid artery

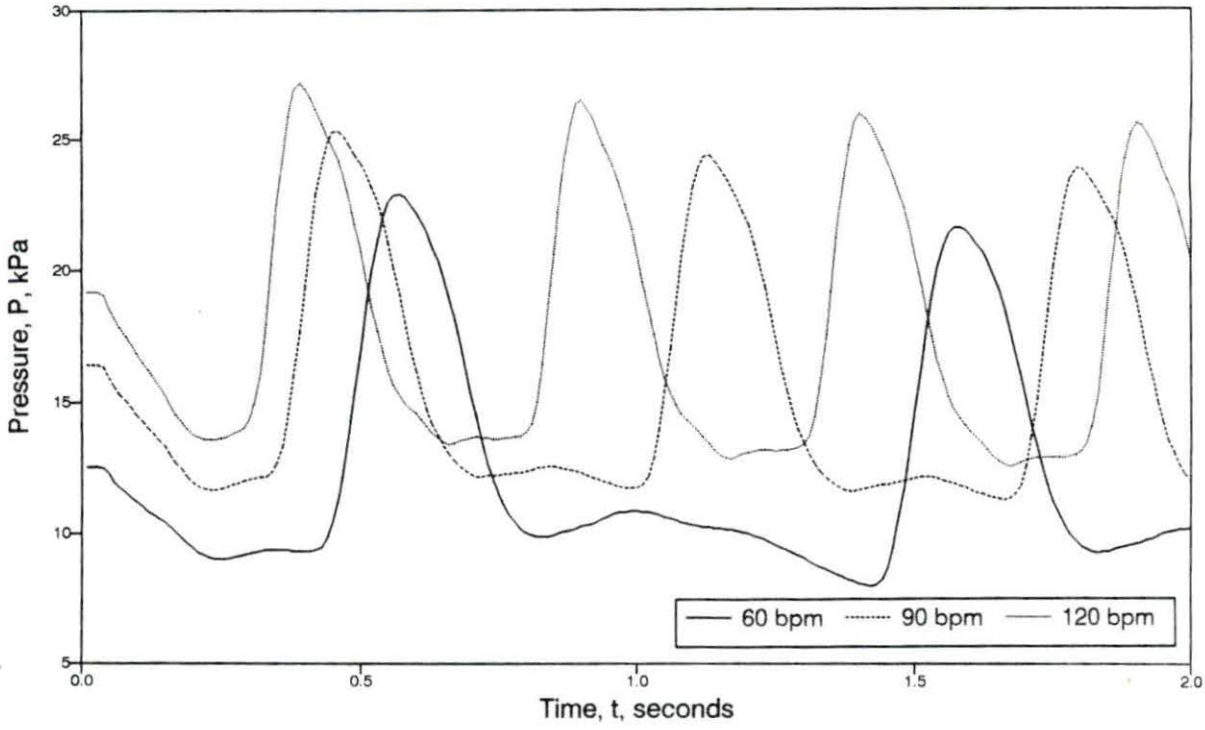

Figure 4.7: Pressure sensitivity to heart rate in the femoral artery

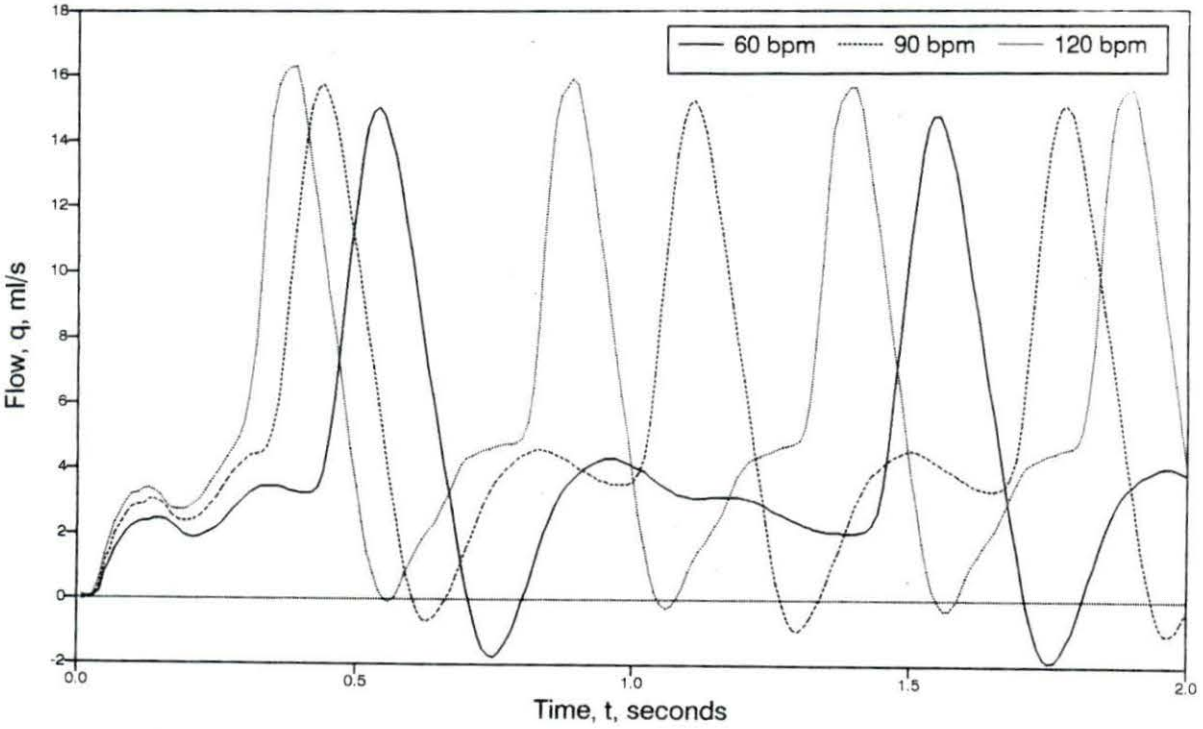

Figure 4.8: Flow sensitivity to heart rate in the femoral artery

modified proximal flow waveform are shown in Figure 4.9.

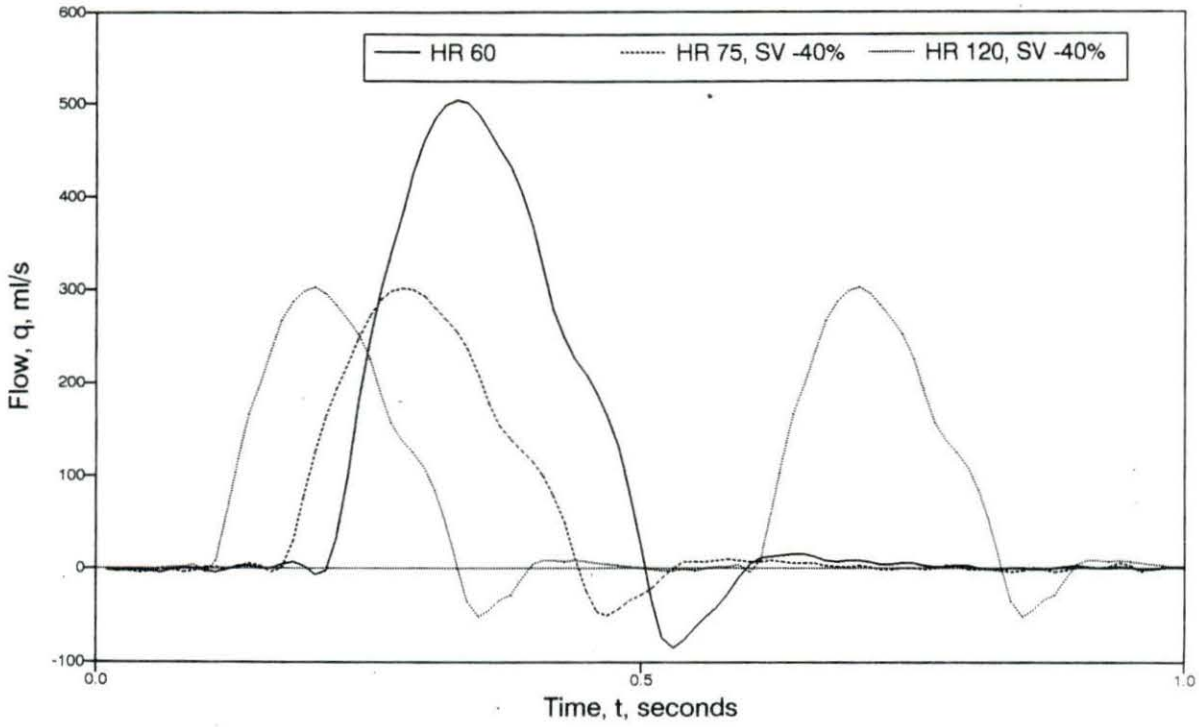

Figure 4.9: Input flow boundary condition with decreased stroke volume

Increasing stroke volume without changing heart rate systemically raises blood pressures and flows as shown in Figures 4.10 through 4.13. Mean pressures and flows are shown in Table 4.2.

Peripheral Resistance

Physiologically, peripheral resistance is determined by the number of arterioles open to flow just proximal to the capillaries. To change peripheral resistances in the model, both the R_1 and R_2 terms of the windkessel model are changed in all

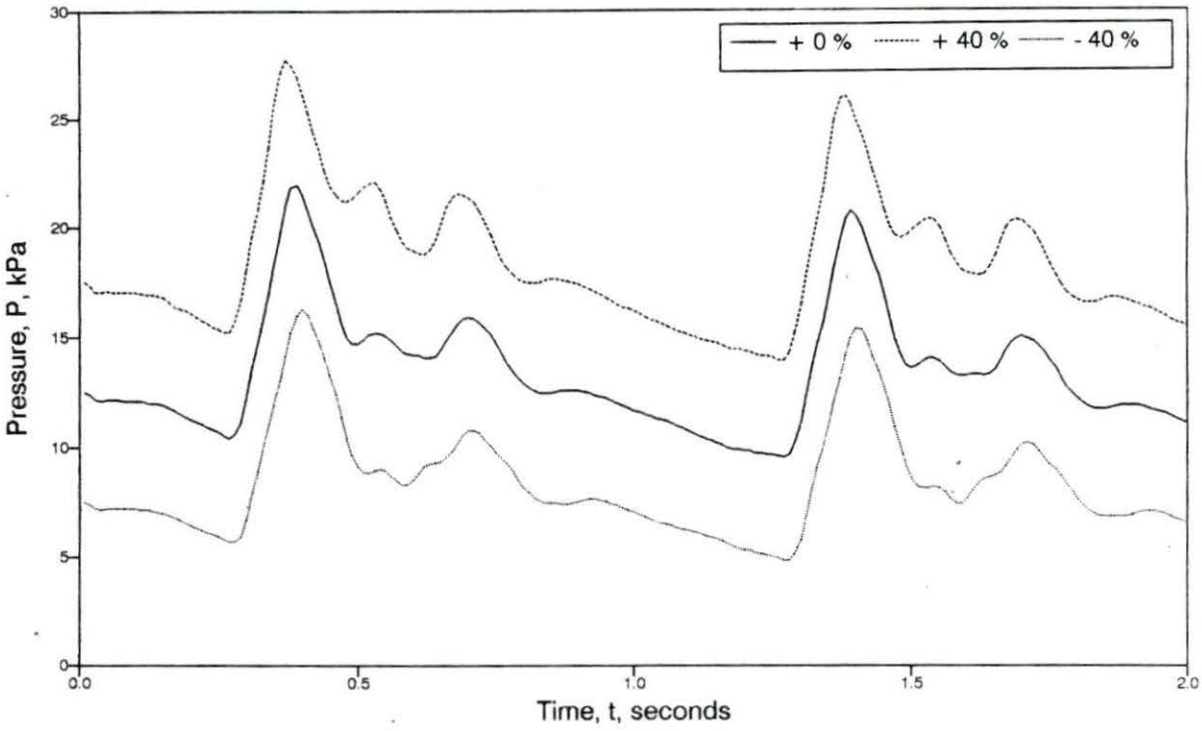

Figure 4.10: Pressure sensitivity to stroke volume in the L. external carotid artery

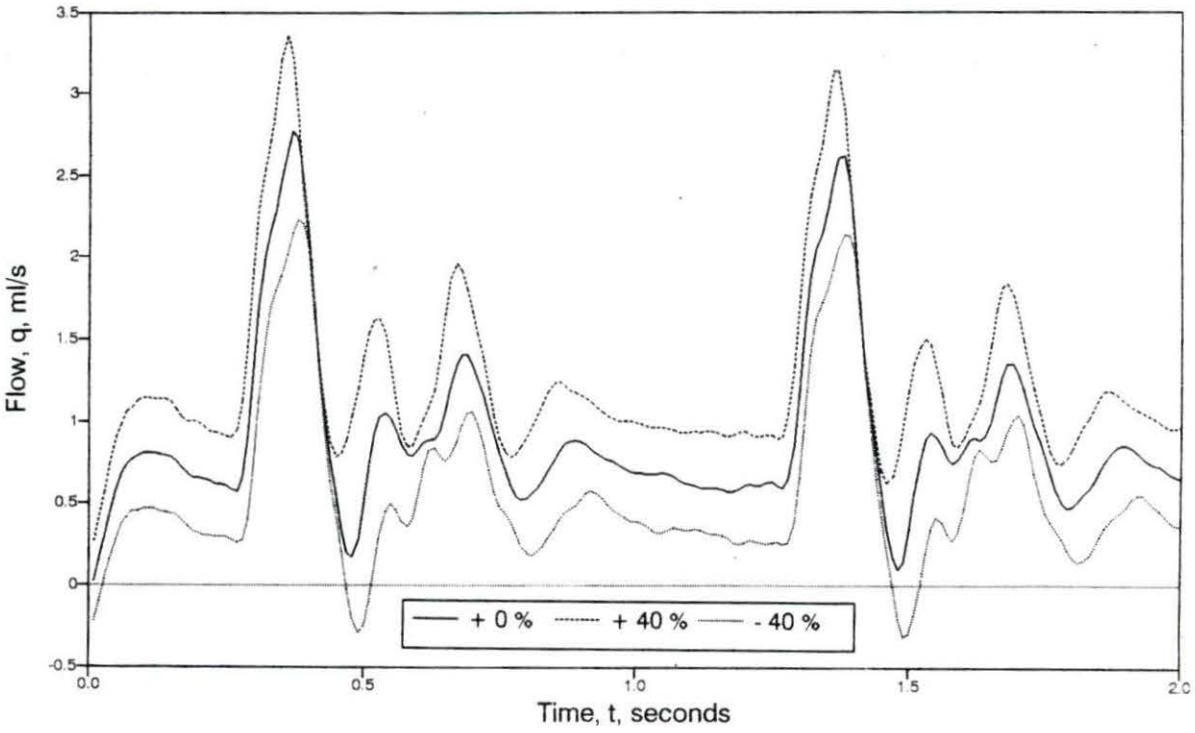

Figure 4.11: Flow sensitivity to stroke volume in the L. external cartotid artery

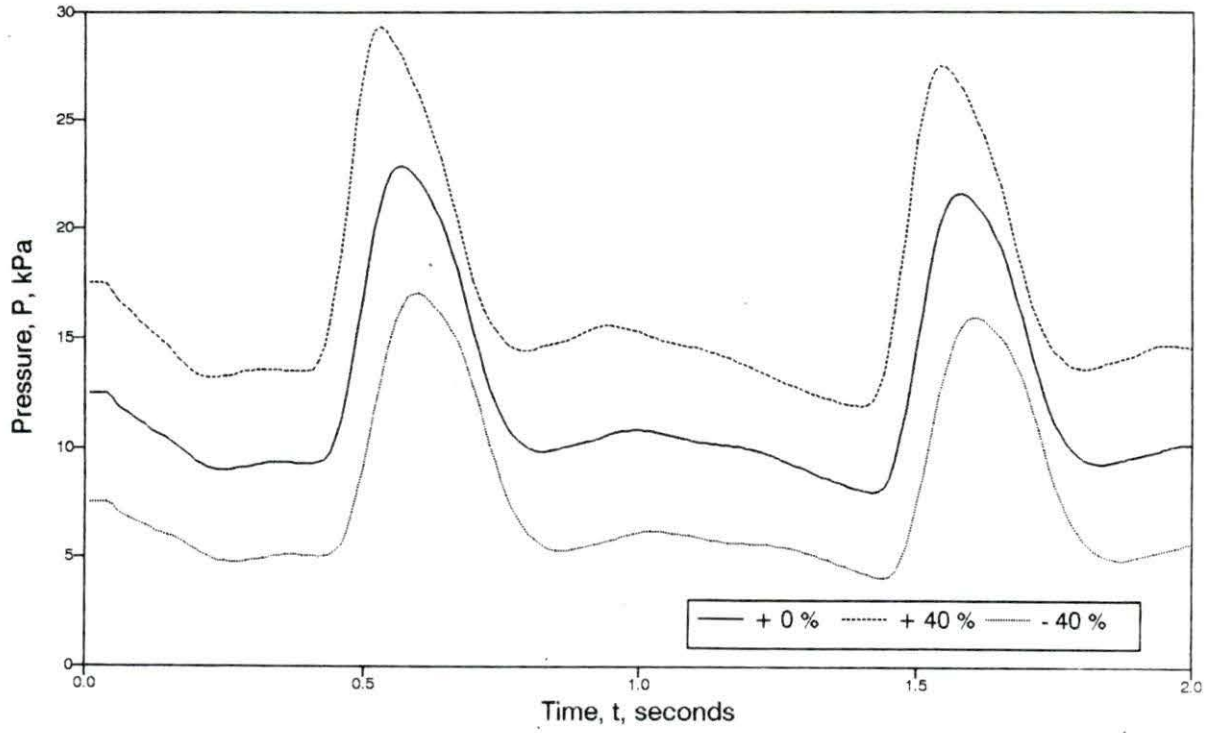

Figure 4.12: Pressure sensitivity to stroke volume in the femoral artery

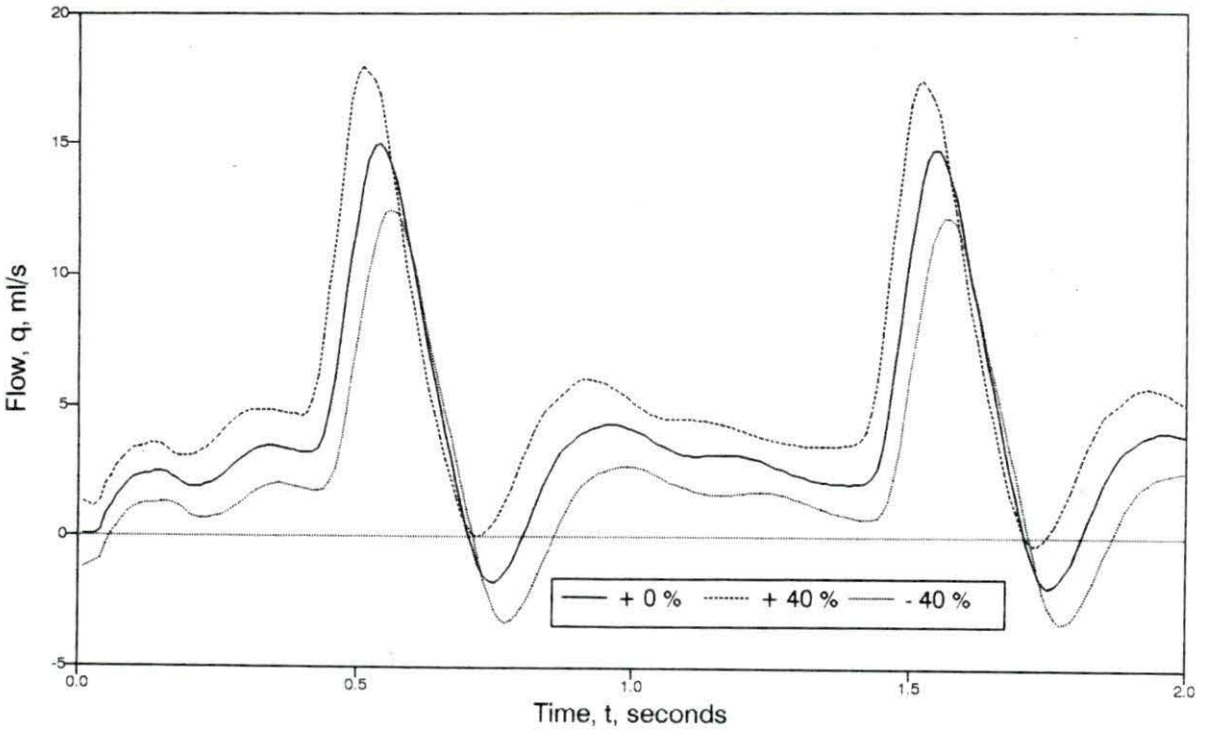

Figure 4.13: Flow sensitivity to stroke volume in the femoral artery

Table 4.2: Mean pressures and flows in the L. external carotid and femoral arteries with varying stroke volume

(2 Cycle avg.)	L. Ext. Carotid		Femoral	
Stroke Vol., ($m\ell$)	$\bar{P}$, kPa (mm Hg)	$\bar{q}$, $m\ell/s$	$\bar{P}$, kPa	$\bar{q}$, $m\ell/s$
-40%	8.039 (60)	0.555	7.330	2.464
Control	12.93 (97)	0.895	11.77	3.968
+40%	17.79 (134)	1.232	16.16	5.457

the terminal vessels. At present, this is accomplished by manually changing the input data file parameters. For systemic changes, all the terminal vessels except those supplying the cranium (segments 6, 12, 13, 16, 17, and 20 in Figure 3.4) are modified. For cerebral resistance changes during cerebral autoregulation, the cranium terminal resistances are changed.

Using the supine control case, systemic peripheral resistances are changed plus and minus 40% from the control values and plotted results for the external carotid and femoral arteries as shown in Figures 4.14 through 4.17. Mean pressures and flows are presented in Table 4.3.

Table 4.3: Mean pressures and flows in the L. external carotid and femoral arteries with varying systemic periperal resistance

(2 Cycle avg.)	L. Ext. Carotid		Femoral	
Terminal PR	$\bar{P}$, kPa (mm Hg)	$\bar{q}$, $m\ell/s$	$\bar{P}$, kPa	$\bar{q}$, $m\ell/s$
-40%	8.482 (64)	0.586	7.284	3.822
Control	12.93 (97)	0.895	11.17	3.968
+40%	17.33 (130)	1.200	16.19	4.022

As expected by the windkessel model, an increase in systemic peripheral resistance without changes in compliance in the extremities raises arterial pressure. From Equation 3.8, flow is a function of $\frac{\bar{P}_a}{R_T}$ and $\frac{\partial P_a}{dt}$. Since the model uses lumped

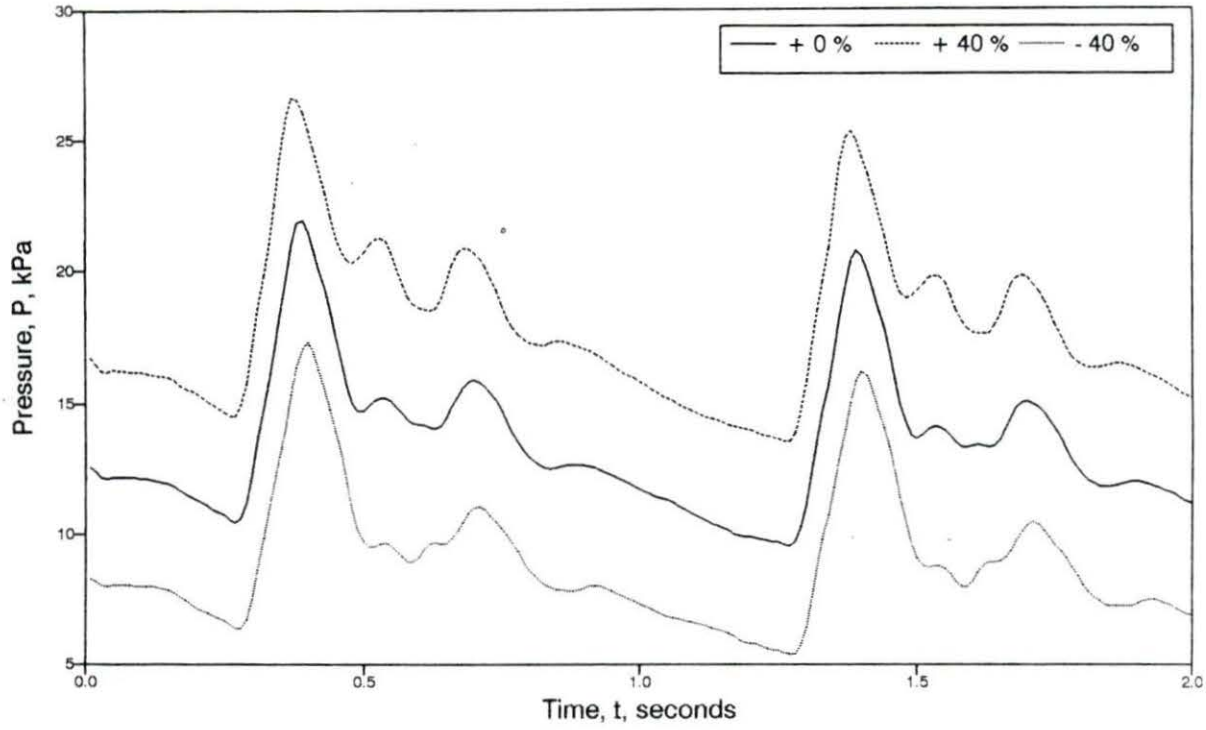

Figure 4.14: Pressure sensitivity to systemic peripheral resistance in the L. external carotid artery

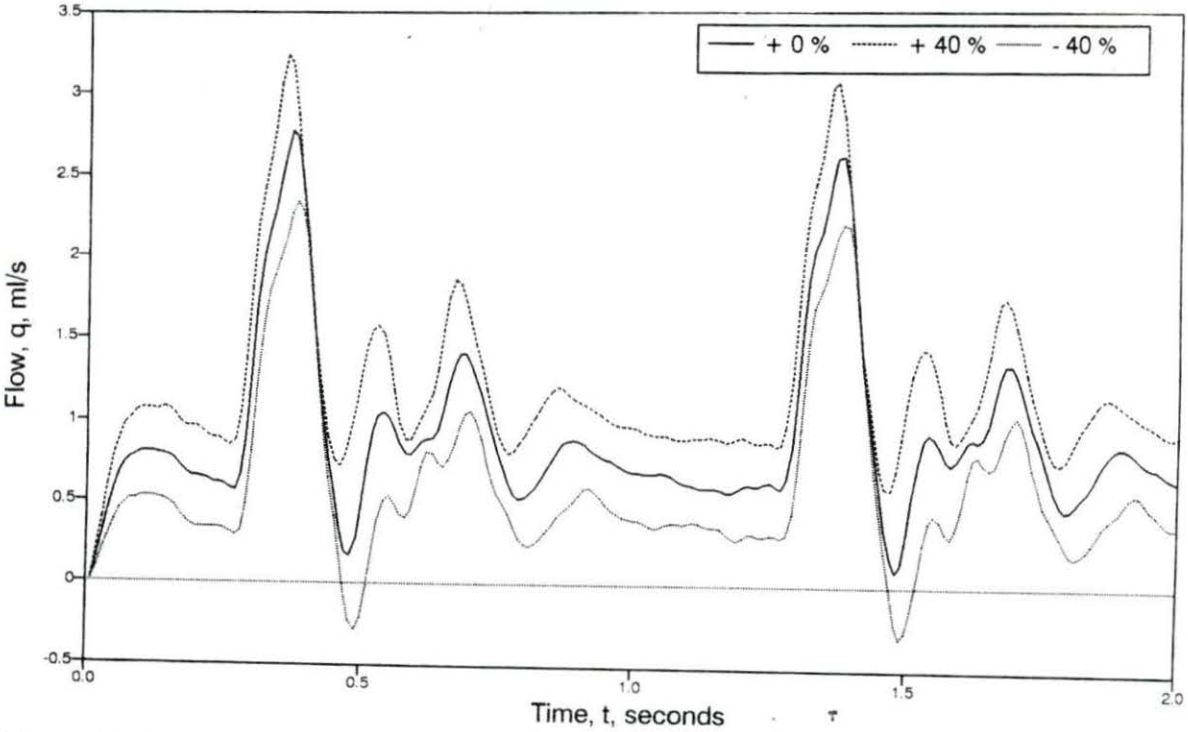

Figure 4.15: Flow sensitivity to systemic peripheral resistance in the L. external carotid artery

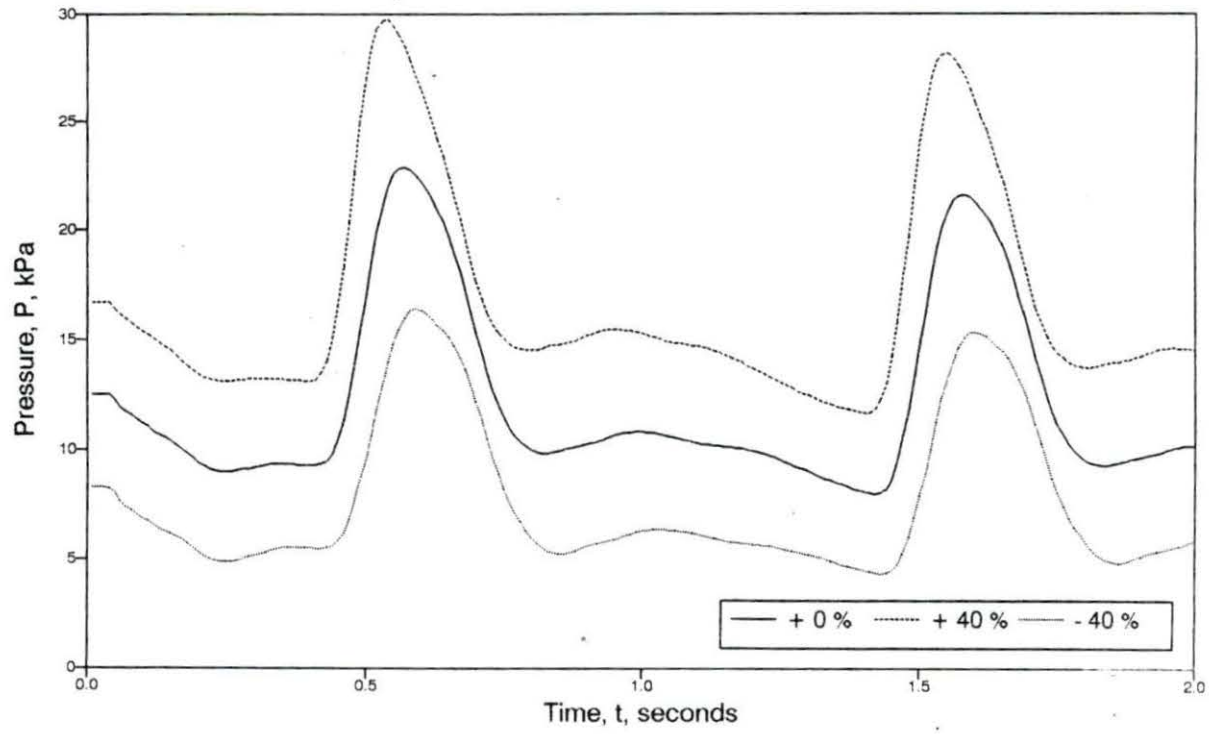

Figure 4.16: Pressure sensitivity to systemic peripheral resistance in the femoral artery

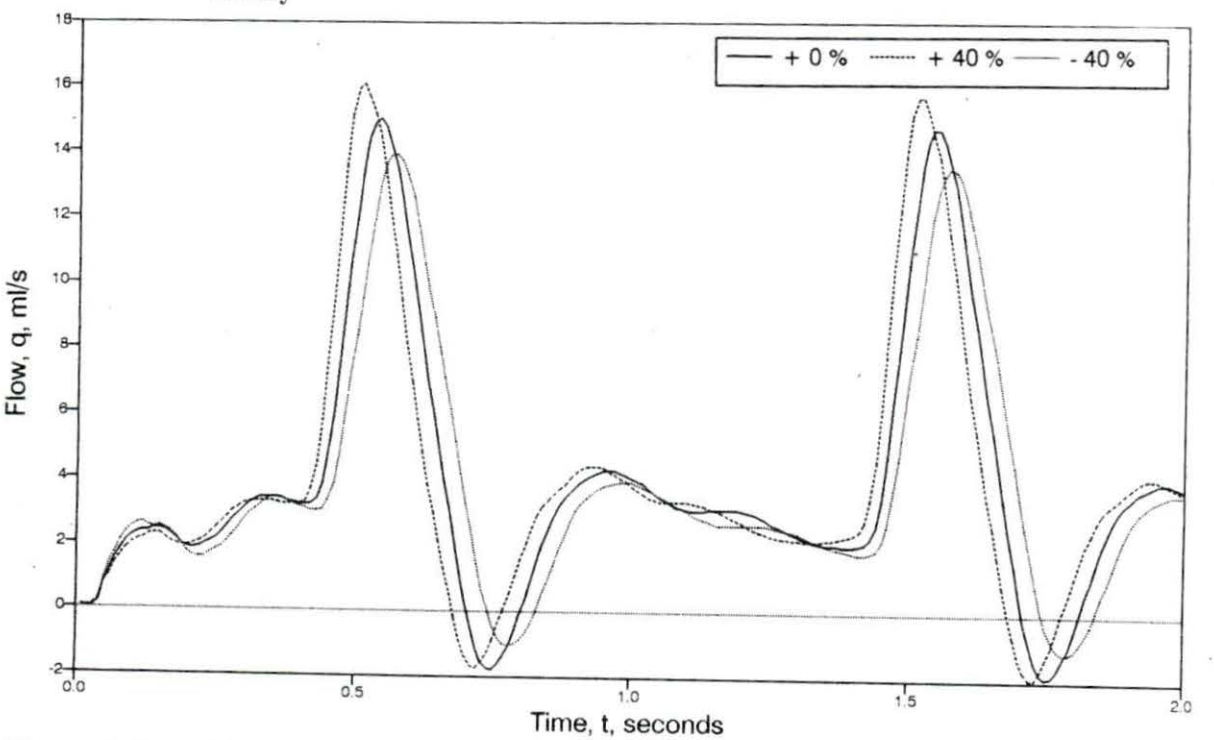

Figure 4.17: Flow sensitivity to systemic peripheral resistance in the femoral artery

parameter terminal resistances, flow will increase only if the percentage change in calculated arterial pressure rises faster than an input percentage change in R_T. For a 40% decrease in peripheral resistance, femoral artery mean pressures and flows decreased, so the % ΔR_T was greater than % $\Delta \bar{P}_a$. During $+G_z$ acceleration, the addition of a body force term will increase $\bar{P}_a$ dramatically. A decrease in flow is therefore expected for an increase in peripheral resistance during $+G_z$, rather than the increase as shown in Table 4.3.

The increase in systemic peripheral resistance raised cranial blood pressure as well. Since impedances did not change in the cerebral cavity, flow increases.

Variations in cranial peripheral resistances are plotted in Figures 4.18 through 4.21 and mean pressures and flows listed in Table 4.4. A decrease in cerebral peripheral resistance decreases cerebral presssure and increases cerebral flow. The effect on the systemic circulation is negligible but tends to decrease systemic pressures and resistances.

Table 4.4: Mean pressures and flows in the L. external carotid and femoral arteries with varying cerebral peripheral resistance

(2 Cycle avg.)	L. Ext. Carotid		Femoral	
Cerebral PR	$\bar{P}$, kPa (mm Hg)	$\bar{q}$, $m\ell/s$	$\bar{P}$, kPa	$\bar{q}$, $m\ell/s$
-40%	12.20 (92)	1.383	11.19	3.771
Control	12.93 (97)	0.895	11.77	3.968
+40%	13.29 (100)	0.660	12.04	4.062

External Acceleration

Again, using only the supine control case input parameters, external $+G_z$ acceleration was applied to the model. Figures 4.22 through 4.27 show the results of

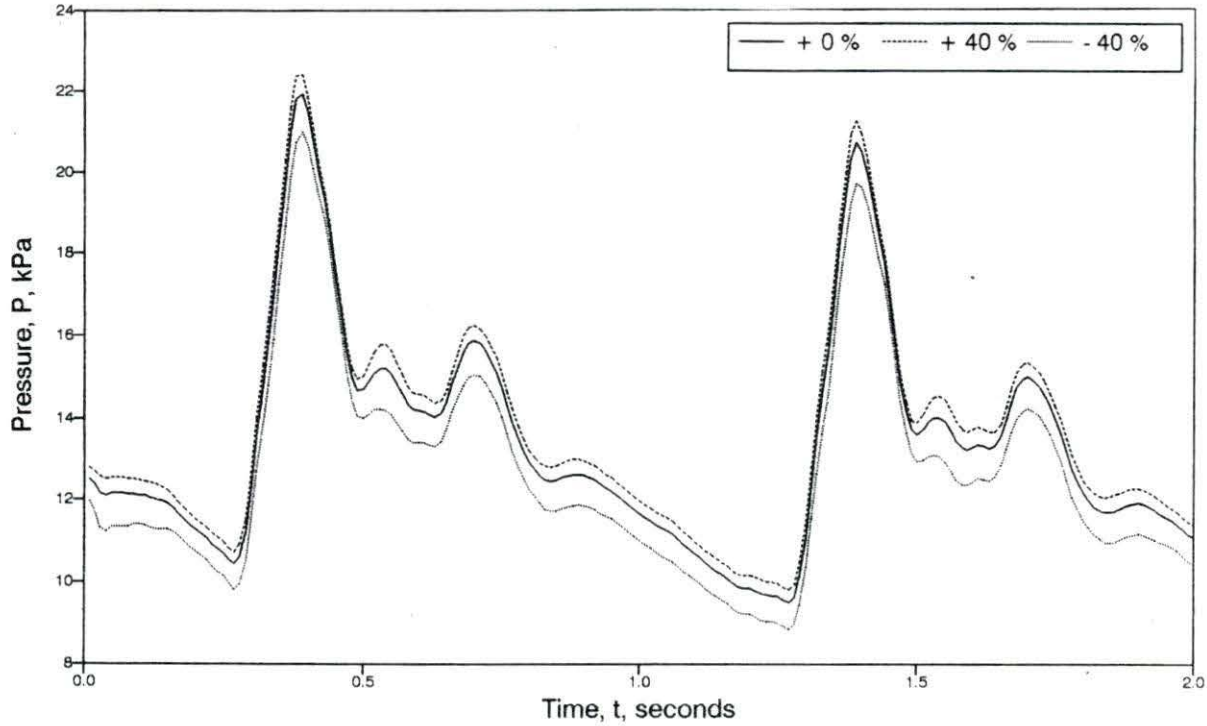

Figure 4.18: Pressure sensitivity to cerebral peripheral resistance in the L. external carotid artery

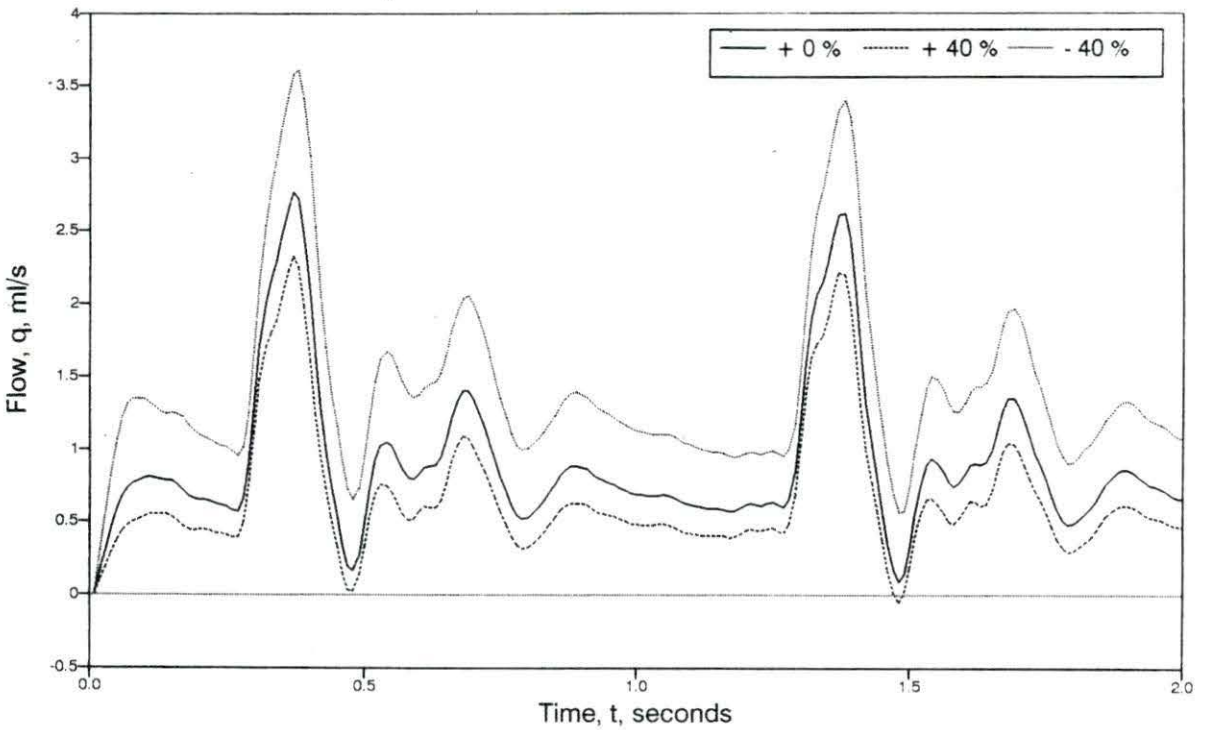

Figure 4.19: Flow sensitivity to cerebral peripheral resistance in the L. external carotid artery

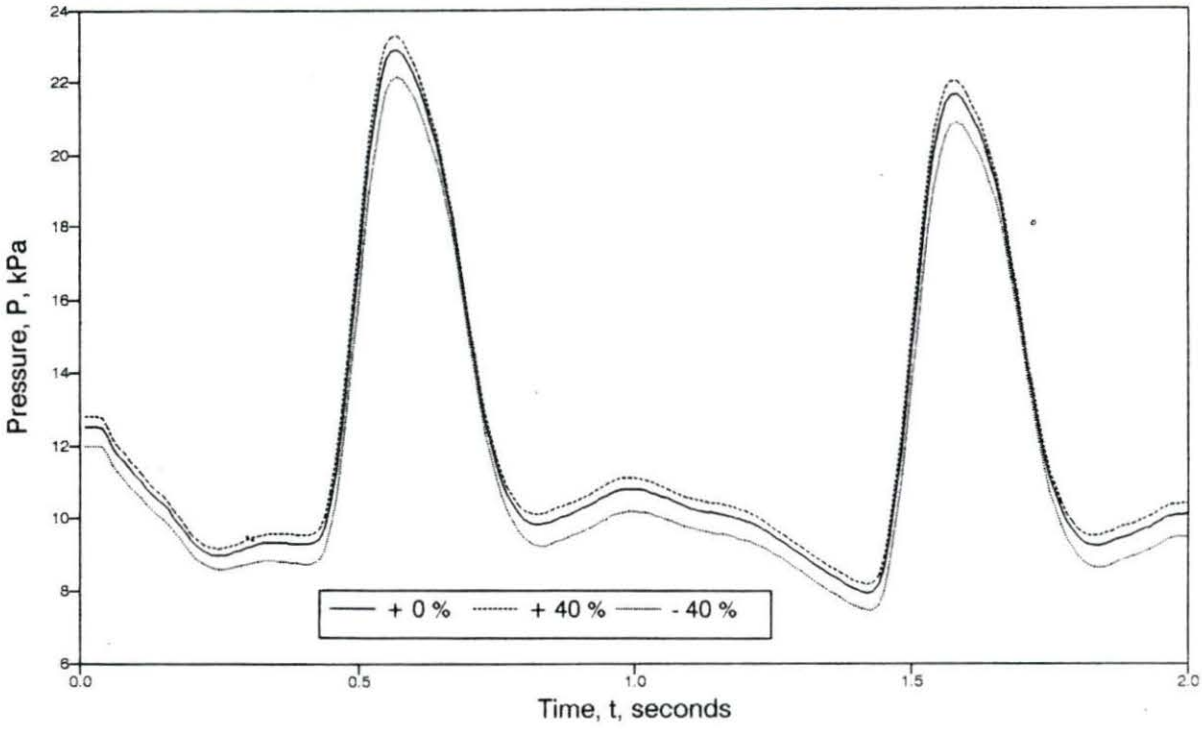

Figure 4.20: Pressure sensitivity to cerebral peripheral resistance in the femoral artery

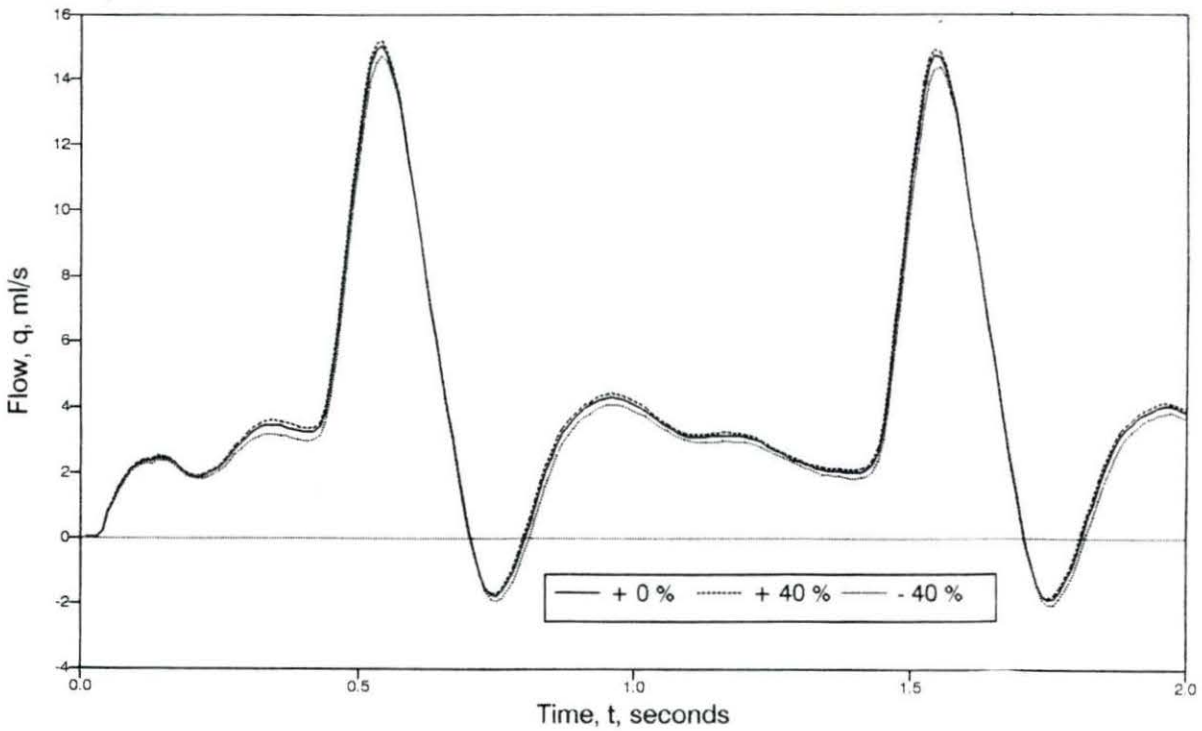

Figure 4.21: Flow sensitivity to cerebral peripheral resistance in the femoral artery

the external body force on the supine model. Pressures and flows are simply shifted downwards in proportion to the externally applied body force. Mean pressures and flows are shown in Table 4.5. It is easily seen that mean pressures and flows fall nearly linearly with external acceleration. Deviation from a linear curve becomes more pronounced as G-forces increase. This is primarily due to the fact that the model tends towards instability at higher Gs. As shown in Figure 4.22, mean aortic pressures on a per beat basis drop steadily in high $+G_z$ applications until a steady-state is reached in the fourth cycle. The supine case converges to a steady-state in two cycles. Mean pressures for the fourth cycle only, after all cases have converged to steady-state, fall nearly linearly. The values listed in Table 4.5 are mean pressures measured over the entire first four cycles, not just the fourth cycle. For low-G applications, steady-state convergence occurs within 2 beats but requires more cycles for higher G loads.

Table 4.5: Mean pressures and flows in the L. external carotid and femoral arteries with varying $+G_z$ acceleration

(4 Cycle avg.)	L. Ext. Carotid		Femoral	
$+G_z$	$\bar{P}$, kPa (mm Hg)	$\bar{q}$, $m\ell/s$	$\bar{P}$, kPa	$\bar{q}$, $m\ell/s$
0	12.27 (92)	0.854	11.14	3.793
1	6.739 (51)	0.422	16.77	6.871
2	1.246 (9)	-0.007	22.45	9.962
3	-4.136 (-31)	-0.430	28.23	13.09

For stability, a typical simulation requires a 40% reduction of the non-linear term in the p-A relationship (Equation 3.4) regardless of $+G_z$ (Stergiopulos, 1990). For +3 G_z, a 55% reduction of the non-linear term is required for stability. In addition, time steps in the numerical solving routine must be smaller for the solution to converge. The normal time step used in +0 G_z and +1 G_z cases is 10^{-3} seconds. For +2 G_z, the time step is reduced to 10^{-4} seconds. For +3 G_z, a time step of 10^{-5} seconds

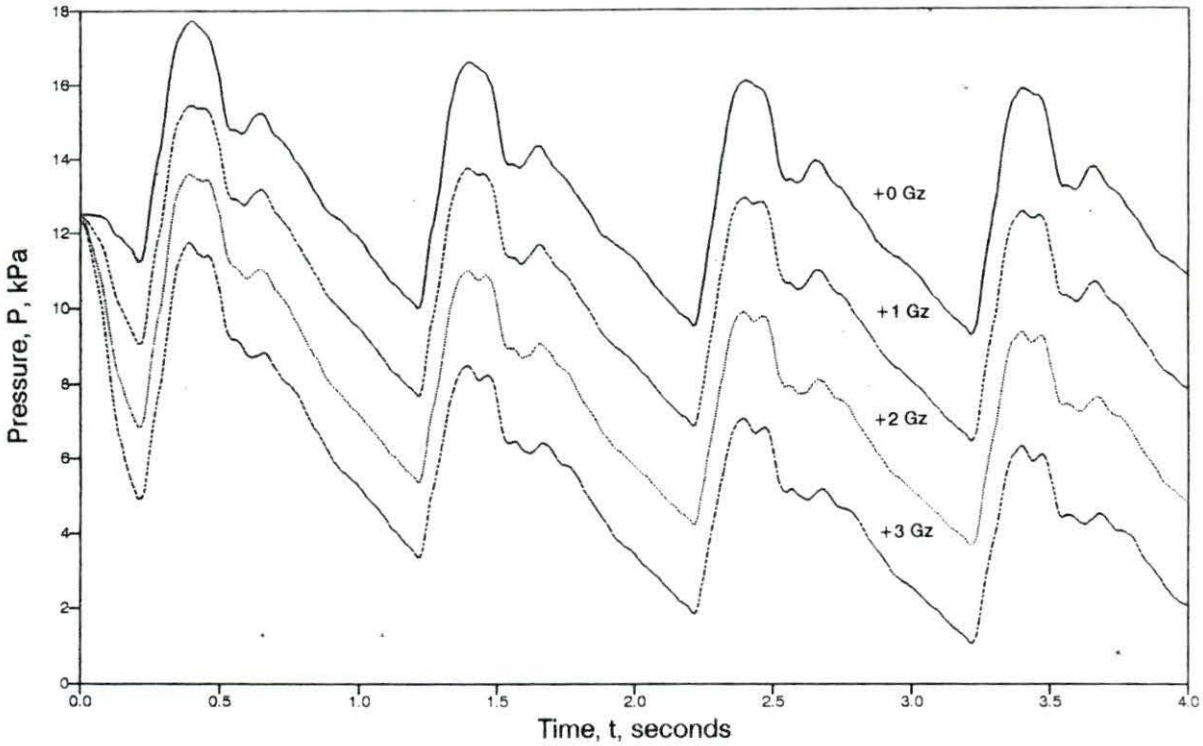

Figure 4.22: Effect of $+G_z$ acceleration on the pressure waveforms in the ascending aorta

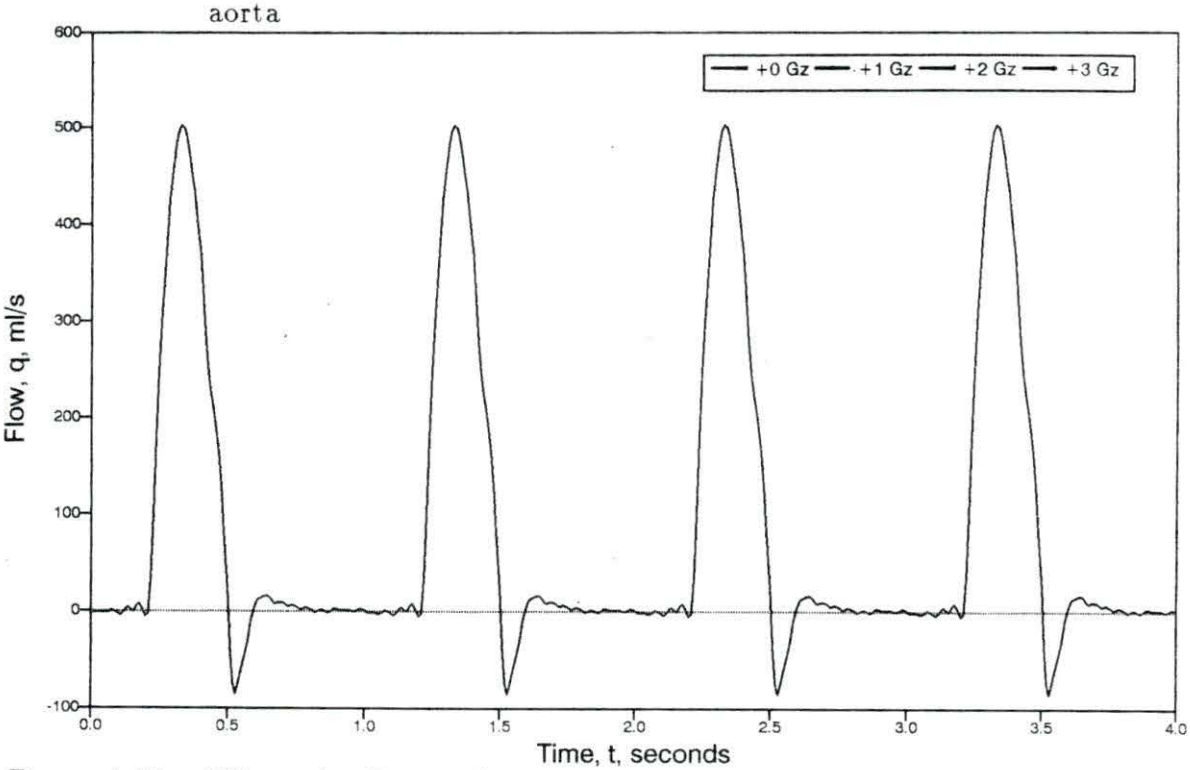

Figure 4.23: Effect of $+G_z$ acceleration on the flow waveforms in the ascending aorta (proximal boundary condition)

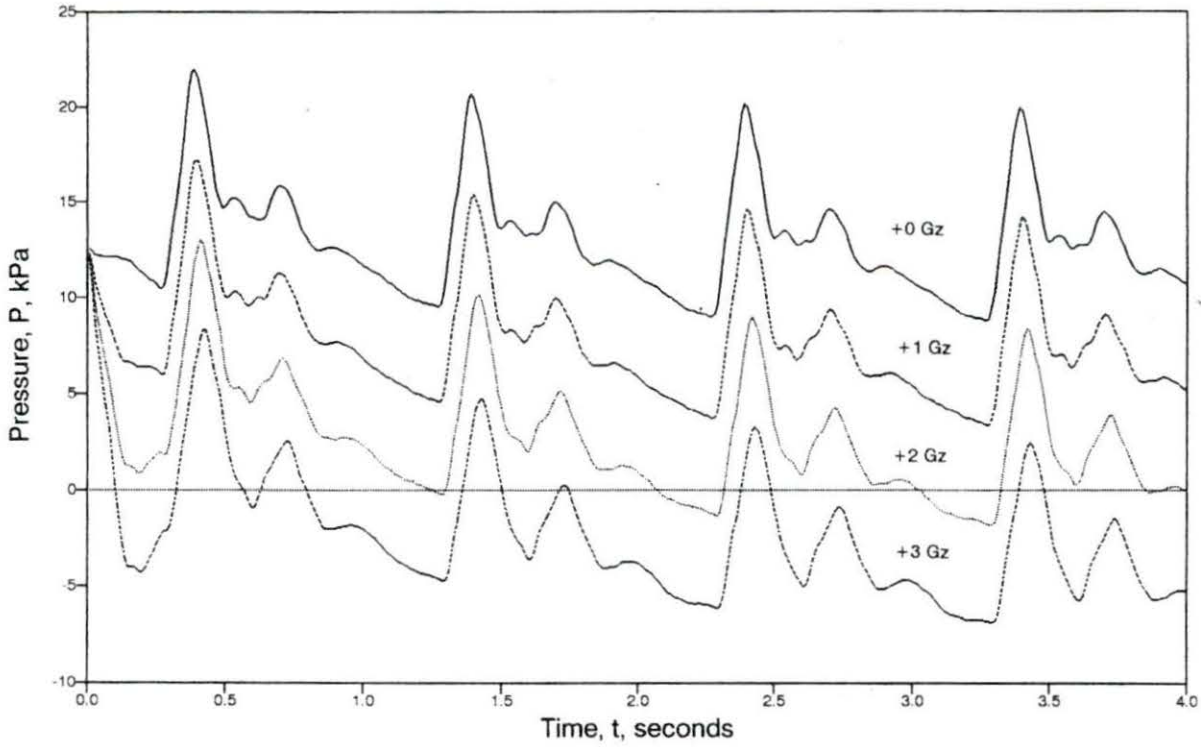

Figure 4.24: Effect of $+G_z$ acceleration on the pressure waveforms in the L. external carotid artery

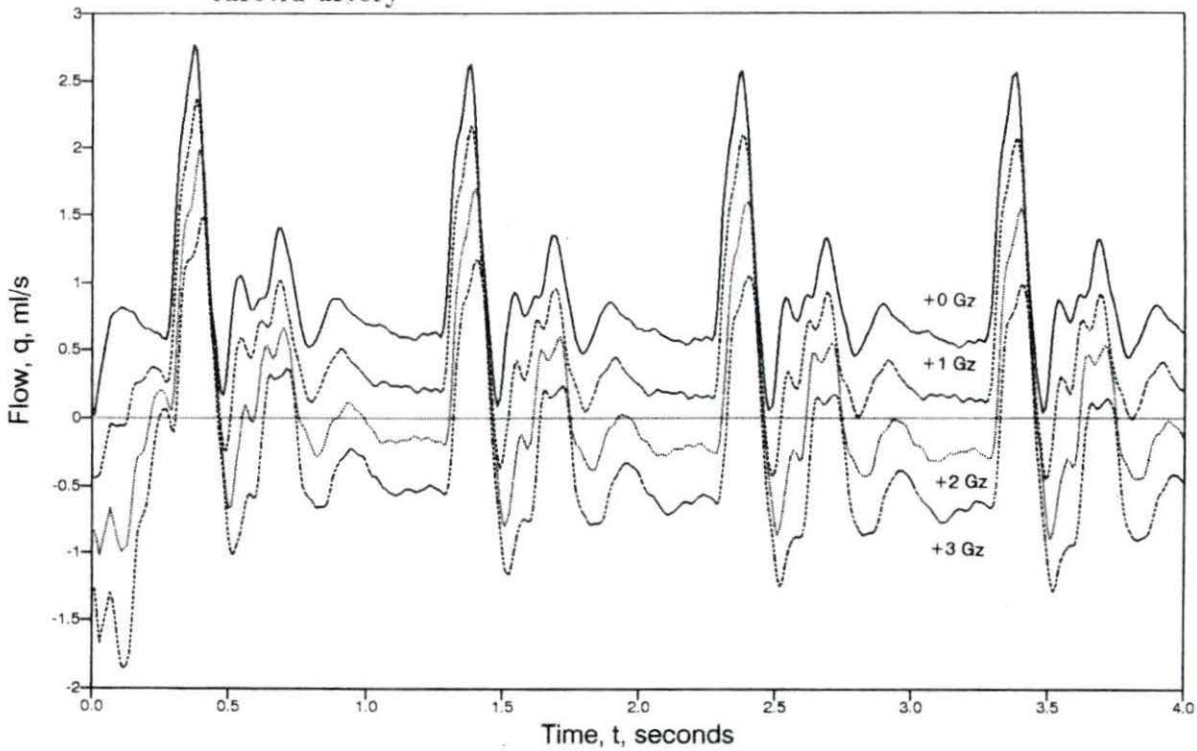

Figure 4.25: Effect of $+G_z$ acceleration on the flow waveforms in the L. external carotid artery

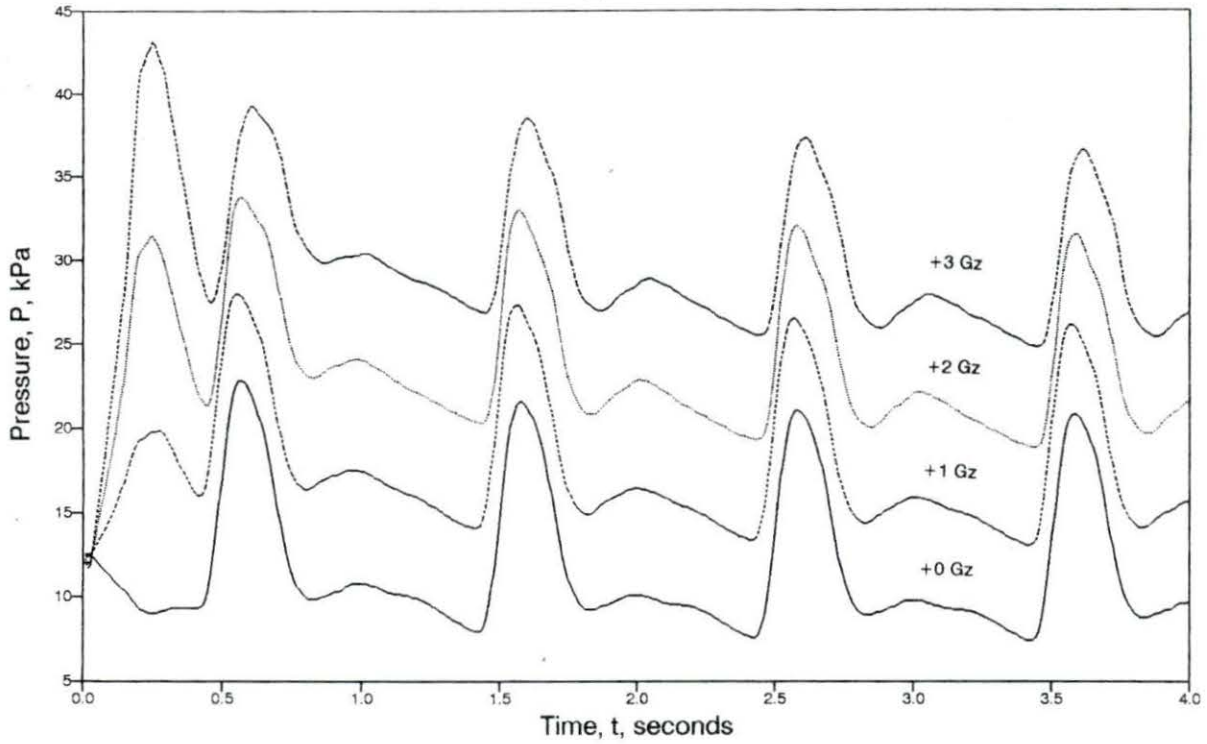

Figure 4.26: Effect of $+G_z$ acceleration on the pressure waveforms in the femoral artery

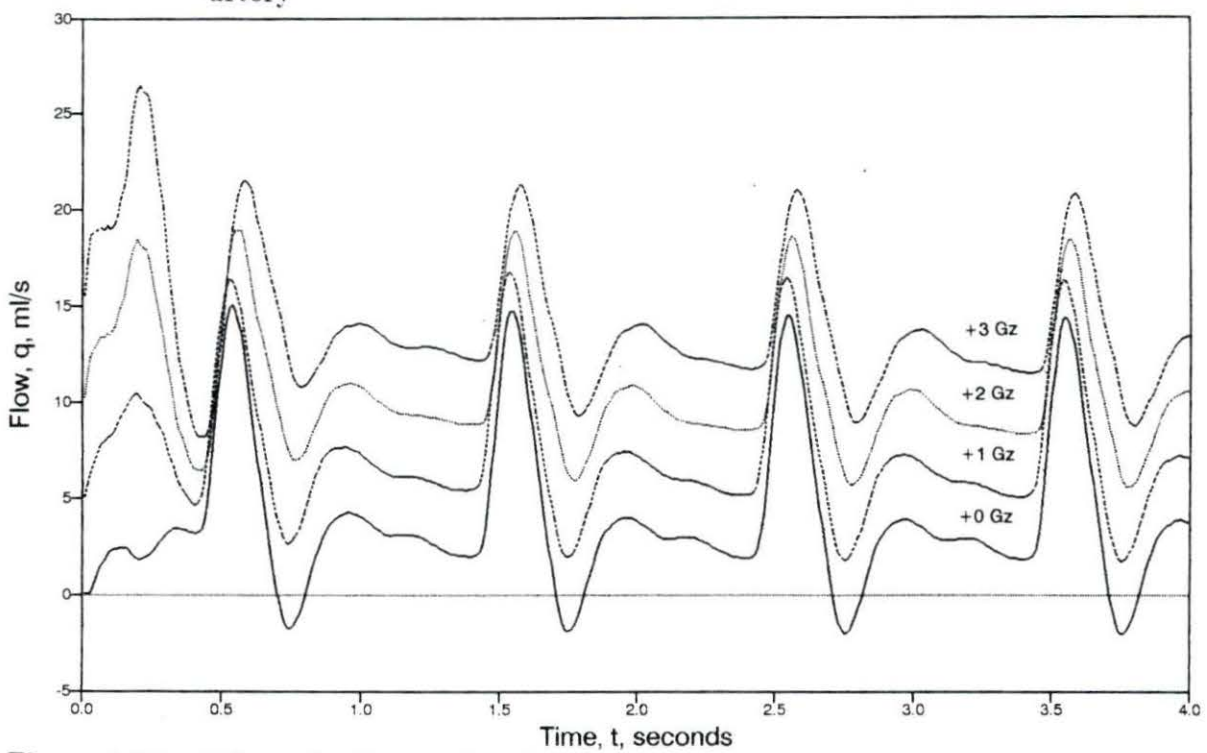

Figure 4.27: Effect of $+G_z$ acceleration on the flow waveforms in the femoral artery

is required. Increases in heart rates or peripheral resistance require the time steps to become even smaller and the non-linear reduction to become more pronounced. If all of the simulations were run at the time step and attenuation of the worst case (+3 G_z), pressure and flow drops are expected to be close to linear.

Burns et al. (1986) state that eye-level blood pressure drops off linearly at 25 mm Hg per G with flow cessation and PLL at 50 mm Hg. Without compensation, eye-level blood pressure in the model drops 41 mm Hg per G with flow cessation at a mean pressure of approximatly 10 mm Hg. Peak pressure at flow cessation, however, is 62 mm Hg, which better corresponds with experimental findings in the literature. Stergiopulos (1990) reports flow cessation at a systolic pressure of 5.8 kPa (44 mm Hg) with the same model. The discrepancy is because Stergiopulos probably assumed the model converged at two beats regardless of $+G_z$ loading. It has been found that for +2 G_z, convergence takes four cycles.

The hydrostatic indifference point for the human body should lie just at the proximal input point (just distal of the aortic valve). Figure 4.23 shows such occurance for the pressure waveforms. Aortic flow (Figure 4.24) does not change with $+G_z$ acceleration as it is the input boundary condition. If pressure is used as an input boundary condition, flow is expected to change with $+G_z$. Further study of this phenomena requires the addition of venous and cardiac dynamics to eliminate dependancy on the proximal input condition.

Even though the values do not exactly match those found in literature, the trend is identical. With physiological compensation added (Chapter 5), the model values should match those found in literature more closely.

CHAPTER 5. EFFECTS OF $+G_z$ ACCELERATION AND COMPENSATION

Supine versus Standing

Many physiological changes occur in man from the $+0$ G_z (supine) position to the $+1$ Gz (standing) position. These changes are time dependent, but develop rapidly. Since compensatory mechanisms in this model are not time dependent but are merely a change in an input parameter, only the steady-state, fully developed compensatory mechanisms will be considered.

According to the Standard Man data presented in Chapter Three, heart rate should increase 25% upon standing due to baroreflex as blood volume shifts caudally. A total of 350–400 $m\ell$ of blood will be lost to the capacitance vessels in the legs, reducing venous return and resulting in a stroke volume drop of 40%. These two factors lead to a net cardiac output drop of 25%. Peripheral resistance increases 25% to compensate. Cerebral autoregulation is not stated quantitativly, but one could assume only minor changes occur in cerebral vascular tone during $+1$ G_z.

Figures 5.1 and 5.2 show the results of incorporating compensatory mechanism values (heart rate, stroke volume, and peripheral resistance) found in the literature (labelled as "Lit. values" in the plots) on external carotid artery pressure and flow at $+1$ G_z. For comparision, the $+0$ G_z and $+1$ G_z control cases (control cases have no

changes from the +0 G_z supine case except for the body force term) are also plotted. Mean pressures and flows are shown in Table 5.1.

Burns et al. (1986) and Ganong (1989) show that mean carotid pressures and flow rates drop approximatly 31% and 20% respectively during $+G_z$. In the model, carotid flow is taken to be the critical factor and a measure of compensatory performance. A 20% drop in mean carotid flow (from 0.895 $m\ell/s$ in CONTROL 0) is therefore the target value.

Experimental Doppler ultrasound studies of the superficial temporal artery show retrograde flow does not occur until high sustained $+G_z$ acceleration. In addition to the mean flow requirement, a +1 G_z compensated model must not have any carotid artery retrograde flow.

Using the literature values for compensation, Table 5.1 shows an external carotid artery flow rate of 0.375 $m\ell/s$, far less than the the target flow rate of 0.716 $m\ell/s$. Retrograde eye-level flow is also present, as shown in Figure 5.1. Mean pressure is 45.8 mm Hg, which is below the critical Peripheral Light Loss pressure and below the minimum value for complete cerebral correction of the impaired flow. Since, in the absence of pathology, humans do not lose consciousness upon standing, further compensation within the model is needed.

A heart rate of 75 bpm is a reasonable average for a physically fit standing human. From the model sensitivity studies, increases in heart rate raise mean flow per unit time but do not significantly raise mean flow on a per beat basis. No retrograde characteristics are altered. Heart rate is therefore held constant but can be used to finely adjust the model. Stroke volume also cannot be changed because the literature values represent the venous dynamics of $+G_z$ loading that are not modelled and

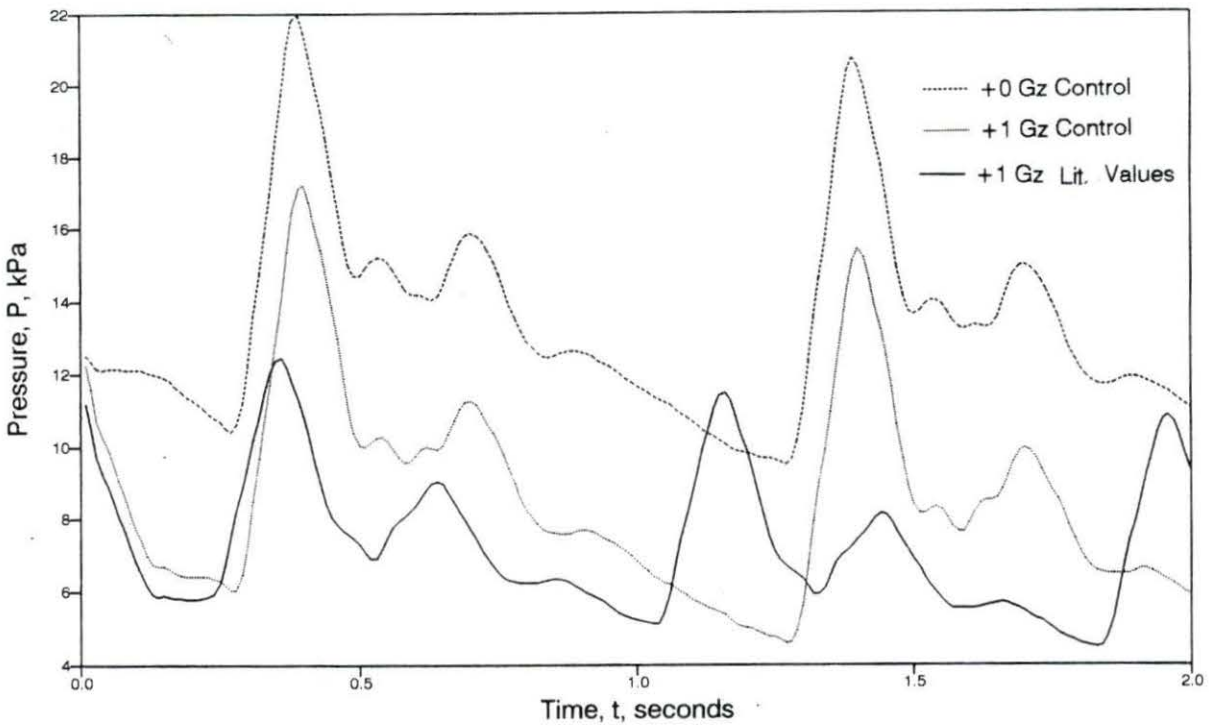

Figure 5.1: Effect of literature values of $+1$ G_z compensation on the pressure waveforms in the L. external carotid artery

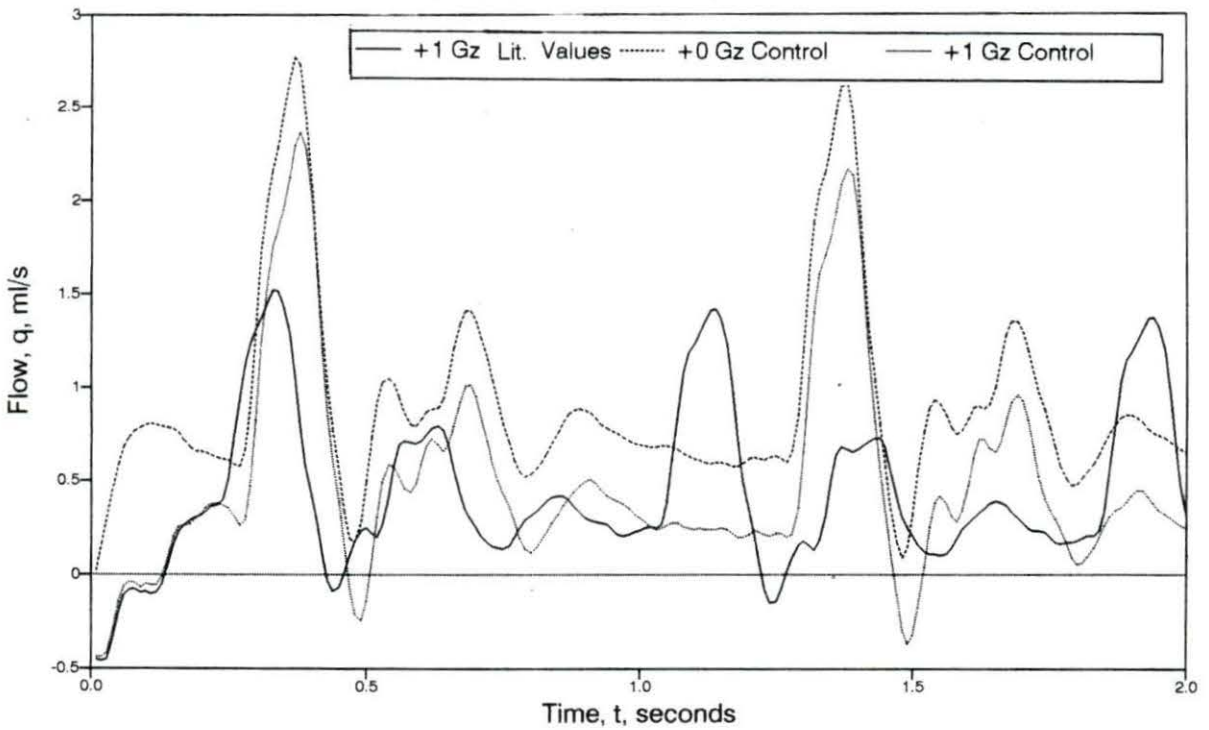

Figure 5.2: Effect of literature values of $+1$ G_z compensation on the flow waveforms in the L. external carotid artery

cannot be readily estimated within the scope of this study. What remains as the primary driving force for increasing eye-level flow is peripheral resistance.

An increase in systemic peripheral resistance of +55% is found to very nearly match the target parameter. A -30% change in cerebral resistance fine-tuned the model well. Figures 5.3 and 5.4 show the results of this model, labelled as "Full compensation" or "Model Compensation." Mean flow in the external carotid artery is 0.723 $m\ell$/s, only 1.0% above the target value. Mean external carotid pressure is 60.5 mm Hg, 7 mm Hg lower than predicted in literature. Aside from biological variations, the low carotid pressure would imply that the cerebral resistance does not change as much as the model suggests.

Table 5.1: Mean pressures and flows in the L. external carotid and femoral arteries during +1 G_z

(4 Cycle avg.)	L. Ext. Carotid		Femoral	
	$\bar{P}$, kPa (mm Hg)	$\bar{q}$, $m\ell$/s	$\bar{P}$, kPa	$\bar{q}$, $m\ell$/s
Control +1 G_z	6.739 (51)	0.422	16.77	6.871
Lit. Compensation	6.092 (46)	0.375	16.46	5.520
Model Compensation	8.043 (60)	0.723	18.63	5.032

Using a simple $\bar{q} = \frac{\bar{P}_a}{R_T}$ relationship, peripheral resistance for +0 G_z eye-level blood pressure and flow at 96 mm Hg and 0.895 $m\ell$/s, respectively (found in the CONTROL 0 model) is 107.3 (mm Hg-s)/$m\ell$. If mean pressure drops to 50 mm Hg (minimum pressure for cerebral autoregulation) and flow is assumed to be maintained by cerebral autoregulation, peripheral resistance must fall 48%.

Since cerebral resistance has been predicted to reach a maximum at -48%, a -30% change in cerebral resistance would be expected to be a bit high for +1 G_z acceleration, despite +G_z venous drainage helping to maintain perfusion pressure.

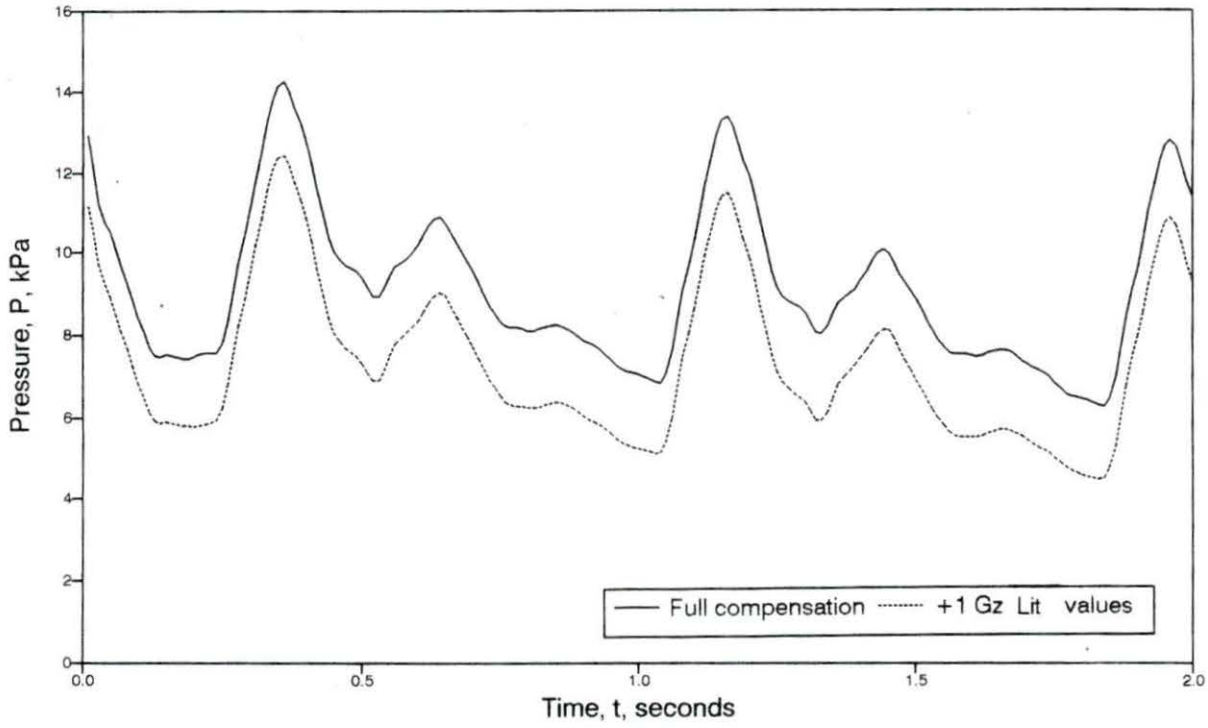

Figure 5.3: L. external carotid artery pressure waveforms in the +1 G_z fully compensated model

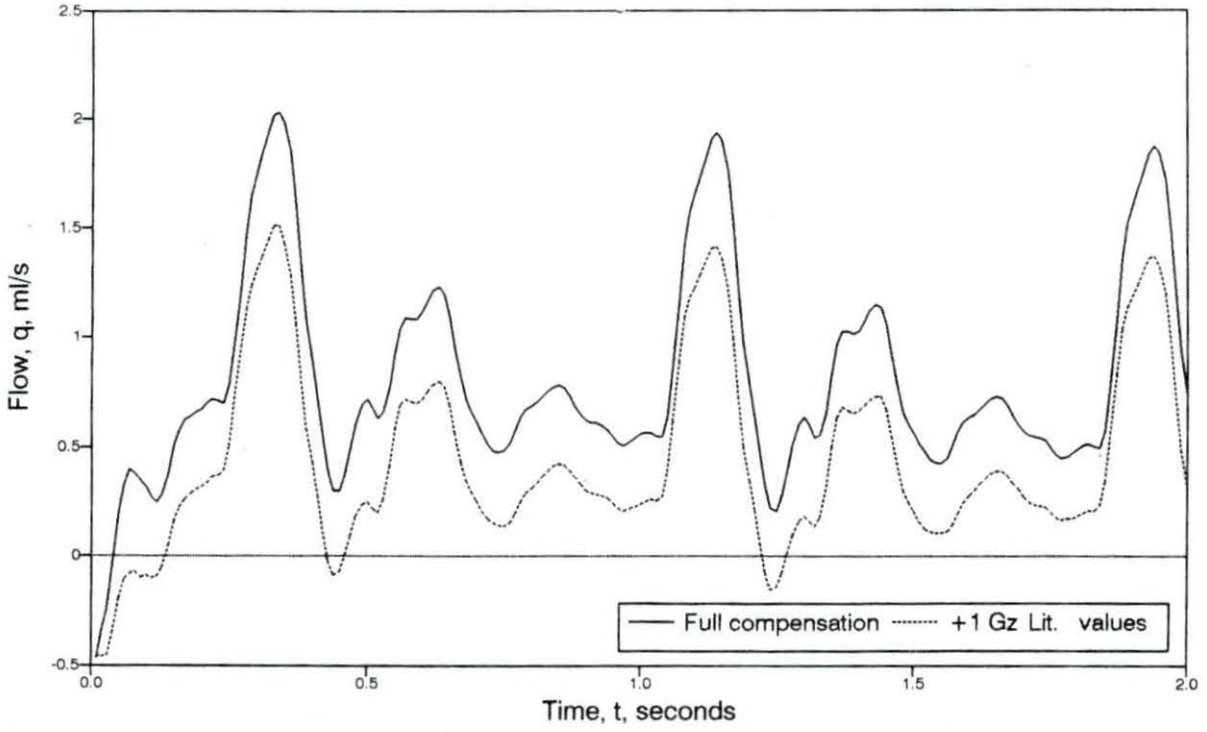

Figure 5.4: L. external carotid artery flow waveforms in the +1 G_z fully compensated model

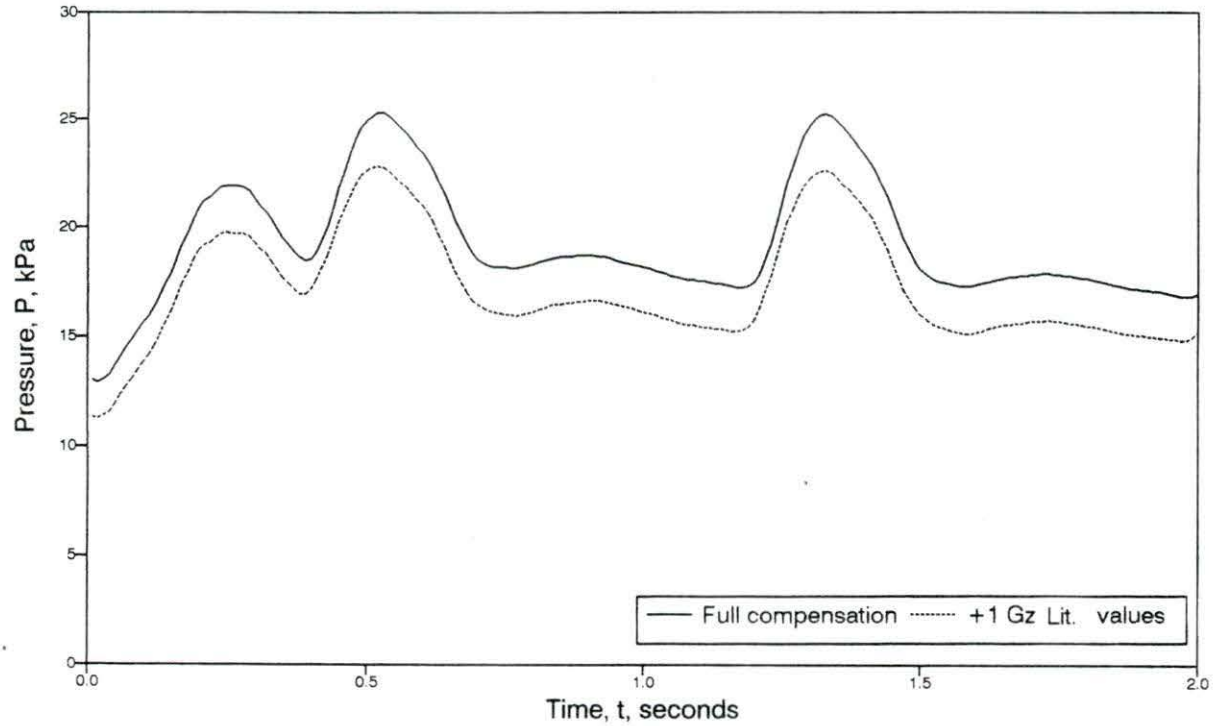

Figure 5.5: Femoral artery pressure waveforms in the +1 G_z fully compensated model

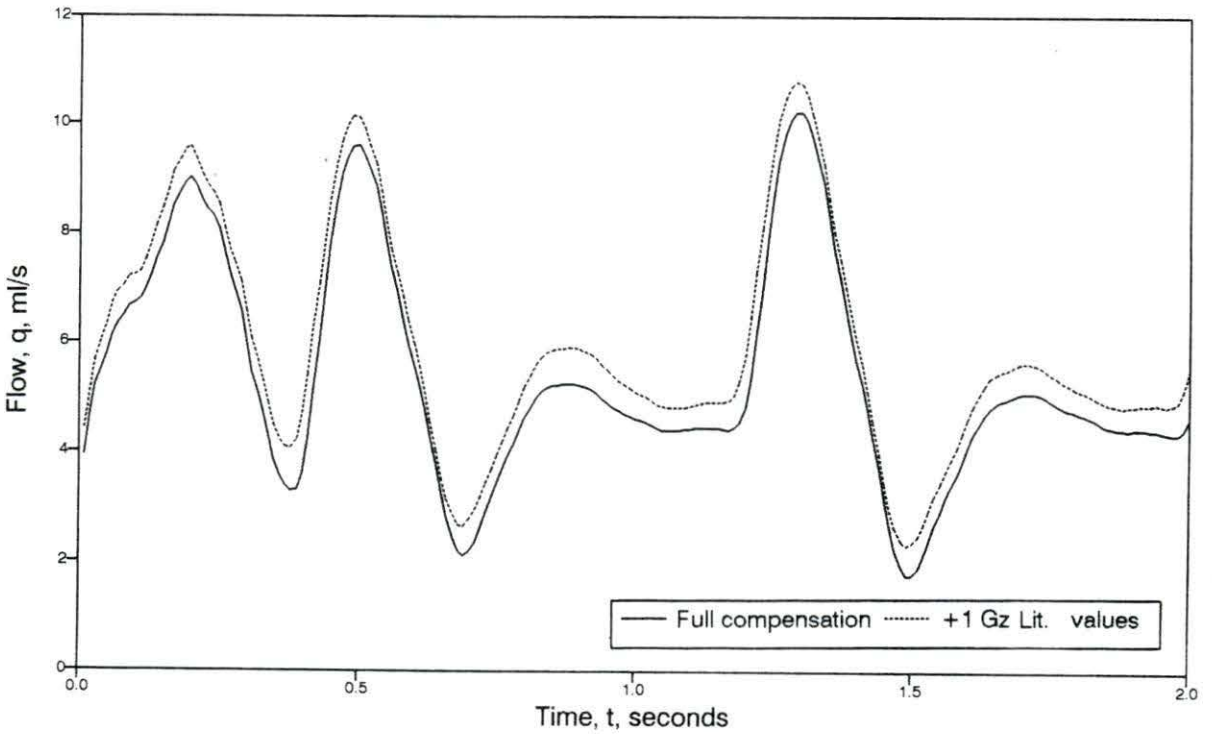

Figure 5.6: Femoral artery flow waveforms in the +1 G_z fully compensated model

A slight increase in systemic peripheral resistance would allow less cerebral autoregulation of cranial blood flow. Since reliable values for cerebral autoregulation do not exist, one particular pair of systemic and cerebral resistances that represent the most accurate solution cannot be found. However, this model is a reasonable solution to the problem.

In this model of the standing human, a peripheral resistance increase of 55% is much higher than the published +25%. However, some of the literature values for peripheral resistance are based on 70° tilt (30° from vertical) experiments on humans, not on fully standing humans. In centrifuge studies on dogs, total peripheral resistance was found to have an average maximum increase of +40% at +1 G_z (Peterson, 1975). In a recent study published after the conclusion of this study, Gotshall et al. (1991) measured average changes in peripheral resistance from +0 G_z to +1 G_z for men and women. While women tended to have the lower response, (+35% as compared to men with +75%) an average of +55% for the combination of the sexes can be calculated (n = 10 for each group), which is the same as in the model.

Pressures and flows for the femoral artery in the compensated +1 G_z case are shown in Figures 5.5 and 5.6. Note that the first cycle is very different than the second. This is an example of the estimation error of the program as discussed in Chapter Three. Peripheral resistance increases femoral pressure and reduces femoral flow, as predicted. However, pressures and flows are not as high as they would be without any compensation from +1 G_z acceleration body force.

Hyper-Gravity

Acceleration of +2 G_z

When the +0 G_z control case is run at +2 G_z (Figures 4.22 through 4.27), mean flow in the external carotid artery (Figure 4.25) is retrograde (negative) and near zero.

Experimental data from Wood (1987) show that at +2 G_z, stroke volume falls 24% from +1 G_z. This is a 54% reduction in flow from the supine position. Cardiac output falls 7% from standing (30% from supine). To compensate, heart rate increases 27% (58% from supine) and peripheral resistance increases 20% (+50% from supine).

Figures 5.7 and 5.8 show external carotid pressures and flows for the above parameters. For comparison, the uncompensated +2 G_z control case and the fully compensated +1 G_z case are also plotted. Mean external carotid flow from the literature value compensation model is 0.079 $m\ell/s$. Flow is no longer retrograde but is still 89% lower than the fully compensated +1 G_z model.

Burns et al. (1986) indicate that mean temporal pressure should be approximately 50 mm Hg during +2 G_z acceleration (-25 mm Hg/G). Since temporal pressure varies nearly linearly with G-loading (Burns et al., 1986), it is reasonable to assume that without any other changes, temporal flow will also fall linearly. Using mean flows from previous models, a linear flow drop of -0.179 $m\ell/s/G$ is assumed. Since supine flow is 0.895 $m\ell/s$, a target value of 0.537 $m\ell/s$ is established for +2 G_z. To determine if the solution is reasonable, Wood (1987) indicates ascending aortic pressure at +2 G_z should be 9% more than at +1 G_z. Here, a 9% increase in aortic pressure from +1 G_z model would be 88 mm Hg.

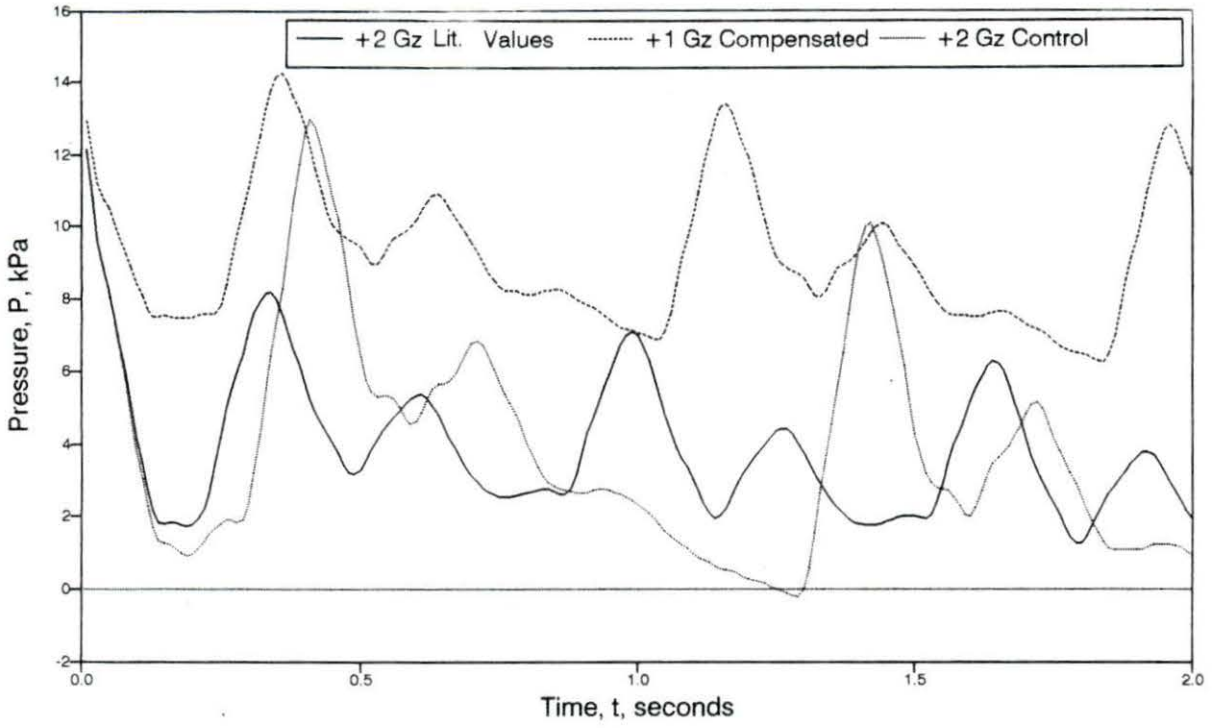

Figure 5.7: Effect of literature values of +2 G_z compensation on pressure waveforms in the L. external carotid artery

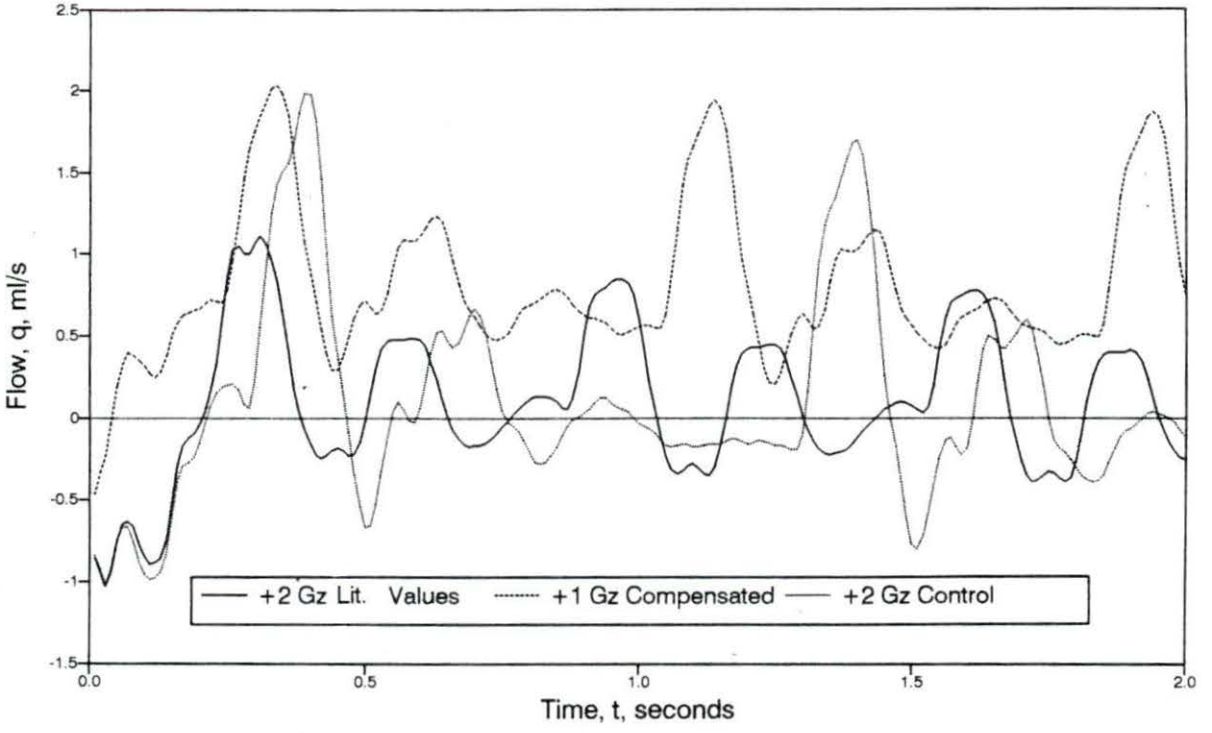

Figure 5.8: Effect of literature values of +2 G_z compensation on flow waveforms in the L. external carotid artery

Using +2 G_z values found in Wood (1987) for stroke volume (39.4 $m\ell$) and heart rate (92 bpm), the target external carotid artery flow rate is reached with a systemic peripheral resistance change of +120% from supine and a cerebral peripheral resistance change of -25% from supine. Under these conditions, mean external carotid flow is found to be 0.537 $m\ell/s$, matching the target value. Mean external carotid pressure is 54 mm Hg, slightly less than the literature indicates. Mean pressure in the ascending aorta is 93 mm Hg, slightly above the literature data. Figures 5.9 through 5.12 show the results for the external carotid and femoral arteries and mean pressures and flows shown in Table 5.2.

Table 5.2: L. external carotid artery pressure waveforms in the fully compensated +2 G_z model

(4 Cycle avg.)	L. Ext. Carotid		Femoral	
	$\bar{P}$, kPa (mm Hg)	$\bar{q}$, $m\ell/s$	$\bar{P}$, kPa	$\bar{q}$, $m\ell/s$
Control +2 G_z	1.246 (9)	-0.007	22.45	9.962
Lit. Compensation	2.549 (19)	0.079	24.32	7.308
Model Compensation	6.746 (51)	0.530	29.00	6.026

From the peripheral resistance curve in Howard (1965) (Figure 2.8), peripheral resistance should increase nearly linearly with +G_z accelerations greater than +1 G_z. From the Standard Man data presented in Chapter Three, systemic peripheral resistance doubled as G-loading increased from +1 G_z to +2 G_z. Since a peripheral resistance change of +55% found by the +1 G_z model has been found to be reasonable, a +120% change in peripheral resistance from +0 G_z to +2 G_z becomes reasonable. Canine data (presented in Chapter Three) show systemic peripheral resistance changing +82% as G-loading increases from +0 G_z to +2 G_z, double that of a +0 G_z to +1 G_z change of +40%. If one takes into consideration that the canine

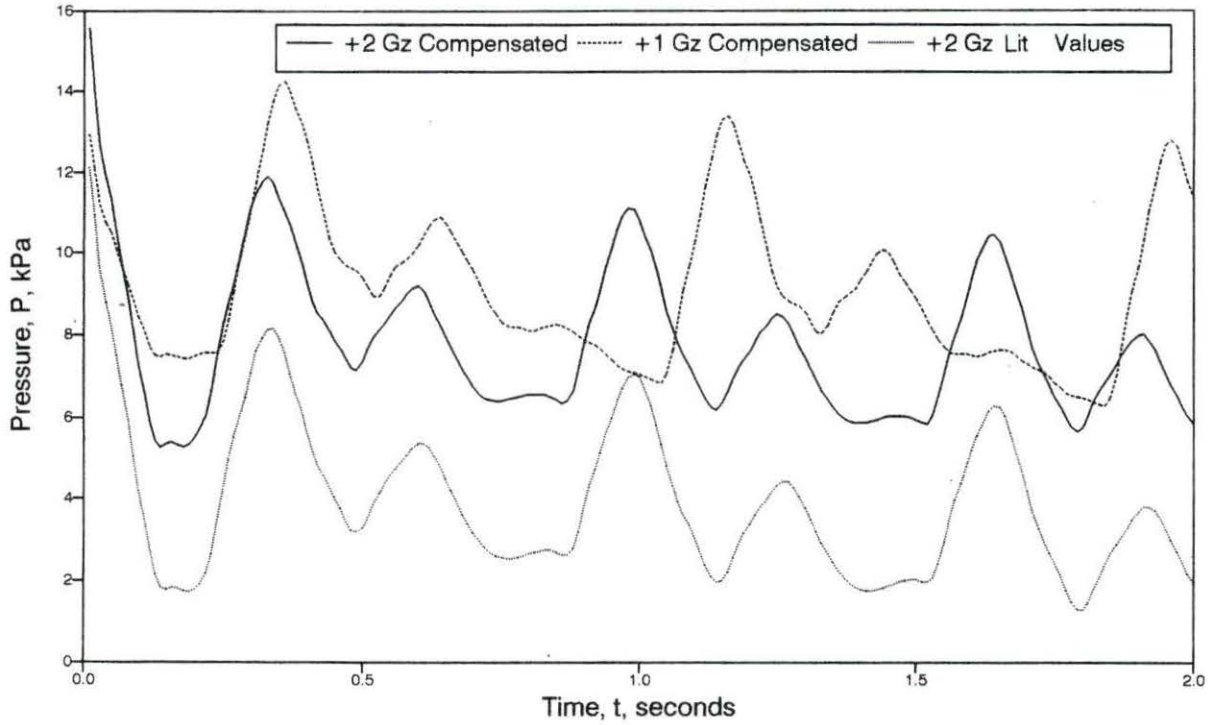

Figure 5.9: L. external carotid artery pressure waveforms in the +2 G_z fully compensated model

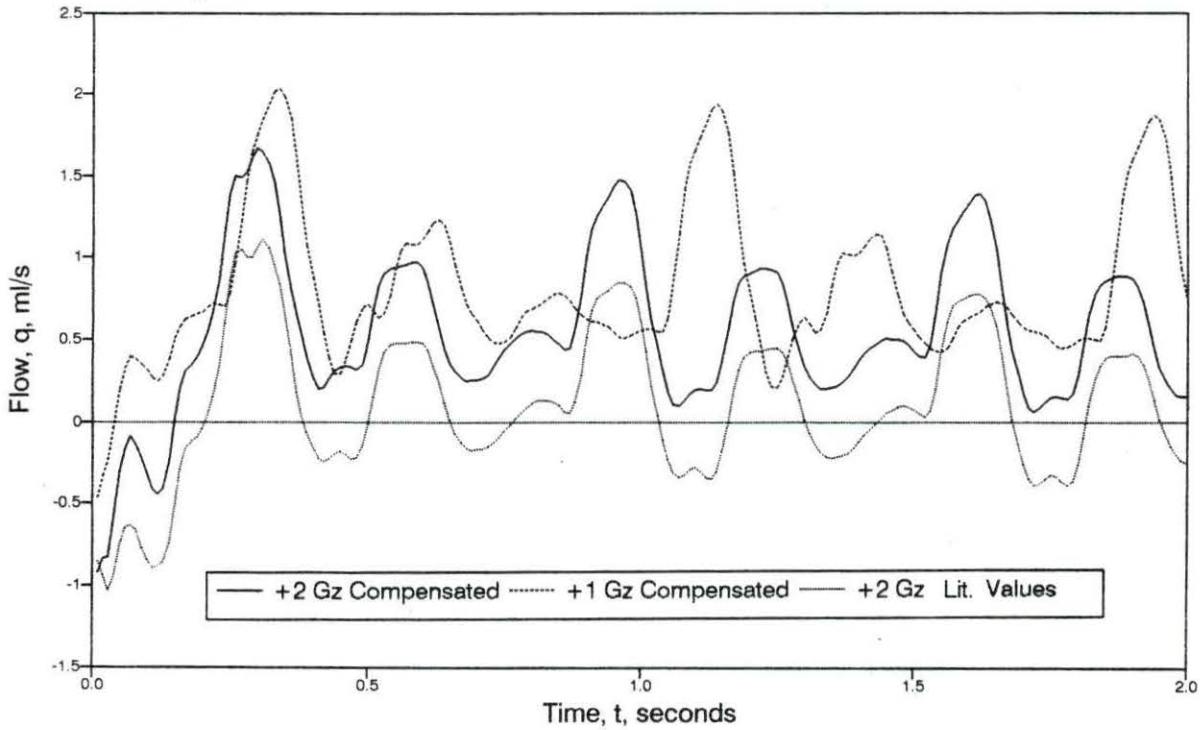

Figure 5.10: L. external carotid artery flow waveforms in the +2 G_z fully compensated model

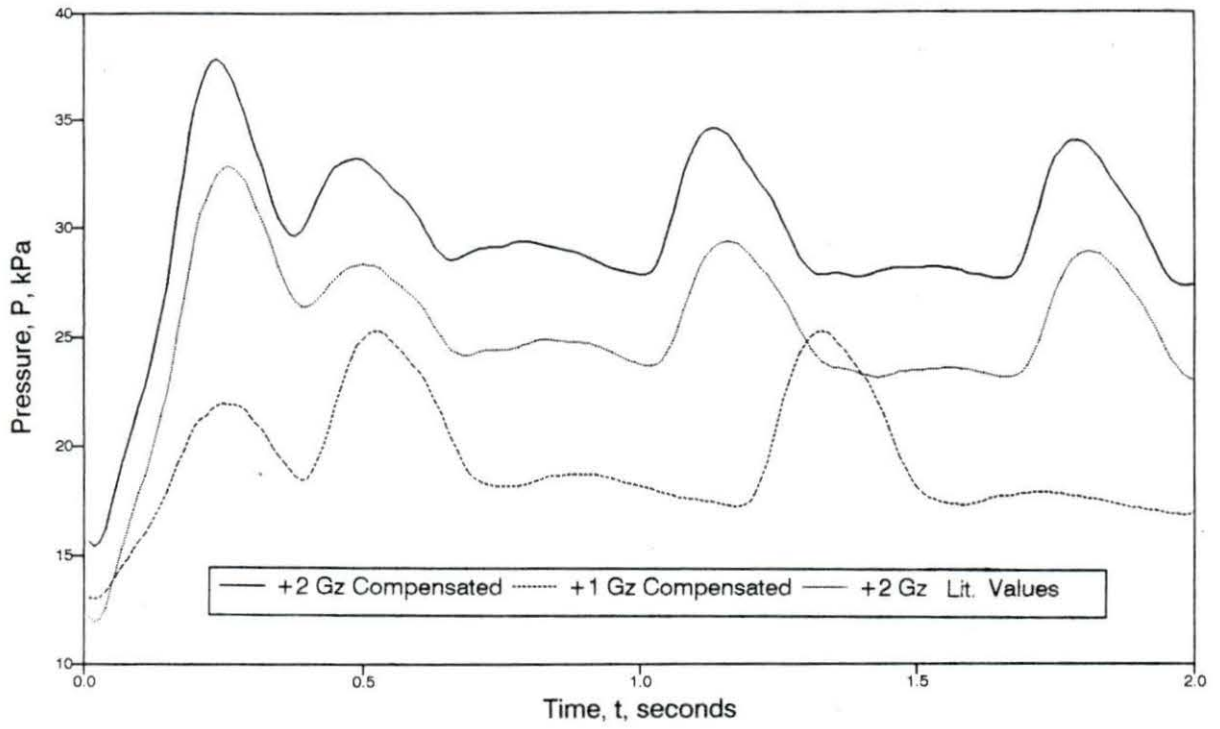

Figure 5.11: Femoral artery pressure waveforms in the +2 G_z fully compensated model

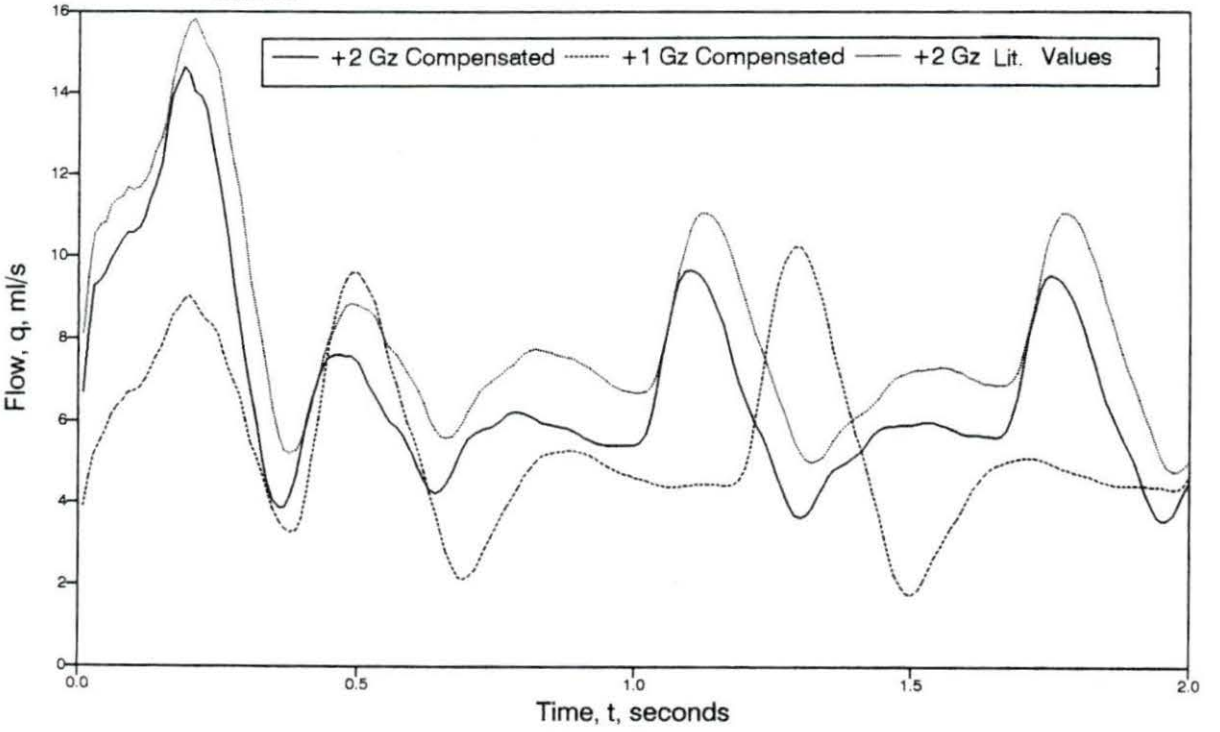

Figure 5.12: Femoral artery flow waveforms in the +2 G_z fully compensated model

hindlimb has a lower percentage of total volume than a human leg, one could assume a smaller blood volume will pool in the canine legs. Therefore, the canine does not need as much of a peripheral resistance change to withstand $+G_z$ acceleration as does man. Since canine peripheral resistance increases +82% at +2 G_z, a +120% peripheral resistance change in man seems reasonable.

Accelerations of +3 G_z

Gravitational accelerations greater than +2 G_z are not easily studied in this model, especially when compensation is involved. In order to keep the model solution from going unstable, time steps become very small, leading to high CPU usage and long execution times. In addition, the non-linear terms in the p-A relationship must be reduced to keep a stable solution. While elimination of the non-linear p-A terms does not greatly affect the pressure and flow waveforms (Stergiopulos, 1990), mean pressures and flows at +3 G_z should not be compared to those having different reductions of the non-linear term since the p-A relationship has been altered.

While a fully compensated +3 G_z model has not been developed, Table 5.3 shows the results of using the Standard Man data from Chapter Three as input parameters. Mean external carotid flow is -0.240 $m\ell/s$ with a mean pressure of -10 mm Hg. Since findings by Burton et al. (1974) and others state that man can withstand +3 G_z without support, additional peripheral resistance changes are clearly necessary, but cannot be simulated due to the instability of the program. It is expected that systemic peripheral resistance would be approximatly +190% from supine based on the previous models.

Table 5.3: L. external carotid artery pressure waveforms in the +3 G_z model

(4 Cycle avg.)	L. Ext. Carotid		Femoral	
	$\bar{P}$, kPa (mm Hg)	$\bar{q}$, $m\ell/s$	$\bar{P}$, kPa	$\bar{q}$, $m\ell/s$
Control +3 G_z	-4.136 (-31)	-0.430	28.23	13.09
Lit. Compensation	-1.338 (10)	-0.240	32.10	8.39

Effects of Anti-G Suits

Literature data presented in Chapter Three show many physiological changes occuring during G-suit inflation. Because G-suits apply external pressure to the legs and abdomen, blood pooled in the legs is forced into the thoracic cavity, improving venous return and increasing stroke volume. For a 2 psi inflation, stroke volume increases 23% from the standing (+1 G_z) stroke volume. Cardiac output is found to increase 32% from standing without any change in heart rate. Mean arterial blood pressure increases 9% from standing. In the model, a 23% increase in stroke volume without any change in heart rate is a 23% rise in cardiac output.

Experiments by Seaworth et al. (1985) show peripheral resistance decreasing 18% after 1 minute of G-suit inflation in a standing man. Ganong (1989) states peripheral resistance falls 25%. Yet, Burton (1974), Burns (1986), and other acceleration physiologists show an increase in peripheral resistance upon inflation. The difference likely lies in the system over which the measurements were taken.

If the 32% rise in cardiac output and the 9% rise in mean arterial blood pressure are substituted into Equation 2.1 , peripheral resistance for the entire system drops 11%. Locally, an external pressure of 2 psi (approx. 104 mm Hg) will collapse small arteries and vascular beds, decreasing flow and increasing peripheral resistance.

The first model run to study the effects of a G-suit used literature values as

they were listed: stroke volume up 23%, no change in heart rate, and all terminal resistances except those in the cranium were reduced 18%. All changes were done to the +1 G_z fully compensated model. The premise behind using these values was to allow the compensatory mechanisms to act as though the body was in the supine state due to the G-suit action.

The second run used a 23% increase in stroke volume but left the terminal resistances at the +1 G_z state (no changes from +1 G_z to +2 G_z. In effect, the G-suit was only allowed to act on the venous system in the legs and not the arterial system, by only preventing blood pooling in the legs but not increasing mean arterial pressure.

Finally, the computer model was developed in a unique way to model a totally occlusive G-suit. A 97% stenosis (maximum occlusion before model instability) was placed in the abdominal aorta (segment #39). No changes were made in the stroke volume from the +1 G_z case to study only the effect of the occlusion.

The resulting waveforms for all three runs observed in the carotid and femoral arteries and the aorta are shown in Figures 5.13 through 5.18. For the G-suit to afford 1 G of protection, mean pressures and flows during +1 G_z with an inflated G-suit should match the conditions found in the supine position. For this comparision, the +0 G_z pressure and flow waveforms are plotted.

Pressure and flow waveforms in the L. external carotid artery (Figures 5.15 – 5.16) in the first run (literature value models for compensation) are virtually identical to those in the +1 G_z compensated model. The conclusion that can be drawn is that the increase in stroke volume upon G-suit inflation allows terminal resistances (vascular tone) to decrease and still maintain +1 G_z homeostasis.

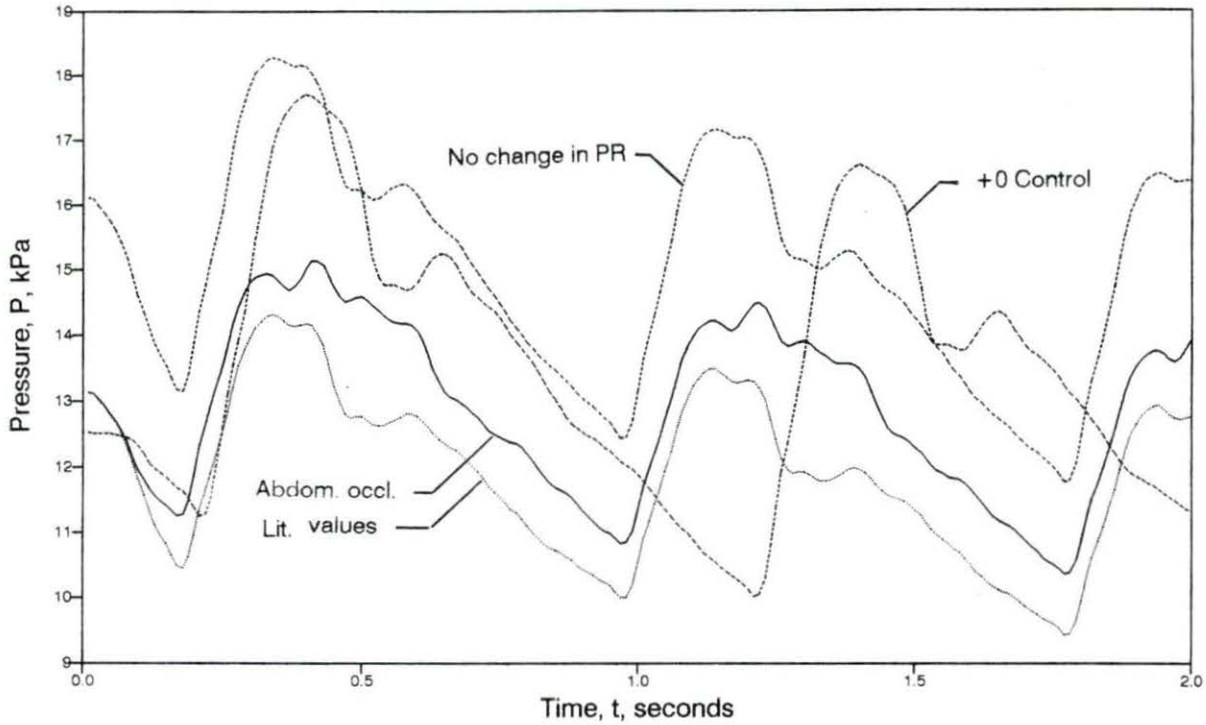

Figure 5.13: Effect of 2 psi inflation of a five bladder G-suit and a 97% abdominal occlusion on pressure waveforms in the ascending aorta at $+1\ G_z$

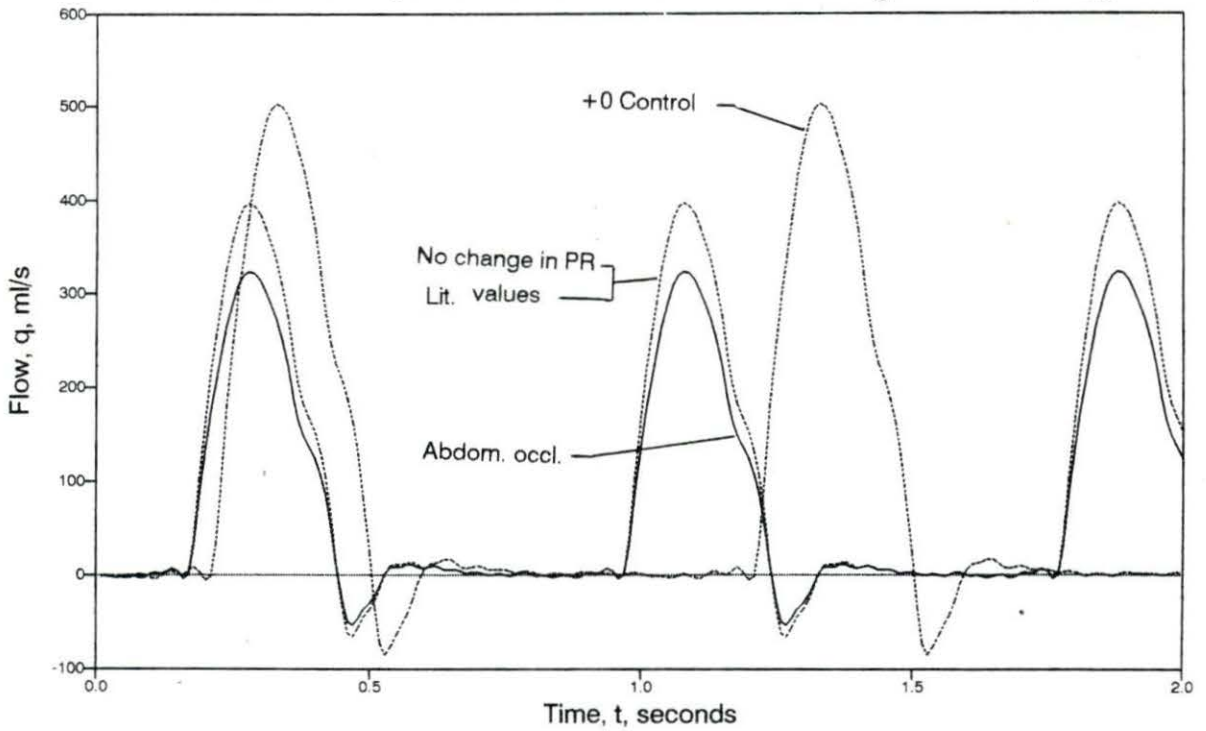

Figure 5.14: Effect of 2 psi inflation of a five bladder G-suit and a 97% abdominal occlusion on flow waveforms in the ascending aorta at $+1\ G_z$

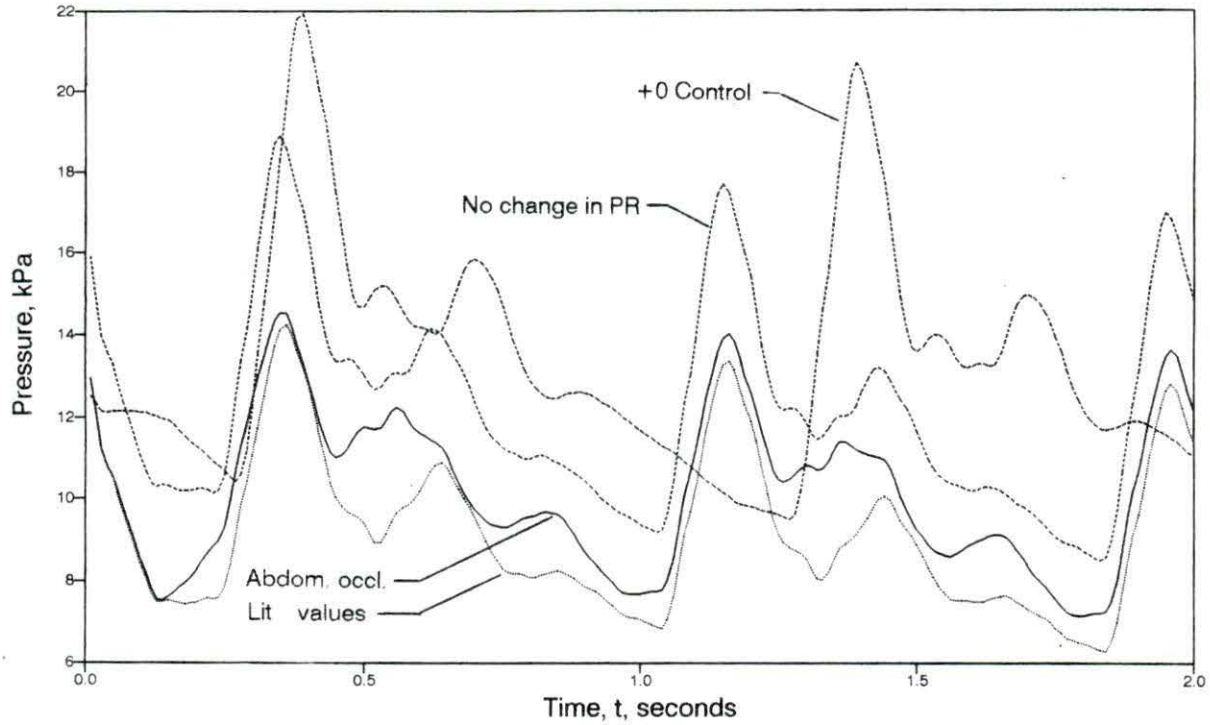

Figure 5.15: Effect of 2 psi inflation of a five bladder G-suit and a 97% abdominal occlusion on pressure waveforms in the L. external carotid artery at +1 G_z

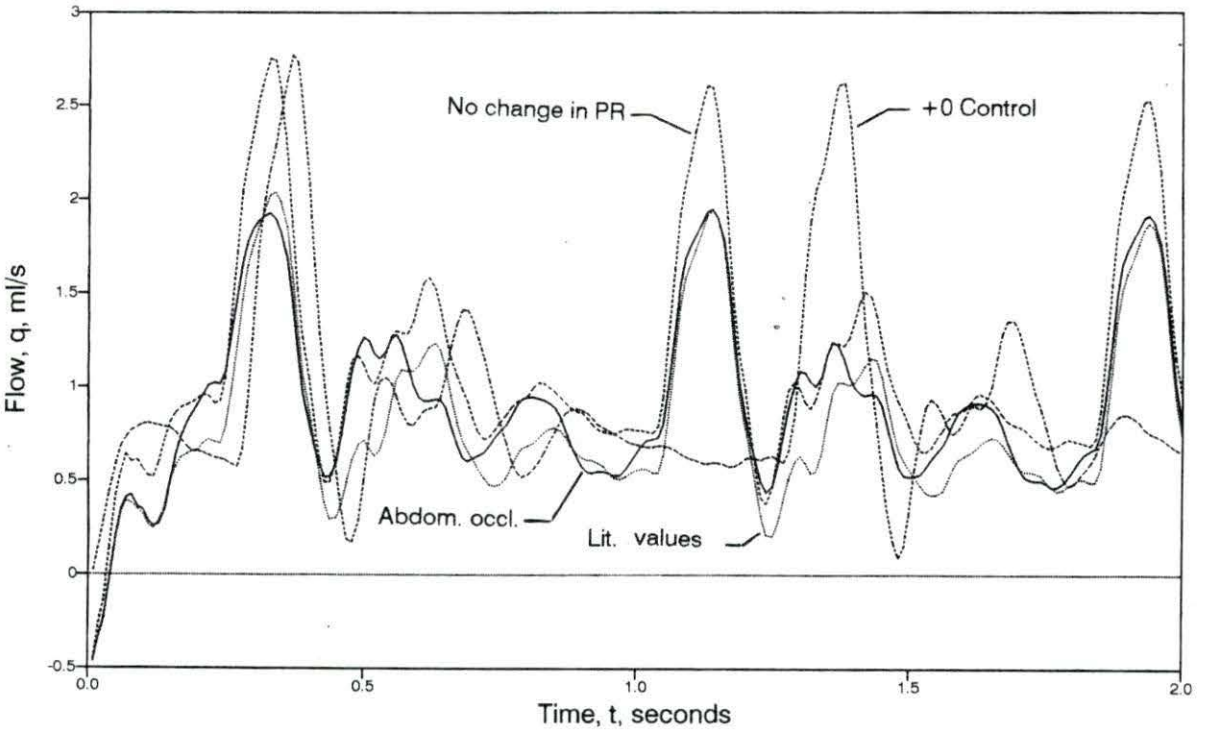

Figure 5.16: Effect of 2 psi inflation of a five bladder G-suit and a 97% abdominal occlusion on flow waveforms in the L. external carotid artery at +1 G_z

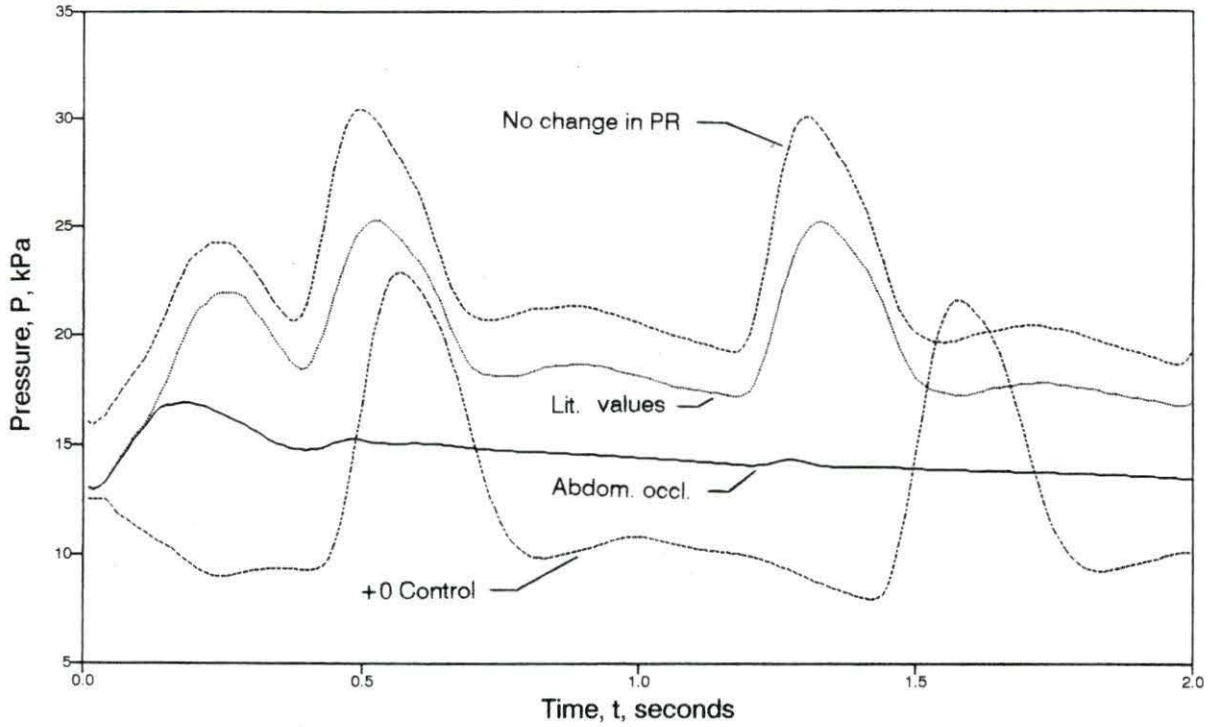

Figure 5.17: Effect of 2 psi inflation of a five bladder G-suit and a 97% abdominal occlusion on pressure waveforms in the femoral artery at +1 G_z

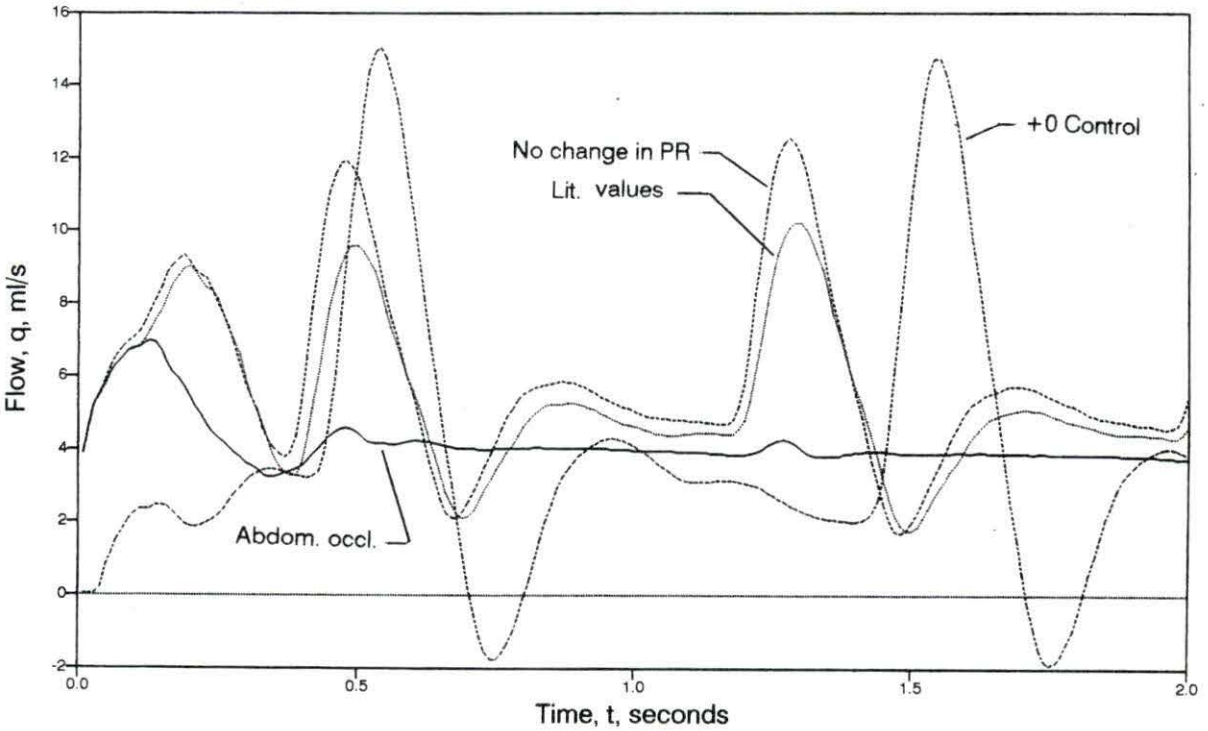

Figure 5.18: Effect of 2 psi inflation of a five bladder G-suit and a 97% abdominal occlusion on flow waveforms in the femoral artery at +1 G_z

Raising terminal resistances further by external pressure could only improve the situation. The second run shows flow rates in the L. external carotid artery to be similar to the supine case on a per beat basis. Since the heart rate is higher in the standing man, the mean flow per unit time is higher. The G-suit effect of raising local peripheral resistance allows the heart rate to return to the supine condition and still maintain +1 G_z homeostasis. Ganong (1989) shows that a G-suit inflated on a standing man does in fact allow response mechanisms to return to the supine state while maintaining cerebral perfusion.

The occlusion of the abdominal aorta raised pressures and flows above the levels found by the literature value model, which had a rise in stroke volume. An occlusion causes a pressure drop proportional to the flow. A dampening out the pulsatile nature of the waveforms distal to the occlusion is shown in Figures 5.17 – 5.18. In comparison to the supine case, flow in the femoral artery during G-suit inflation is slightly higher than the mean flow during the supine condition. A complete model of such a suit would require a qualitative determination of the increase in stroke volume during inflation. The occlusive suit already outperforms the purely resistive suit but it can be easily seen, however, that any increase in stroke volume (as is suggested in the literature) will only improve the overall performance of the occlusive suit. The model suggests that an occlusive-type G-suit affords the best protection against G-LOC, which is in agreement with Wood (1987).

The above G-suit simulations assume complete coverage of the legs and abdomen. In actuality, the suit has borders around the ankles, knees, buttocks, and genitalia. With an improved model geometry, the pressures and flows around these areas could be studied.

While a G-suit cannot be accurately modelled because of the relative lack of physiological information, the results of this study are consistent with the known effects of G-suits (for which there is a wealth of data).

Effects of Stenosis

One of the common phenomena of aging is the buildup of arterial plaque in the region of the carotid bifurcation. It is well documented that stenotic buildup does not drastically affect arterial flow until approximately 80% of the vessel lumen is occluded (Young, 1979). Changes is the peripheral resistance in microvascular beds distal to the stenosis can permit normal blood flow up to about 90% occlusion of the lumen.

No experimental work or computer simulations have been done to study the effect of carotid stenosis on the head-level arterial pressures and flows during $+G_z$ acceleration. Experimental work done by Young and Tsai (1973b) on pulsatile flow through a stenosis model indicates the pressure drop across a stenosis is a function of flow and stenosis geometry. It is expected that as flow decreases in the carotid artery with $+G_z$ acceleration, the pressure drop across a stenosis will become less pronounced.

To keep consistant peripheral resistances, the control case input data files for $+0$ G_z to $+2$ G_z were modified to include a concentric, blunt stenosis in the right carotid artery just proximal to the carotid bifurcation. The length of the stenosis is 1.5 cm, beginning 4.55 cm from the proximal node in segment #15. Figures 5.19 and 5.20 show eye-level mean pressures and flows in the external carotid artery as a function of percent occlusion and $+G_z$ acceleration.

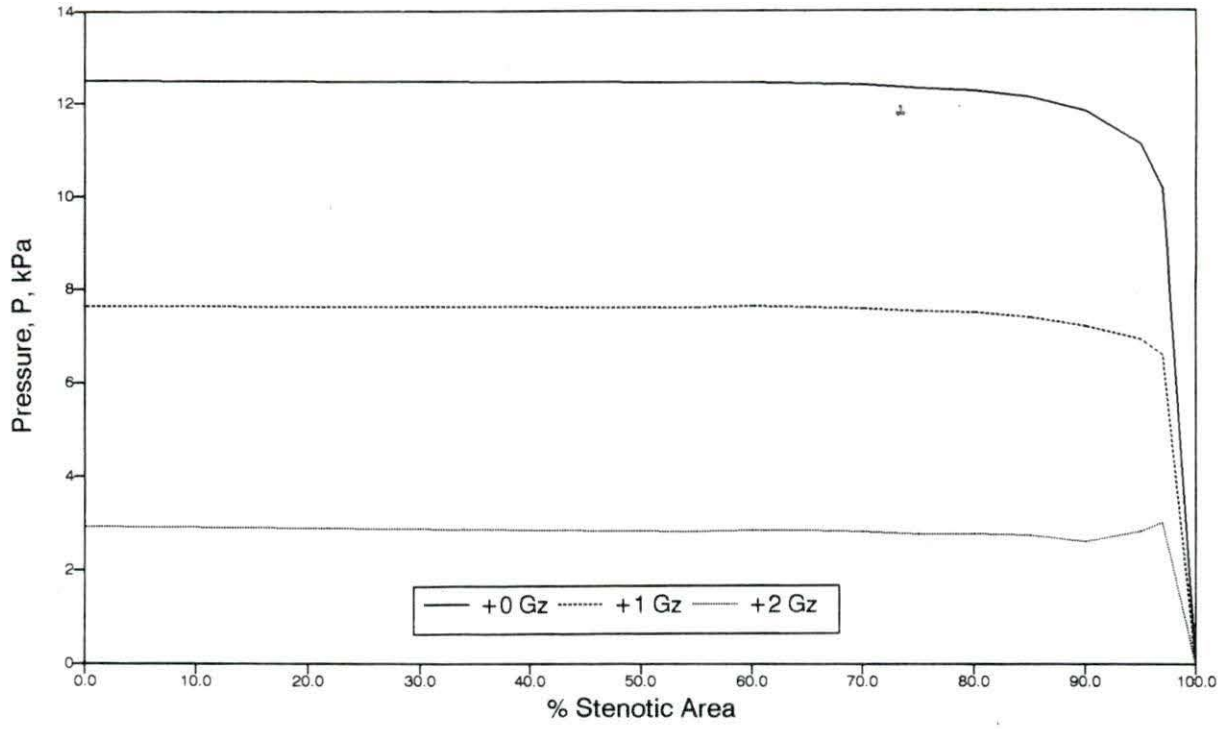

Figure 5.19: Mean pressures in the L. external carotid artery versus percentage stenosis and $+G_z$ acceleration

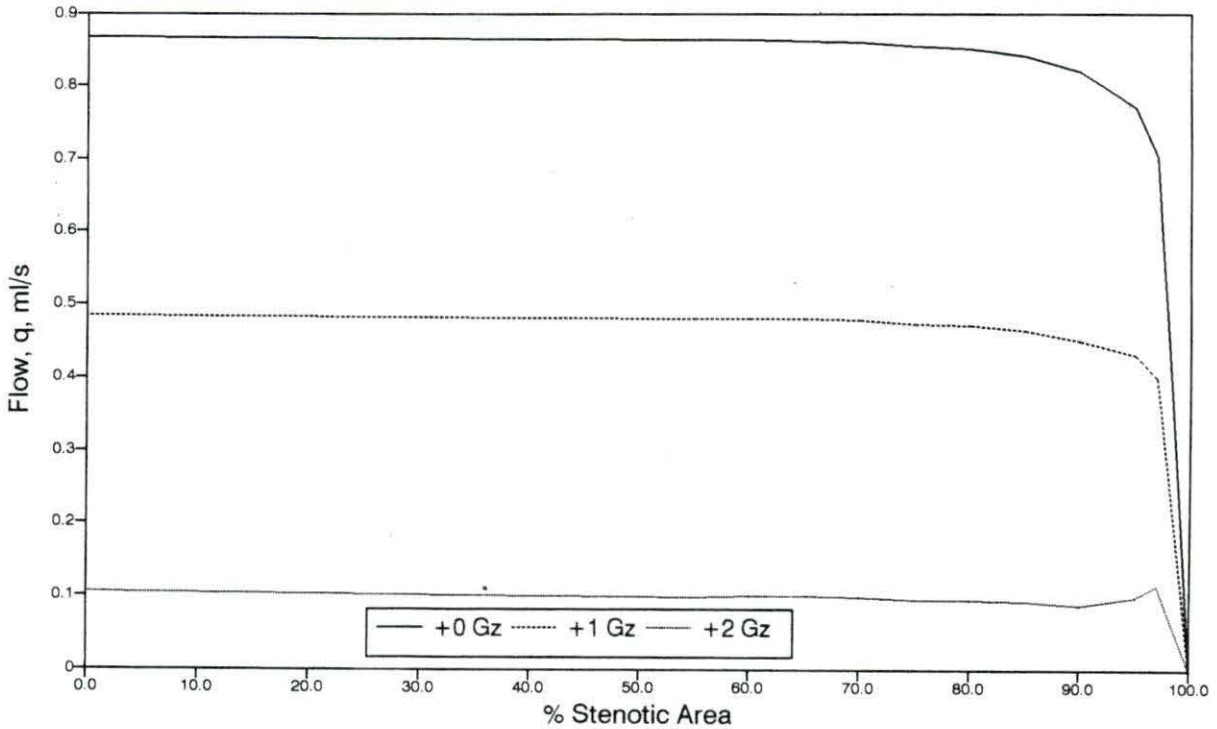

Figure 5.20: Mean flows in the L. external carotid artery versus percentage stenosis and $+G_z$ acceleration

In the +0 G_z model, the mean pressure and flow plots look identical to those found in the literature. The critical stenosis (the minimal occlusion where flow becomes profoundly affected), is about 80%. For +1 G_z acceleration, the critical stenosis occurs just before 90% occlusion. This is consistant with predicted behavior.

For +2 G_z, the mean pressures and flows remain nearly constant as a function of occlusion until 90% stenosis. At 90% stenosis, the numerical solving routine becomes unstable. A combination of the elevated body force with the high degree of lumen narrowing created instability in the finite difference code despite small time steps and increased attenuation of the non-linear p-A terms. Pressures and flows do not increase after 90% stenosis as the plots indicate.

Figures 5.19 and 5.20 show that the presence of a carotid stenosis during $+G_z$ acceleration does not adversely affect cerebral pressures and flows. In fact, the model suggests that the percentage occlusion for a critical stenosis at +0 G_z is less than the percentage occlusion for a critical stenosis at +1 G_z.

Using Figures 5.19 and 5.20, it is expected that the pressure drop across a stenosis in the lower extremities during $+G_z$ would become more pronounced, reducing blood flow distal to the stenosis. While this would help maintain cerebral pressures and flows, circulation in the extremity would be impaired. In effect, a mini G-suit is applied to a single artery.

A stenosis in the carotid bifurcation would be expected to hinder the effect of anti-G straining maneuvers and G-suits. The pressure drop across the stenosis would counteract the pressure rise in the carotid artery from these protective measures.

A stenosis in the carotid bifurcation would be expected to aid the pilot in high $-G_z$ acceleration because during high $-G_z$, the headward body force raises pressures

and flows above the normal standing (or even supine) pressures and flows. The stenosis would lower pressures and flows during $-G_z$ in the external and internal carotid arteries distal to the stenosis, minimizing the risk of red-out (too much blood to the brain, as shown in Figure 1.3). Again, in effect, a mini G-suit has been applied to a single artery.

According to the model, it can be hypothesized that carotid stenosis should not adversly affect pilots in their flight worthiness. The presence of a stenosis should affect these men and women in their everyday activities prior to symptoms at elevated $+G_z$ acceleration. As the medically flightworthy community ages, more data will become available from medical records as to the validity of the hypothesis.

CHAPTER 6. CONCLUSIONS AND RECOMMENDATIONS

A previously developed computer model of the human arterial system, based on the one dimensional momentum and continuity equations, is used to study the effects of $+G_z$ acceleration on head-level pressures and flows. Using empirical stroke volume, cardiac output, heart rate, and peripheral resistance data found in the literature, the model yields a good first approximation of arterial pressures and flows during external acceleration of the system.

Of course, the model is only as good as the input data it requires. Physiological acceleration data are subject to a high degree of variation because of differences in acceleration gradients between centrifuges. Physiological responses are also dependent upon G onset. Using the data set assembled in this study, the following conclusions can be made:

- The model can be used to simulate $+G_z$ loadings if the physiological changes in stroke volume, heart rate, and peripheral resistance are known.

- If only two of the above parameters are known, the third can be estimated if a mean head-level pressure or flow during $+G_z$ acceleration (a target value) is found in the literature.

- The model becomes unstable at $+G_z$ loadings of 3 Gs despite drastic reduc-

tions in the non-linear terms of the pressure-area relationship and solving the equations at extremely small time increments.

- From available data, a reasonable approximation of the eye-level pressures and flows for supine ($+0\ G_z$), standing ($+1\ G_z$), and $+2\ G_z$ cases can be simulated.

- Using G-suit data available in the literature, the model shows an occlusive-type G-suit affords better protection to $+G_z$ acceleration than the purely resistive-type (lower inflation pressure) G-suit presently used in modern high-performance aircraft.

- If a stenosis in the carotid bifurcation does not significantly alter pressures and flows in the $+0\ G_z$ case (stenotic area less than the critical occlusion), there still will be no significant stenotic effects to pressures and flows in the carotid artery during $+G_z$ acceleration.

Several improvements can be made to the model to more accurately represent arterial dynamics under external acceleration. At present, the model depends upon empirical data for stroke volume and cardiac output to represent venous pooling. If venous and cardiac dynamics were added to the model, such dependence would be eliminated.

With the addition of venous and cardiac systems, the model would be a closed-loop system. Closure would eliminate the present proximal input boundary condition, allowing the hydrostatic indifference point to be found.

Quantitative studies of the changes in vascular tone during $+G_z$ acceleration are necessary to build a model that incorporates the peripheral resistance compensatory

mechanism. A mathematical function relating vascular tone to pressures in the aortic and carotid baroreceptors is required.

The use of computer models can yield insight into G-suit design as well as straining techniques. Compartmental, lumped-parameter models (both analog and digital) have been developed by acceleration research centers such as the NADC (Naval Air Development Center) and have been shown to correspond well to experimental studies. However, these models fail to accurately model wave propagation. As more compartments are added, the model begins to show wave propagation more closely but at the expense of changing the equations in all the compartments.

The model presented here shows wave propagation phenomena during $+G_z$ acceleration. To see the waveform at any particular point in the arterial tree, a new compartment need not be added. Adding a new node at the point of interest is all that is required.

The geometry and physiology of the model are easily changed without re-writing the governing equations — an advantage that would alone recommend this model to acceleration researchers.

Higher order interpolation techniques could improve the accuracy of the solution. However, until the detail and consistency of anatomical and physiological data improves, more accurate numerical techniques will be of little value to the researcher.

ACKNOWLEGEMENTS

I would like to express my sincere appreciation and gratitude to Dr. Donald F. Young for his knowledge and guidance throughout this study. In addition, I would like to thank Dr. Tom Rogge for his suggestions in the development of FLOW, Dr. Nikolas Stergiopulos for helping me understand his work, and Dr. Frederick Hembrough for serving on my committee. Special thanks go to Benjamin Dehner for the use of his computer, apartment, and time at all hours. Also, I would like to thank all the professors and graduate students in Biomedical Engineering for their support and assistance.

I would also like to express my appreciation to the physicians and staff of the Iowa State Student Health Center, most notably Rebecca Fritzsche, M.D., for their efforts in maintaining my continued health.

This work is dedicated to my parents, Henry and Kathleen Cornet, for their understanding and emotional support, as well as my brothers Erik, Jac, and Patrick, whose help I could count on when I needed it most, and most especially to Karen Wagner, my fiancée, for her continual understanding and Love through house fires, hospitalizations, long work days, weeks apart, and everyday frustrations.

BIBLIOGRAPHY

Burns, J. W. 1988. Prevention of loss of consciousness with Positve Pressure Breathing and supinating seat. Aviat., Space and Envir. Med. 59:20–22.

Burns, J. W., M. J. Parnell, and R. R. Burton. 1986. Hemodynamics of miniature swine during $+G_z$ stress with and without anti-G support. J. Appl. Physiol. 60:1628–1637.

Burton, R. R. 1988. Anti-G suit inflation requirements. Aviat., Space and Envir. Med. 59:601–605.

Burton, R. R., S. D. Leverett, Jr., and E. D. Michaelson. 1974. Man at high sustained $+G_z$ acceleration. AGARD–AG–190.

Caro, C. G., T. J. Pedley, R. C. Schroter, and W. A. Seed. 1978. The mechanics of circulation. Oxford University Press, Oxford.

Chien, S. 1985. Cerebral blood flow and metabolism. Pages 845–852 *in* Kandel, E. R. and J. H. Schwartz, ed. Principles of neuro science, 2nd ed. Elsevier Science Publishing, New York.

Erickson, H. H., H. Sandler, and H. L. Stone. 1976. Cardiovascular function during sustained $+G_z$ stress. Aviat., Space and Envir. Med. 47(7):750–758.

Etkin, B. 1982. Dynamics of flight — Stability and control, 2nd ed. John Wiley and Sons, New York.

Fung, Y. C. 1984. Biodynamics, Circulation. Springer-Verlag, New York.

Ganong, W. F. 1989. Review of medical physiology, 14th ed. Appleton and Lange, New Jersey.

Gaur, O. H. 1961(a). The hydrostatic pressures. Pages 16–27 *in* Gaur, O. H., and G. D. Zuidema, ed. Gravitational stress in aerospace medicine. Little, Brown, and company, Boston.

Gaur, O. H. 1961(b). Magnitude, direction, and time course of acceleration forces. Pages 10–15 *in* Gaur, O. H., and G. D. Zuidema, ed. Gravitational stress in aerospace medicine. Little, Brown, and company, Boston.

Gaur, O. H., and E. W. Salzman. 1961. Reflex responses of the circulation. Pages 46–51 *in* Gaur, O. H., and G. D. Zuidema, ed. Gravitational stress in aerospace medicine. Little, Brown, and company, Boston.

Gillingham, K. K. 1988. High-G stress and orientational stress: Physiologic effects of aerial maneuvering. Aviat., Space and Envir. Med. 59(11, Suppl.):A10–20.

Gillingham, K. K., and J. P. Fosdick. 1988. High-G training for fighter aircrew. Aviat., Space and Envir. Med. 59:12–19.

Glaeser, D., S. Gum, and B. Walters. 1985. An invitation to fly, 2nd ed. Wadsworth Publishing Co., California.

Glaister, D. H. 1990. Cardiovasular responses to sustained acceleration. The Physiologist 33(1):S121–124.

Gotshall, R. W., P-F Tsai, and M. A. B. Frey. 1991. Gender-based differences in cardiovascular response to standing. Aviat., Space and Envir. Med. 62(9):823–922.

Gray, S., III, J. A. Shaver, F. W. Kroetz, and J. J. Leonard. 1969. Acute and prolonged effects of G suit inflation on cardiovascular dynamics. Aerospace Med. 40(1):40–43.

Howard, P. 1965. The physiology of positive acceleration. Pages 551–687 *in* Gilles, J. A., ed. A textbook of aviation physiology. Pergamon Press, New York.

Krutz, R. W., Jr., S. A. Rositano, and R. E. Mancini. 1973. Correlation of eye-level blood flow velocity and blood pressure during $+G_z$ acceleration. SAM-TR-73-36.

Laughlin, M. H. 1986. The effects of $+G_z$ on the coronary circulation: A review. Aviat., Space and Envir. Med. 57:5–16.

Leverett, S. D., Jr., R. R. Burton, R. J. Crossley, E. D. Michaelson, and S. J. Shubrooks, Jr. 1973. Physiologic responses to high sustained $+G_z$ acceleration. USAF SAM-TR-73-21.

Martini, F. 1989. Fundamentals of anatomy and physiology. Prentice Hall, New Jersey.

McCulloch, J. 1988. The physiology and regulation of cerebral blood flow. Pages 1-24 *in* Knezevic, S., A. Maximilian, Z. Mubrin, I. Prohovnik, and J. Wade. ed. Handbook of regional cerebral blood flow. Lawrence Erlbaum Associates, New Jersey.

McDonald, D. A. 1974. Blood flow in arteries, 2nd ed. Camelot Press, Ltd., Southampton.

Milnor, W. R. 1982. Hemodynamics. Williams and Wilkins, Baltimore.

Moore, T. W., J. Bai, F. Kepica, L. Hrebien, and D. Jaron. 1988. Studies of cardiovascular responses during acceleration stress. Proceedings. IEEE Engineering in medicine and biology society 10th annual international conference.

O'Bryon, J. F. 1991. Unlocking G-LOC. Aerospace America 29(9):60-63.

Peterson, D. F., V. S. Bishop, and H. H. Erickson. 1975. Cardiovascular changes during and following 1-min exposure to $+G_z$ stress. Aviat., Space and Envir. Med. 46(6):775-779.

Porenta, G., D. F. Young, and T. R. Rogge. 1986. A finite-element model of blood flow in arteries including taper, branches, and obstructions. J. Biomechanical Engineering 108:161-167.

Raines, J. K., M. Y. Jaffrin, and A. H. Shapiro. 1974. A computer simulation of arterial dynamics in the human leg. J. Biomechanics 7:77-91.

Rooz, E., D. F. Young, and T. R. Rogge. 1982. A finite-element simulation of pulsatile flow in flexible obstructed tubes. J. Biomechanical Engineering 104:119-124.

Sandler, H., S. A. Rositano, and E. P. McCutcheon. 1977. An objective determination of $+G_z$ acceleration tolerance. Acta Astronautica 4:541–553.

Seaworth, J. F., T. J. Jennings, L. L. Howell, J. W. Frazier, C. D. Goodyear, and E. D. Grassman. 1985. Hemodynamic effects of anti-G suit inflation in a 1-G environment. J. Applied Physiology 59(4):1145–1151.

Seeley, B. D. and D. F. Young. 1976. Effect of geometry on pressure loss across models of arterial stenosis. J. Biomechanics 5:345–364.

Shubrooks, S. J., and S. D. Leverett, Jr. 1973. Effect of the valsalva maneuver on tolerance to $+G_z$ acceleration. J. Appl. Physiol. 34(4):460–466.

Sieker, H. O. 1961. Effect of acceleration on the heart. Pages 52–60 *in* Gaur, O. H., and G. D. Zuidema, ed. Gravitational stress in aerospace medicine. Little, Brown, and company, Boston.

Stergiopulos, N. 1987. Pulsating flow through models of compliant stenosis. M. S. Thesis. Iowa State University, Ames.

Stergiopulos, N. 1990. Computer simulation of arterial flow. Ph. D. Thesis. Iowa State University, Ames.

Sud, V. K., and G. S. Sekhon. 1986. Analysis of blood flow through a model of the human arterial system under periodic body acceleration. J. Biomechanics 19(11):929–941.

Van Patten, R. E.. 1988. Advances in anti-G valve technology: What's in the future? Aviat., Space and Envir. Med. 59:32–35.

Voge, V. M. 1980. Acceleration forces on the human subject. Aviat., Space and Envir. Med. 51(9):970–980.

Whinnery, J. E. 1988. Converging research on $+G_z$ induced loss of consciousness. Aviat., Space and Envir. Med. 59:9–11.

Wood, E. H. 1991. Aerial combat, physiology and clinical medicine. Presentation at the 28th annual rocky mountain bioengineering symposium, Mayo Clinic, April 12–13.

Wood, E. H. 1987. Development of anti-G suits and their limitations. Aviat., Space and Envir. Med. 58:699–706.

Young, D. F., and F. Y. Tsai. 1973(a). Flow characteristics in models of arterial stenosis. I. Steady Flow. J. Biomechanics 6:395–410.

Young, D. F., and F. Y. Tsai. 1973(b). Flow characteristics in models of arterial stenosis. II. Unsteady flow. J. Biomechanics 6:547–559.

Young, D. F. 1979. Fluid mechanics of arterial stenosis. J. Biomechanical Engineering 101:157–175.

Young, D. F., T. R. Rogge, T. A. Gray, and E. Rooz. 1981. Indirect evaluation of system parameters for pulsatile flow in flexible tubes. J. Biomechanics 14(5):339–347.

APPENDIX. PROGRAM SOURCE CODES

PQYPLOT

Written by Dr. Nikos Stergiopulos, PQYPLOT numericaly solves the momentum, continuity, p-A, and shear stress equations for arterial flow using a finite difference scheme. Any geometry can be specified, as all geometry and mechanical properties are contained in an input data file.

PQYPLOT.FOR, as listed below, is written in Microsoft Fortran (version 5.0). To convert this program to standard FORTRAN 77, only the file handling statements must be changed.

```
CCCCCCCCCCCCCCCCCCCCCCCCCCCCCCCCCCCCCCCCCCCCCCCCCCCCCCCCCCCCCCCCCC
C                                                                  C
C     FINITE ELEMENT PROGRAM FOR THE ANALYSIS OF                   C
C           MULTI-BRANCHED ARTERIAL FLOW                           C
C                                                                  C
C                    MAIN PROGRAM                                  C
C                                                                  C
CCCCCCCCCCCCCCCCCCCCCCCCCCCCCCCCCCCCCCCCCCCCCCCCCCCCCCCCCCCCCCCCCC
      IMPLICIT REAL*8(A-H,O-Z)
      CHARACTER*30
      FILE,INFILE,OUTFILE,PLTFILE,AVGFILE,INF,OUTF,AVGF,PLF
C
      COMMON/AREADT/AIN(150),AOUT(150),AVA(500)
      COMMON/BOUND/QBOUN(30,2),PBOUN(30,2)
```

```
      COMMON/CONDCT/CONDUCT(150)
      COMMON/COORDN/X(500),DX(500),XLAST(150),COORD(800,2)
     1             ,CLAST(150,2)
      COMMON/FLUPRO/DENS,VISC
      COMMON/YOUNG/CV(500),CU(500),PAR1(500)
      COMMON/GRAVT/GRAV,GLOAD,GA(2),GZ(500)
      COMMON/ISEGMT/NNODES(150),INDBRA(150),INDPAR(150),INDSTE(150)
      COMMON/NBOUN/NQB,NPB
      COMMON/NDATA/NS,NT,NCYC
      COMMON/NODES/NFIRST(150),NLAST(150)
      COMMON/PEE/PI
      COMMON/SEGDAT/COMPL0(150),COMPL1(150),SLEN(150),SPG(150)
     1              ,DA(150,2)
      COMMON/STENOS/XSTEN(150),STELEN(150),PRC(150)
     1              ,ST1(150),ST2(150),ST3(150)
      COMMON/TERMZ/RES1(150),RES2(150),CT(150)
      COMMON/TDATA/DT,FREQ
      COMMON/VAINIT/PINIT(500),QINIT(500)
C
      WRITE(*,'(A \)') ' Enter file name: '
      READ(*,'(A20)') FILE
C
      DO 5 I=20,1,-1
      IF(FILE(I:I).NE.' ') GOTO 7
    5 CONTINUE
    7 CONTINUE
      INFILE=FILE(1:I)//'.DAT'
      OUTFILE=FILE(1:I)//'.OUT'
      AVGFILE=FILE(1:I)//'.AVG'
      PLTFILE=FILE(1:I)//'.PLT'
C
      INF='f:\dac\files\'//INFILE
      OUTF='f:\dac\files\'//OUTFILE
      AVGF='f:\dac\files\'//AVGFILE
      PLF='f:\dac\files\'//PLTFILE
      OPEN (UNIT=5,FILE=INF,STATUS='UNKNOWN')
      OPEN (UNIT=6,FILE=OUTF,STATUS='UNKNOWN')
      OPEN (UNIT=7,FILE=AVGF,STATUS='UNKNOWN')
      OPEN (UNIT=8,FILE=PLF,STATUS='UNKNOWN')
C
```

```
      CALL INPUT
      CALL SETUP
      CALL INIVAL
      CALL SOLVE
C
      STOP
      END
C
C
C
      SUBROUTINE INPUT
CCCCCCCCCCCCCCCCCCCCCCCCCCCCCCCCCCCCCCCCCCCCCCCCCCCCCCCCCCCCCCCCCC
C                                                                 C
C     THIS SUBROUTINE READS INPUT DATA                            C
C                                                                 C
CCCCCCCCCCCCCCCCCCCCCCCCCCCCCCCCCCCCCCCCCCCCCCCCCCCCCCCCCCCCCCCCCC
C
C-----INPUT PARAMETERS:
C
C--------------NS: # OF ARTERIAL SEGMENTS
C-------INDBRA(I): # OF THE FIRST BRANCH OF THE Ith SEGMENT
C                  (0 INDICATES TERMINAL BRANCH)
C-------INDPAR(I): # OF THE PARENT SEGMENT OF THE Ith SEGMENT
C-------INDSTE(I): LOCATION (ELEMENT #) OF STENOSIS (=0, NO STENOSIS)
C---------SLEN(I): SEGMENT LENGTH
C-------NNODES(I): # OF NODES IN EACH SEGMENTS
C----------AIN(I): AREA AT THE BEGINING OF THE SEGMENT
C---------AOUT(I): AREA AT THE END OF THE SEGMENT
C-------COMPL0(I): COMPLIANCE COEFFICIENT OF THE ARTERIAL WALL [C0]
C-------COMPL1(I): COMPLIANCE COEFFICIENT OF THE ARTERIAL WALL [C1]
C----------SPG(I): SEEPAGE OF THE SEGMENT
C-------DA(I,1-2): DIRECTIONAL ANGLES OF THE SEGMENT
C---------RES1(I): TERMINAL RESISTANCE 1
C---------RES2(I): TERMINAL RESISTANCE 2
C-----------CT(I): TERMINAL CAPACITANCE
C--------XSTEN(I): DISTANCE FROM BEGINING OF SEGMENT TO STENOSIS
C-------STELEN(I): LENGTH OF STENOSIS
C----------PRC(I): PERCENT AREA REDUCTION IN STENOSIS
C------------DENS: DENSITY
C------------VISC: VISCOSITY
```

```
C------------NCYC: # OF CYCLES
C------------FREQ: BASIC FREQUENCY OF EACH CYCLE
C-------------NQB: # OF FLOW HARMONICS
C-------------NPB: # OF PRESSURE HARMONICS
C----QBOUN(I,1-2): FLOW HARMONICS (INPUT)
C----PBOUN(I,1-2): PRESSURE HARMONICS (INPUT)
C-----------GLOAD: BODY FORCE IN MULTIPLES OF g (ACCL. OF GRAVITY)
C---------GA(1-2): ANGLES OF THE GLOAD VECTOR WRT COORDINATE SYSTEM
C--------------DT: TIME INCREMENT
C
      IMPLICIT REAL*8(A-H,O-Z)
      COMMON/AREADT/AIN(150),AOUT(150),AVA(500)
      COMMON/BOUND/QBOUN(30,2),PBOUN(30,2)
      COMMON/FLUPRO/DENS,VISC
      COMMON/YOUNG/CV(500),CU(500),PAR1(500)
      COMMON/GRAVT/GRAV,GLOAD,GA(2),GZ(500)
      COMMON/ISEGMT/NNODES(150),INDBRA(150),INDPAR(150),INDSTE(150)
      COMMON/NBOUN/NQB,NPB
      COMMON/NDATA/NS,NT,NCYC
      COMMON/SEGDAT/COMPL0(150),COMPL1(150),SLEN(150),SPG(150)
     1             ,DA(150,2)
      COMMON/STENOS/XSTEN(150),STELEN(150),PRC(150)
     1             ,ST1(150),ST2(150),ST3(150)
      COMMON/TERMZ/RES1(150),RES2(150),CT(150)
      COMMON/TDATA/DT,FREQ
      WRITE(*,'(A \)') ' p-A ? (1=linear, 2=log type, 3=change C): '
      READ(*,*) NPA
C
      WRITE(*,'(A \)') ' Peripheral resistance? (Pure = 1): '
      READ(*,*) NPR
C
      READ (5,1000) NS
C
      DO 10 I=1,NS
         READ (5,2000)
      INDBRA(I),INDPAR(I),INDSTE(I),NNODES(I),SLEN(I),
     1                 AIN(I),AOUT(I)
   10 CONTINUE
C
      READ (5,9000)
```

```
C
      IF(NPA.EQ.2.OR.NPA.EQ.3) THEN
         WRITE(*,'(A \)') ' Enter compliance coefficient: '
         READ(*,*) CCF
      ELSE
         CONTINUE
      END IF
      DO 15 I=1,NS
         READ (5,2500)  COMPL0(I),COMPL1(I),SPG(I),ANGL
         ANGL=ANGL*3.14159D0/180.D0
         DA(I,1)=DCOS(ANGL)
         DA(I,2)=DSIN(ANGL)
         IF(NPA.EQ.1) THEN
            COMPL0(I)=COMPL0(I)+12900.D0*COMPL1(I)
            COMPL1(I)=0.0D0
         ELSE IF(NPA.EQ.2) THEN
            COPRIME=COMPL0(I)+12900.D0*COMPL1(I)
            C1PRIME=-COPRIME/(2.0D0*12900.D0)
            COMPL0(I)=2.0D0*COPRIME
            COMPL1(I)=CCF*2.0D0*C1PRIME
         ELSE IF(NPA.EQ.3) THEN
            COPRIME=(COMPL0(I)+12900.D0*COMPL1(I))*CCF
            C1PRIME=COPRIME**2
            COMPL0(I)=COPRIME-2.0D0*12900.D0*C1PRIME
            COMPL1(I)=2.0D0*C1PRIME
         ELSE
            CONTINUE
         END IF
   15 CONTINUE
C
      READ (5,9000)
C
      WRITE(*,'(A \)') ' Enter first segment for R change : '
      READ(*,*) NRST
      IF(NRST.EQ.0) GOTO 19
      WRITE(*,'(A \)') ' Enter Resistance coefficients : '
      READ(*,*) RCOEFF1,RCOEFF2
   19 CONTINUE
      DO 20 I=1,NS
         IF (INDBRA(I).GT.0) GOTO 20
```

```
         READ (5,3000) RES1(I),RES2(I),CT(I)
         IF(I.GE.NRST.AND.NRST.NE.0) THEN
            RES1(I)=RES1(I)*RCOEFF1
            RES2(I)=RES2(I)*RCOEFF2
         ELSE
            CONTINUE
         END IF
         IF(NPR.EQ.1) CT(I)=0.0D0
   20 CONTINUE
C
      KS=0
      DO I=1,NS
         KS=KS+INDSTE(I)
      END DO
      IF (KS.EQ.0) GOTO 26
C
      READ (5,9000)
C
      DO 25 I=1,NS
         IF (INDSTE(I).EQ.0) GOTO 25
         READ (5,3000)  XSTEN(I),STELEN(I),PRC(I)
   25 CONTINUE
   26 CONTINUE
C
      READ (5,4000) DENS,VISC
      READ (5,5000) NCYC,FREQ,DT
C
      READ (5,6000) NPB,NQB
      IF (NPB.GT.0) THEN
         DO 30 I=1,NPB
            READ (5,7000) PBOUN(I,1),PBOUN(I,2)
   30    CONTINUE
      ELSE
         DO 40 I=1,NQB
            READ (5,7000) QBOUN(I,1),QBOUN(I,2)
   40    CONTINUE
      END IF
C
      READ (5,8000) GRAV,GLOAD,GANGL
      GANGL=GANGL*3.14159D0/180.D0
```

```
      GA(1)=DCOS(GANGL)
      GA(2)=DSIN(GANGL)
C
C-----CALL VERIPT TO VERIFY INPUT DATA
C
      CALL VERIPT
      RETURN
C
C
 1000 FORMAT(1X/I3//)
 2000 FORMAT(3X,4(2X,I3),3(2X,D12.5))
 2500 FORMAT(3X,4(2X,D12.5))
 3000 FORMAT(3X,3(2X,D12.5))
 4000 FORMAT(//2(2X,D12.5))
 5000 FORMAT(//2X,I3,2(2X,D12.5))
 6000 FORMAT(//2(2X,I3)//)
 7000 FORMAT(2(2X,D12.5))
 8000 FORMAT(//3(2X,D12.5))
 9000 FORMAT(/)
C
      END
C
C
      SUBROUTINE VERIPT
CCCCCCCCCCCCCCCCCCCCCCCCCCCCCCCCCCCCCCCCCCCCCCCCCCCCCCCCCCCCCCCCCC
C                                                                 C
C      THIS SUBROUTINE VERIFIES INPUT DATA                        C
C                                                                 C
CCCCCCCCCCCCCCCCCCCCCCCCCCCCCCCCCCCCCCCCCCCCCCCCCCCCCCCCCCCCCCCCCC
      IMPLICIT REAL*8(A-H,O-Z)
      COMMON/AREADT/AIN(150),AOUT(150),AVA(500)
      COMMON/BOUND/QBOUN(30,2),PBOUN(30,2)
      COMMON/FLUPRO/DENS,VISC
      COMMON/YOUNG/CV(500),CU(500),PAR1(500)
      COMMON/GRAVT/GRAV,GLOAD,GA(2),GZ(500)
      COMMON/ISEGMT/NNODES(150),INDBRA(150),INDPAR(150),INDSTE(150)
      COMMON/NBOUN/NQB,NPB
      COMMON/NDATA/NS,NT,NCYC
      COMMON/SEGDAT/COMPL0(150),COMPL1(150),SLEN(150),SPG(150)
     1             ,DA(150,2)
```

```
      COMMON/STENOS/XSTEN(150),STELEN(150),PRC(150)
     1             ,ST1(150),ST2(150),ST3(150)
      COMMON/TERMZ/RES1(150),RES2(150),CT(150)
      COMMON/TDATA/DT,FREQ
C
      WRITE (6,500)
      WRITE (6,1000) NS
C
      WRITE (6,1500)
      DO 10 I=1,NS
         WRITE (6,2000)
         I,INDBRA(I),INDPAR(I),INDSTE(I),NNODES(I),
     1                  SLEN(I),AIN(I),AOUT(I)
   10 CONTINUE
C
      WRITE (6,2100)
      DO 15 I=1,NS
         WRITE (6,2200)
         I,COMPL0(I),COMPL1(I),SPG(I),DA(I,1),DA(I,2)
   15 CONTINUE
C
      WRITE (6,2500)
C
      DO 20 I=1,NS
         IF (INDBRA(I).GT.0) GOTO 20
         WRITE (6,3000) I,RES1(I),RES2(I),CT(I)
   20 CONTINUE
C
C
      WRITE (6,3100)
C
      DO 25 I=1,NS
         IF (INDSTE(I).EQ.0) GOTO 25
         WRITE (6,3000) I,XSTEN(I),STELEN(I),PRC(I)
   25 CONTINUE
C
      WRITE (6,3500)
      WRITE (6,4000) DENS,VISC
C
      WRITE (6,4500)
```

```
      WRITE (6,5000) NCYC,FREQ,DT
C
      WRITE (6,5500)
      WRITE (6,6000) NPB,NQB
      IF (NPB.GT.0) THEN
         WRITE (6,6500)
         DO 30 I=1,NPB
            WRITE (6,7000) PBOUN(I,1),PBOUN(I,2)
   30    CONTINUE
      ELSE
         WRITE (6,7500)
         DO 40 I=1,NQB
            WRITE (6,7000) QBOUN(I,1),QBOUN(I,2)
   40    CONTINUE
      END IF
C
      WRITE (6,8500)
      WRITE (6,8000) GRAV,GLOAD,GA(1),GA(2)
C
      RETURN
C
  500 FORMAT(' NUMBER OF SEGMENTS')
 1000 FORMAT(7X,I4,//)
 1500 FORMAT('  SEG  BRA  PAR  STE  NEL  SEGM. LENGTH  INPUT AREA',
     1   11X,'   OUTPUT ')
 2000 FORMAT(1X,I3,4(2X,I3),6(2X,D12.5),2(2X,F4.1))
 2100 FORMAT(/'  SEG     COMPLO        COMPL1       SEEPAGE
     1   DIRECTIONAL COSINES')
 2200 FORMAT(1X,I3,5(2X,D12.5))
 2500 FORMAT(/'  SEG      RES1          RES2          CT')
 3000 FORMAT(1X,I3,3(2X,D12.5))
 3100 FORMAT(/'  SEG   X STENOSIS   STENOSIS LNGTH     %')
 3500 FORMAT(/'     DENSITY      VISCOSITY')
 4000 FORMAT(2(2X,D12.5))
 4500 FORMAT(/' # OF CYCLES    FREQUENCY    TIME INCREMENT')
 5000 FORMAT(4X,I3,2(7X,D12.5))
 5500 FORMAT(/' # OF PRESSURE FOURIER COEF.',5x,
     1         '# OF FLOW FOURIER COEFF.')
 6000 FORMAT(10X,I3,25X,I3)
 6500 FORMAT(/'   P COS TERM    P SIN TERM')
```

```
 7000 FORMAT(2(2X,D12.5))
 7500 FORMAT(/'   Q COS TERM    Q SIN TERM')
 8000 FORMAT(4(2X,D12.5))
 8500 FORMAT(/'  ACCEL. GRAV.    GRAVIT. LOAD        ORIENT. ANGLES')
C
      END
C
C
C
      SUBROUTINE SETUP
CCCCCCCCCCCCCCCCCCCCCCCCCCCCCCCCCCCCCCCCCCCCCCCCCCCCCCCCCCCCCCCCC
C                                                               C
C      THIS SUBROUTINE SETS UP THE ELEMENTS,                    C
C      CALCULATES THE ELEMENT LEGTHS AND TYPES                  C
C      ASSIGNS THEIR CHARACTERISTIC VALUES, AND                 C
C      SETS UP A COORDINATE SYSTEM                              C
C                                                               C
CCCCCCCCCCCCCCCCCCCCCCCCCCCCCCCCCCCCCCCCCCCCCCCCCCCCCCCCCCCCCCCCC
      IMPLICIT REAL*8(A-H,O-Z)
      COMMON/AREADT/AIN(150),AOUT(150),AVA(500)
      COMMON/COORDN/X(500),DX(500),XLAST(150),COORD(800,2)
     1             ,CLAST(150,2)
      COMMON/FLUPRO/DENS,VISC
      COMMON/ISEGMT/NNODES(150),INDBRA(150),INDPAR(150),INDSTE(150)
      COMMON/NDATA/NS,NT,NCYC
      COMMON/NODES/NFIRST(150),NLAST(150)
      COMMON/PEE/PI
      COMMON/SEGDAT/COMPL0(150),COMPL1(150),SLEN(150)
     1             ,SPG(150),DA(150,2)
      COMMON/STENOS/XSTEN(150),STELEN(150),PRC(150)
     1             ,ST1(150),ST2(150),ST3(150)
      COMMON/TERMZ/RES1(150),RES2(150),CT(150)
      COMMON/TDATA/DT,FREQ
C
      PI=4.0D0*DATAN(1.0D0)
C
C-----NT: TOTAL # OF NODES
C-----NFIRST(I): THE FIRST NODE OF THE Ith SEGMENT
C-----NLAST(I): THE LAST NODE OF THE Ith SEGMENT
C
```

```
      K=0
      DO 10 I=1,NS
         NFIRST(I)=K+1
         K=K+NNODES(I)
         NLAST(I)=K
   10 CONTINUE
      NT=K
C
C-----CALCULATE THE GRID SPACING DX(J) TO THE RIGHT OF EACH NODE
C
      DO 50 I=1,NS
         NF=NFIRST(I)
         NL=NLAST(I)
         IS=INDSTE(I)
         IF(IS.EQ.0) THEN
C-----------NO STENOSES
            DO 20 J=NF,NL-1
               DX(J)=SLEN(I)/(NNODES(I)-1)
   20       CONTINUE
         ELSE
C-----------THERE ARE STENOSES IN THE SEGMENT
            DO 30 J=NF,NF+IS-2
               DX(J)=XSTEN(I)/(IS-1)
   30       CONTINUE
            DX(NF+IS-1)=STELEN(I)
            DO 40 J=NF+IS,NL-1
            DX(J)=(SLEN(I)-XSTEN(I)-STELEN(I))/(NNODES(I)-IS-1)

   40       CONTINUE
         END IF
   50 CONTINUE
C
C-----CALCULATE THE COORDINATES OF EACH NODE X(I)(ARC-LENGTH),
C-----COORD(I,1) (X-COORDINATE), AND COORD(I,2) (Y-COORDINATE)
C
C-----XLAST(I): THE COORDINATE OF THE LAST NODE OF Ith SEGMENT
C-----CLAST(I,1-2): X AND Y COORDINATES OF LAST NODE OF Ith SEGMENT
C
      X(1)=0.0D00
      COORD(1,1)=0.0D00
```

```
      COORD(1,2)=0.0D00
      DO 80 I=1,NS
         NF=NFIRST(I)
         NL=NLAST(I)
         L=INDPAR(I)
         IF (L.EQ.0) GOTO 60
         X(NF)=XLAST(L)
         COORD(NF,1)=CLAST(L,1)
         COORD(NF,2)=CLAST(L,2)
   60    CONTINUE
         DO 70 J=NF+1,NL
            X(J)=X(J-1)+DX(J-1)
            COORD(J,1)=COORD(J-1,1)+DX(J-1)*DA(I,1)
            COORD(J,2)=COORD(J-1,2)+DX(J-1)*DA(I,2)
   70    CONTINUE
         XLAST(I)=X(NL)
         CLAST(I,1)=COORD(NL,1)
         CLAST(I,2)=COORD(NL,2)
   80 CONTINUE
C
C
C-----CALCULATE THE MEAN AREA FOR EACH ELEMENT
C
      CALL AREA
C
C-----CALCULATE THE WALL SHEAR STRESS COEFFICIENTS
C-----CV AND CU AT EACH NODE
C
      CALL WALLSHEAR
C
C-----CALCULATE THE BODY FORCE PROJECTION ON EACH SEGMENT
C
      CALL GRAVIT
C
C-----CALCULATE THE STENOSIS COEFFICIENTS SKV(I),SK1(I),SK2(I),
C     AND SK3(I)
C
      CALL STENOSIS
C
C-----PRINT OUT THE FIRST AND LAST NODE OF EACH SEGMENT
```

```
C-----AND THE COORDINATES OF THE LAST NODE
C
      WRITE (6,4000)
      DO 110 I=1,NS
         WRITE (6,5000) I,NFIRST(I),NLAST(I),XLAST(I),
     1                  CLAST(I,1),CLAST(I,2)
  110 CONTINUE
C
C-----PRINT OUT THE TOTAL NUMBER OF NODES AND THE
C-----COORDINATES OF EACH NODE
C
      WRITE (6,6000) NT
      WRITE (6,7000)
      DO 120 K=1,NT,5
         L=K+4
         WRITE (6,8000) (I,X(I),I=K,L)
  120 CONTINUE
C
      RETURN
C
 4000 FORMAT(/' SEGMENT  FIRST_NODE  LAST_NODE   LAST_POINT_CCORD.')
 5000 FORMAT(2X,I3,2(8X,I3),3(2X,D12.5))
 6000 FORMAT(//' NUMBER OF NODES'/5X,I3)
 7000 FORMAT(/20X,'NODE COORDINATES')
 8000 FORMAT(2X,5(I3,D12.5,1X))
      END
C
C
      SUBROUTINE AREA
CCCCCCCCCCCCCCCCCCCCCCCCCCCCCCCCCCCCCCCCCCCCCCCCCCCCCCCCCCCCCCCCCC
C                                                                  C
C      THIS SUBROUTINE CALCULATES THE ELEMENT AREA                 C
C                                                                  C
CCCCCCCCCCCCCCCCCCCCCCCCCCCCCCCCCCCCCCCCCCCCCCCCCCCCCCCCCCCCCCCCCC
      IMPLICIT REAL*8(A-H,O-Z)
      COMMON/AREADT/AIN(150),AOUT(150),AVA(500)
      COMMON/COORDN/X(500),DX(500),XLAST(150),COORD(800,2)
     1             ,CLAST(150,2)
      COMMON/ISEGMT/NNODES(150),INDBRA(150),INDPAR(150),INDSTE(150)
      COMMON/NDATA/NS,NT,NCYC
```

```
      COMMON/NODES/NFIRST(150),NLAST(150)
      COMMON/SEGDAT/COMPL0(150),COMPL1(150),SLEN(150),SPG(150)
     1             ,DA(150,2)
      COMMON/TERMZ/RES1(150),RES2(150),CT(150)
C
C
      DO 20 I=1,NS
         SLOPE=(AOUT(I)-AIN(I))/SLEN(I)
         KF=NFIRST(I)
         KL=NLAST(I)
         DO 10 J=KF,KL
            AVA(J)=AIN(I)+SLOPE*(X(J)-X(KF))
   10    CONTINUE
   20 CONTINUE
C
      RETURN
      END
C
C
      SUBROUTINE WALLSHEAR
CCCCCCCCCCCCCCCCCCCCCCCCCCCCCCCCCCCCCCCCCCCCCCCCCCCCCCCCCCCCCCCCCC
C                                                                  C
C      THIS SUBROUTINE CALCULATES THE WALL SHEAR STRESS C
C      COEFFICIENTS CU AND CV AT EACH NODE             C
C                                                                  C
CCCCCCCCCCCCCCCCCCCCCCCCCCCCCCCCCCCCCCCCCCCCCCCCCCCCCCCCCCCCCCCCCC
      IMPLICIT REAL*8(A-H,O-Z)
      COMMON/AREADT/AIN(150),AOUT(150),AVA(500)
      COMMON/FLUPRO/DENS,VISC
      COMMON/ISEGMT/NNODES(150),INDBRA(150),INDPAR(150),INDSTE(150)
      COMMON/NDATA/NS,NT,NCYC
      COMMON/NODES/NFIRST(150),NLAST(150)
      COMMON/PEE/PI
      COMMON/TERMZ/RES1(150),RES2(150),CT(150)
      COMMON/TDATA/DT,FREQ
      COMMON/YOUNG/CV(500),CU(500),PAR1(500)
C
C
C-----SELECTION OF THE HARMONIC TO BE USED ON ALPHA
C-----PARAMETER CALCULATION
```

```
C
      WRITE(*,'(A \)') ' Enter harmonic for alpha parameter: '
      READ(*,*) IHAR
      DO 20 I=1,NS
         KF=NFIRST(I)
         KL=NLAST(I)
         DO 10 J=KF,KL
            A=SQRT(DFLOAT(IHAR)*2.0D0*AVA(J)*FREQ*DENS/VISC)
            IF(A.LT.2.0D0) THEN
               CV(J)=1.0D0
               CU(J)=4.0D0/3.0D0
            ELSE
               CV(J)=1.0863-0.1358*A+0.05626*A**2-0.00487*A**3
     +               +0.00020153*A**4-0.0000032042*A**5
               CU(J)=1.3256+0.029858*A-0.01587*A**2+0.0017947*A**3
     +               -0.000083962*A**4+0.0000014297*A**5
            END IF
            PAR1(J)=8.0D0*CV(J)*PI*VISC*DT/DENS/CU(J)
   10    CONTINUE
   20 CONTINUE
C
      RETURN
      END
C
C
      SUBROUTINE GRAVIT
CCCCCCCCCCCCCCCCCCCCCCCCCCCCCCCCCCCCCCCCCCCCCCCCCCCCCCCCCCCCCCCCC
C                                                               C
C      THIS SUBROUTINE CALCULATES THE BODY FORCE                C
C      PROJECTION ON EACH SEGMENT                               C
C                                                               C
CCCCCCCCCCCCCCCCCCCCCCCCCCCCCCCCCCCCCCCCCCCCCCCCCCCCCCCCCCCCCCCCC
      IMPLICIT REAL*8(A-H,O-Z)
      COMMON/GRAVT/GRAV,GLOAD,GA(2),GZ(500)
      COMMON/NDATA/NS,NT,NCYC
      COMMON/SEGDAT/COMPL0(150),COMPL1(150),SLEN(150),SPG(150)
     1             ,DA(150,2)
C
C
      DO 20 I=1,NS
```

```
      PROJ=0.0D0
      DO 10 J=1,2
            PROJ=PROJ+DA(I,J)*GA(J)
   10    CONTINUE
      GZ(I)=PROJ*GLOAD*GRAV
   20 CONTINUE
C
      RETURN
      END
C
C
      SUBROUTINE STENOSIS
CCCCCCCCCCCCCCCCCCCCCCCCCCCCCCCCCCCCCCCCCCCCCCCCCCCCCCCCCCCCCCCCCC
C                                                                 C
C     THIS SUBROUTINE CALCULATES THE STENOSIS                     C
C     COEFFICIENTS                                                C
C                                                                 C
CCCCCCCCCCCCCCCCCCCCCCCCCCCCCCCCCCCCCCCCCCCCCCCCCCCCCCCCCCCCCCCCCC
      IMPLICIT REAL*8(A-H,O-Z)
      COMMON/AREADT/AIN(150),AOUT(150),AVA(500)
      COMMON/FLUPRO/DENS,VISC
      COMMON/ISEGMT/NNODES(150),INDBRA(150),INDPAR(150),INDSTE(150)
      COMMON/NDATA/NS,NT,NCYC
      COMMON/NODES/NFIRST(150),NLAST(150)
      COMMON/PEE/PI
      COMMON/STENOS/XSTEN(150),STELEN(150),PRC(150)
     1             ,ST1(150),ST2(150),ST3(150)
      COMMON/TDATA/DT,FREQ
C
      REAL*8 KV,KT,KU,LA
C
C
      KU=1.20D00
      KT=1.52D00
      DO 10 I=1,NS
         KS=INDSTE(I)
         IF(KS.EQ.0) GOTO 10
         J=NFIRST(I)+KS-1
         A1=PRC(I)*AVA(J)
         D1=DSQRT(4.0D00*A1/PI)
```

```
          LA=0.83D00*STELEN(I)+1.64D00*D1
          D=DSQRT(4.0D00*AVA(J)/PI)
          KV=3.2D01*(LA/D)*(1.0D00/PRC(I))**2
          ST1(I)=AVA(J)/(DENS*STELEN(I)*KU)
          ST2(I)=-(KV*VISC)/(DENS*STELEN(I)*KU*D)
          ST3(I)=-KT/(2.0D00*KU*STELEN(I)*AVA(J))
     1         *(1.0D00/PRC(I)-1)**2
   10 CONTINUE
C
      RETURN
      END
C
C
      SUBROUTINE INIVAL
CCCCCCCCCCCCCCCCCCCCCCCCCCCCCCCCCCCCCCCCCCCCCCCCCCCCCCCCCCCCCCCCCC
C                                                                 C
C      THIS SUBROUTINE ASSIGNS INITIAL PRESSURE AND               C
C      FLOW VALUES AT EACH NODE                                   C
C                                                                 C
CCCCCCCCCCCCCCCCCCCCCCCCCCCCCCCCCCCCCCCCCCCCCCCCCCCCCCCCCCCCCCCCCC
      IMPLICIT REAL*8(A-H,O-Z)
      COMMON/AREADT/AIN(150),AOUT(150),AVA(500)
      COMMON/BOUND/QBOUN(30,2),PBOUN(30,2)
      COMMON/CONDCT/CONDUCT(150)
      COMMON/COORDN/X(500),DX(500),XLAST(150),COORD(800,2)
     1            ,CLAST(150,2)
      COMMON/FLUPRO/DENS,VISC
      COMMON/GRAVT/GRAV,GLOAD,GA(2),GZ(500)
      COMMON/ISEGMT/NNODES(150),INDBRA(150),INDPAR(150),INDSTE(150)
      COMMON/NBOUN/NQB,NPB
      COMMON/NDATA/NS,NT,NCYC
      COMMON/NODES/NFIRST(150),NLAST(150)
      COMMON/PEE/PI
      COMMON/SEGDAT/COMPL0(150),COMPL1(150),SLEN(150),SPG(150)
     1             ,DA(150,2)
      COMMON/TERMZ/RES1(150),RES2(150),CT(150)
      COMMON/VAINIT/PINIT(500),QINIT(500)
      DIMENSION FL(150),GFL(150)
C
C-----CALCULATE THE TOTAL CONDUCTANCE FIRST (RTOTAL=1/CONDUCTANCE)
```

```
C
C--------CALCULATE THE CONDUCTANCE AT THE TERMINAL BRANCHES FIRST
C
      DO 10 I=1,NS
         IF (INDBRA(I).GT.0) GOTO 5
         CONDUCT(I)=1.0D00/(RES1(I)+RES2(I)
     1                      +8.0D00*VISC*SLEN(I)*PI/AOUT(I)**2)
    5    CONTINUE
   10 CONTINUE
C
C--------CALCULATE CONDUCT(I) FOR THE REST OF THE SEGMENTS
C
      DO 20 I=NS,1,-1
         K=INDBRA(I)
         IF (K.EQ.0) GOTO 15
         CONDUCT(I)=1.0D00/(1.0D00/(CONDUCT(K)+CONDUCT(K+1))
     1                      +8.0D00*VISC*PI*SLEN(I)/AOUT(I)**2)
   15    CONTINUE
   20 CONTINUE
C
C--------THE TOTAL RESISTANCE IS THE INVERSE OF THE
C--------CONDUCTIVITY OF THE FIRST SEGMENT
C
      RTOTAL=1.0D00/CONDUCT(1)
C
C
C-----FIX PROXIMAL P AND Q
C
      IF(NPB.GT.0) THEN
         PR=FPRES(0.0D00)
         FL(1)=PBOUN(1,1)/RTOTAL
      ELSE
         FL(1)=FFLOW(0.0D0)
         PR=QBOUN(1,1)*RTOTAL
      END IF
C
C
C-----ASSIGN INITIAL FLOW VALUES BY DIVIDING Q
C-----ACCORDING TO THE CONDUCTIVITY OF EACH ELEMENT
C
```

```
      DO 30 I=1,NS
         IF (INDBRA(I).EQ.0) GOTO 25
         IB1=INDBRA(I)
         IB2=IB1+1
         FL(IB1)=FL(I)*CONDUCT(IB1)/(CONDUCT(IB1)+CONDUCT(IB2))
         FL(IB2)=FL(I)-FL(IB1)
   25    CONTINUE
   30 CONTINUE
C
C-----ADD TO THE INITIAL FLOW VALUES THE PORTION COMING FROM
C-----THE BODY FORCE TERM
C
      DO 40 I=1,NS
         IF(INDBRA(I).GT.0) GOTO 35
            HEAD=CLAST(I,1)*GA(1)+CLAST(I,2)*GA(2)
            GFL(I)=DENS*GRAV*GLOAD*HEAD*CONDUCT(I)
   35    CONTINUE
   40 CONTINUE
      DO 50 I=NS,1,-1
         K=INDBRA(I)
         IF (K.EQ.0) GOTO 50
            GFL(I)=GFL(K)+GFL(K+1)
   50 CONTINUE
C
C-----ASSIGN INITIAL PRESSURE PINIT(I) AND FLOW QINIT(I) VALUES
C     TO ALL NODES
C
      K=0
      DO 70 I=1,NS
         KF=NFIRST(I)
         KL=NLAST(I)
         DO 60 J=KF,KL
            PINIT(J)=PR
            QINIT(J)=FL(I)+GFL(I)
   60    CONTINUE
   70 CONTINUE
C
C-----PRINT OUT INITIAL VALUES FOR ALL NODES
C
      WRITE (6,1000)
```

```
      DO 80 K=1,NT,2
         L=K+1
         WRITE (6,2000) (I,PINIT(I),QINIT(I),I=K,L)
   80 CONTINUE
C
      RETURN
C
 1000 FORMAT(//,15X,'INITIAL PRESSURE AND FLOW VALUES',/)
 2000 FORMAT(2(1X,I3,2X,2(D12.5,1X)))
C
      END
C
C
      SUBROUTINE SOLVE
CCCCCCCCCCCCCCCCCCCCCCCCCCCCCCCCCCCCCCCCCCCCCCCCCCCCCCCCCCCCCCCCCC
C     THIS SUBROUTINE SOLVES THE SYSTEM OF EQUATIONS       C
C     RESULTING FROM THE APPLICATION OF THE IMPLICIT       C
C     FINITE DIFFERENCE METHOD ON THE GOVERNING EQUATIONS. C
C     THE MATRICES ARE FORMED FIRST ARRANGED SO THAT A     C
C     TRIDIAGONAL BLOCK MATRIX SOLVER CAN BE EMPLOYED      C
C     TO SOLVE THE SYSTEM OF EQUATIONS.                    C
CCCCCCCCCCCCCCCCCCCCCCCCCCCCCCCCCCCCCCCCCCCCCCCCCCCCCCCCCCCCCCCCCC
      IMPLICIT REAL*8(A-H,O-Z)
      COMMON/AREADT/AIN(150),AOUT(150),AVA(500)
      COMMON/COORDN/X(500),DX(500),XLAST(150),COORD(800,2)
     1             ,CLAST(150,2)
      COMMON/FLUPRO/DENS,VISC
      COMMON/YOUNG/CV(500),CU(500),PAR1(500)
      COMMON/GRAVT/GRAV,GLOAD,GA(2),GZ(500)
      COMMON/ISEGMT/NNODES(150),INDBRA(150),INDPAR(150),INDSTE(150)
      COMMON/NBOUN/NQB,NPB
      COMMON/NDATA/NS,NT,NCYC
      COMMON/NODES/NFIRST(150),NLAST(150)
      COMMON/PEE/PI
      COMMON/SEGDAT/COMPL0(150),COMPL1(150),SLEN(150),SPG(150)
     1             ,DA(150,2)
      COMMON/STENOS/XSTEN(150),STELEN(150),PRC(150)
     1             ,ST1(150),ST2(150),ST3(150)
      COMMON/TERMZ/RES1(150),RES2(150),CT(150)
      COMMON/TDATA/DT,FREQ
```

```
      COMMON/VAINIT/PINIT(500),QINIT(500)
C
      DIMENSION P(500),Q(500),PAVG(500),PMAX(500),PMIN(500)
     +                        ,QAVG(500),QMAX(500),QMIN(500)
      DIMENSION NPLT(10)
C
C-----DEFINE NODES TO BE PLOTTED
C
      WRITE(*,'(A \)') ' Enter number of nodes to be plotted: '
      READ(*,*) NNP
      WRITE(*,'(A \)') ' Enter nodes to be plotted: '
      READ(*,*) (NPLT(I), I=1,NNP)
      WRITE(*,'(A \)') ' Neglect convective acceleration? (1=yes): '
      READ(*,*) NCA
      IF(NCA.EQ.1) CACF=0.0D0
C
C-----INITIALIZE MAXIMUM AND MINIMUM P AND Q VALUES
C
      DO I=1,NT
         PMAX(I)=0.D0
         QMAX(I)=0.D0
         PMIN(I)=1.D10
         QMIN(I)=1.D10
      END DO
C
C-----NTS: NUMBER OF TIME STEPS
C-----NTSPC: NUMBER OF TIME STEPS PRE CYCLE
C-----NLC: TIME STEP AFTER WHICH LAST CYCLE BEGINS
C
      NTS=IDNINT(NCYC/(DT*FREQ))
      NTSPC=NTS/NCYC
      NLC=NTS-NTSPC
      IPRN=NTS/NCYC/100
C
C-----COPY THE INITIAL VALUES TO D VECTOR
C-----TO START THE INTEGRATION PROCEDURE
C
      DO 10 J=1,NT
         P(J)=PINIT(J)
         Q(J)=QINIT(J)
```

```
   10 CONTINUE
C
C-----START THE SOLUTION - MARCH IN TIME
C
      DO 50 IT=1,NTS
         TIME=IT*DT
C
         DO 30 I=1,NS
C
            NF=NFIRST(I)
            NL=NLAST(I)
C
C-----------WRITE OUT THE EQUATIONS FOR THE FIRST NODE
C
            IF (NF.EQ.1) THEN
C
C--------------PROXIMAL END CONDITION
C
               IF (NPB.GT.0) THEN
C
C-----------------PROXIMAL PRESSURE PRESCRIBED
C
                  P(NF)=FPRES(TIME)
                  Q(NF)=(1.0D0-PAR1(NF)/AVA(NF))*Q(NF)
     1                    -DT/(CU(NF)*DENS)/DX(NF)*AVA(NF)*
     2                    (P(NF+1)-P(NF))
     3                   +AVA(NF)*GZ(I)*DT/CU(NF)
               ELSE
                  Q(NF)=FFLOW(TIME)
                  P(NF)=P(NF)-DT/(COMPL0(I)+COMPL1(I)*P(NF))
     1                /DX(NF)/AVA(NF)*(Q(NF+1)-Q(NF))
               END IF
            ELSE
C
C--------------NODE AT BEGINNING OF A BRANCH
C
               P(NF)=P(NLAST(INDPAR(I)))
               Q(NF)=(1.0D0-PAR1(NF)/AVA(NF))*Q(NF)
     1               -DT/(CU(NF)*DENS)/DX(NF)*AVA(NF)*
     2               (P(NF+1)-P(NF))
```

```
     3               +AVA(NF)*GZ(I)*DT/CU(NF)
            END IF
C
C-----------WRITE OUT THE EQUATIONS FOR INTERIOR NODES
C-----------(BETWEEN FIRST AND LAST) OF EACH SEGMENT
C
            IS=INDSTE(I)
            IF(IS.EQ.0) THEN
C--------------NO STENOSES
               DO 20 J=NF+1,NL-1
                  P(J)=P(J)-DT/(COMPL0(I)+COMPL1(I)*P(J))
     1                /DX(J)/AVA(J)*(Q(J)-Q(J-1))
                  Q(J)=(1.0D0-PAR1(J)/AVA(J))*Q(J)
     1                -DT/(CU(J)*DENS)/DX(J)*AVA(J)*(P(J+1)-P(J))
     2                -CACF*DT/(CU(J)*DX(J))*(Q(J)**2/AVA(J)
     3                -Q(J-1)**2/AVA(J-1))
     4                 +AVA(J)*GZ(I)*DT/CU(J)
   20          CONTINUE
            ELSE
C
C--------------STENOSES PRESENT
C
C--------------EQUATIONS FOR NODES BEFORE THE STENOSIS
C
               DO 22 J=NF+1,NF+IS-2
                  P(J)=P(J)-DT/(COMPL0(I)+COMPL1(I)*P(J))
     1                 /DX(J)/AVA(J)*(Q(J)-Q(J-1))
                  Q(J)=(1.0D0-PAR1(J)/AVA(J))*Q(J)
     1                -DT/(CU(J)*DENS)/DX(J)*AVA(J)*(P(J+1)-P(J))
     2                -CACF*DT/(CU(J)*DX(J))*(Q(J)**2/AVA(J)
     3                -Q(J-1)**2/AVA(J-1))
     4                 +AVA(J)*GZ(I)*DT/CU(J)
   22          CONTINUE
C
C--------------EQUATIONS FOR PROXIMAL NODE OF STENOSIS
C
               J=NF+IS-1
               P(J)=P(J)-DT/AVA(J)/(COMPL0(I)+COMPL1(I)*P(J))
     1              /DX(J-1)*(Q(J)-Q(J-1))
C
```

```
C--------------STENOSIS EQUATION
C
               Q(J)=Q(J)+DT*(ST1(I)*(P(J)-P(J+1))+ST2(I)*Q(J)
     1              +ST3(I)*Q(J)*DABS(Q(J)))
C
C--------------EQUATIONS FOR DISTAL NODE OF STENOSIS
C
               J=NF+IS
               P(J)=P(J)-DT/AVA(J)/(COMPL0(I)+COMPL1(I)*P(J))
     1              /DX(J)*(Q(J+1)-Q(J))
               Q(J)=Q(J-1)
C
C--------------EQUATIONS FOR NODES DISTAL TO STENOSIS
C
               DO 24 J=NF+IS+1,NL-1
                  P(J)=P(J)-DT/(COMPL0(I)+COMPL1(I)*P(J))
     1                 /DX(J)/AVA(J)*(Q(J)-Q(J-1))
                  Q(J)=(1.0D0-PAR1(J)/AVA(J))*Q(J)
     1                -DT/(CU(J)*DENS)/DX(J)*AVA(J)*(P(J+1)-P(J))
     2                -CACF*DT/(CU(J)*DX(J))*(Q(J)**2/AVA(J)
     3                -Q(J-1)**2/AVA(J-1))
     4                 +AVA(J)*GZ(I)*DT/CU(J)
   24            CONTINUE
            END IF
C
C-----------WRITE OUT THE EQUATIONS FOR THE LAST NODE
C
            IF (INDBRA(I).EQ.0) THEN
C
C--------------CASE A. THE SEGMENT ENDS AT A TERMINAL IMPEDANCE
C
               POLD=P(NL)
               IF(CT(I).EQ.0.0D0) THEN
C
C-----------------CASE A.1 SIMPLE RESISTANCE
C
                  P(NL)=P(NL)-DT/(COMPL0(I)+COMPL1(I)*P(NL))
     1                 /DX(NL-1)/AVA(NL)*(Q(NL)-Q(NL-1))
                  Q(NL)=P(NL)/(RES1(I)+RES2(I))
               ELSE
```

```
C
C-----------------CASE A.2 WINDKESSEL MODEL
C
                  P(NL)=P(NL)-DT/(COMPL0(I)+COMPL1(I)*P(NL))
     1                  /DX(NL-1)/AVA(NL)*(Q(NL)-Q(NL-1))
                  Q(NL)=Q(NL)+(P(NL)-POLD)/RES1(I)
     1                  +DT/(RES1(I)*RES2(I)*CT(I))*P(NL)
     2                  -DT*(1.0D0+RES1(I)/RES2(I))/(RES1(I)*CT(I))
     3                  *Q(NL)
               END IF
            ELSE
C
C--------------CASE B. THE SEGMENT BIFURCATES
C
                  P(NL)=P(NL)-DT/(COMPL0(I)+COMPL1(I)*P(NL))
     1                  /DX(NL-1)/AVA(NL)*(Q(NL)-Q(NL-1))
            END IF
   30    CONTINUE
C
C--------APPLY BRANCH FLOW CONDITION
C
         DO 35 I=1,NS
            NL=NLAST(I)
            NF1=NFIRST(INDBRA(I))
            NF2=NFIRST(INDBRA(I)+1)
            IF(INDBRA(I).NE.0) Q(NL)=Q(NF1)+Q(NF2)
   35    CONTINUE
C
         IF(IT.GT.NLC) THEN
            DO I=1,NT
               PAVG(I)=PAVG(I)+P(I)
               QAVG(I)=QAVG(I)+Q(I)
               IF(P(I).GT.PMAX(I)) PMAX(I)=P(I)
               IF(Q(I).GT.QMAX(I)) QMAX(I)=Q(I)
               IF(P(I).LT.PMIN(I)) PMIN(I)=P(I)
               IF(Q(I).LT.QMIN(I)) QMIN(I)=Q(I)
            END DO
         ELSE
            CONTINUE
         END IF
```

```
C
C
C--------PRINT OUT THE NODAL VALUES OF PRESSURE AND FLOW
C--------(PRINT OUT ONLY 100 POINTS PER CYCLE)
C
         ICHECK=IT/IPRN
         IF(ICHECK*IPRN.NE.IT) GOTO 68
         WRITE (*,'(F7.4)') TIME
         WRITE (8,3000) TIME,(P(NPLT(J))/1.D3,Q(NPLT(J))*1.D6,
     1     J=1,NNP)
   40    CONTINUE
   68    CONTINUE
   50 CONTINUE
C
C-----CALCULATE AVERAGE VALUES
C
      DO I=1,NT
         PAVG(I)=PAVG(I)/DFLOAT(NTSPC)
         QAVG(I)=QAVG(I)/DFLOAT(NTSPC)
         WRITE(7,4000)
        1  I,PAVG(I),QAVG(I),PMAX(I),QMAX(I),PMIN(I),QMIN(I)
      END DO
      RETURN
C
 2000 FORMAT(//' TIME = ',D10.4)
 3000 FORMAT(1X,E10.4,10(2X,E10.4))
 4000 FORMAT(1X,I3,6(2X,E10.4))
C
      END
C
C
      FUNCTION FPRES(T1)
CCCCCCCCCCCCCCCCCCCCCCCCCCCCCCCCCCCCCCCCCCCCCCCCCCCCCCCCCCCCCCCCCC
C                                                                 C
C     THIS FUNCTION PROVIDES THE INITIAL VALUE OF                 C
C     THE PRESSURE AT TIME T1                                     C
C                                                                 C
CCCCCCCCCCCCCCCCCCCCCCCCCCCCCCCCCCCCCCCCCCCCCCCCCCCCCCCCCCCCCCCCCC
      IMPLICIT REAL*8(A-H,O-Z)
      COMMON/BOUND/QBOUN(30,2),PBOUN(30,2)
```

```
      COMMON/NBOUN/NQB,NPB
      COMMON/PEE/PI
      COMMON/TDATA/DT,FREQ
C
      P=PBOUN(1,1)
      DO 10 I=2,NPB
         ARG=2.0D00*PI*(I-1)*FREQ*T1
         P=P+PBOUN(I,1)*DCOS(ARG)+PBOUN(I,2)*DSIN(ARG)
   10 CONTINUE
      FPRES=P
C
      RETURN
      END
C
C
      FUNCTION FFLOW(T1)
CCCCCCCCCCCCCCCCCCCCCCCCCCCCCCCCCCCCCCCCCCCCCCCCCCCCCCCCCCCCCCCCCC
C                                                                  C
C     THIS FUNCTION PROVIDES THE INITIAL VALUE OF                  C
C     THE FLOW AT TIME T1                                          C
C                                                                  C
CCCCCCCCCCCCCCCCCCCCCCCCCCCCCCCCCCCCCCCCCCCCCCCCCCCCCCCCCCCCCCCCCC
      IMPLICIT REAL*8(A-H,O-Z)
      COMMON/BOUND/QBOUN(30,2),PBOUN(30,2)
      COMMON/NBOUN/NQB,NPB
      COMMON/PEE/PI
      COMMON/TDATA/DT,FREQ
C
      Q=QBOUN(1,1)
      DO 10 I=2,NQB
         ARG=2.0D00*PI*(I-1)*FREQ*T1
         Q=Q+QBOUN(I,1)*DCOS(ARG)+QBOUN(I,2)*DSIN(ARG)
   10 CONTINUE
      FFLOW=Q
C
      RETURN
      END
```

FLOW

Written by Douglas Cornet, FLOW takes the Fourier coefficients of the proximal flow condition contained in CONTROL 0.DAT and calculates new Fourier coefficients for any desired heart frequency. Systolic and diastolic duration times are modified separately. Duration times are calculated by a linear interpolation of systolic and diastolic duration data supplied in Ganong (1989).

After the new waveform for a given heart rate has been established, any reductions in stroke volume (mean flow) are input and the waveforms recalculated. The roundabout way of doing this is because reductions in stroke volume are measured on a beat-by-beat basis while the Fourier coefficients measure mean flow on a unit time basis. First the mean flow for the new heart rate, based on the "normal" stroke volume are calculated. Then the waveform is reconfigured to reflect a lower stroke volume, if necessary. The output of FLOW is the new Fourier coefficients as well as a plot file of the old and new waveforms for user use.

FLOW cannot handle bradycardia (heart rates less than 60).

This program is intended to be integrated with PQYPLOT as a subroutine. Plotfile outputs and all intermediate waveform outputs will be eliminated prior to its integration. Presented below is the source code in Microsoft FORTRAN (version 5.0) format.

```
C  FLOW.FOR
C  Program recalculates fourier coefficients given an original set
C  of fourier coefficients, a new heart rate (frequency shift), and
C  a new systolic/diastolic time ratio for the new heart rate.
C
C  Base heart rate is 60 bpm (nu = 1.0 cycles/s).  New HR range is
```

```
C  60-200 bpm.

C  File management hardwired for Ben Dehner's 386-33 MHz machine.

C  File management and variable definition

      Implicit Real*8 (a-h,o-z)
      Character*30 infile,pltfile,outfile,inf,plf,otf

      Dimension a(21),b(21),a2(21),b2(21),f(20001)

      pi = 4.0d0 * datan(1.0d0)

      write (*,*) 'Startup Activites...'

      infile = 'flow.dat'
      pltfile = 'flow.plt'
      outfile = 'flow.out'
      inf = 'f:\dac\files\'//infile
      plf = 'f:\dac\files\'//pltfile
      otf = 'f:\dac\files\'//outfile
      open (unit=5,file=inf,status='unknown')
      open (unit=6,file=plf,status='unknown')
      open (unit=7,file=otf,status='unknown')

C  Initial frequency is 1 cycle/second.
      freq = 1.0d0
      p = 1.0d0/freq

      write (*,*) 'Enter new frequency'
      read (*,*) freq2
      write (*,38)
      p2 = 1.0d0/freq2
   38     format (1x,/)

C  Input Basal Heart Rate Fourier Coefficients (Nik, 1990)
      write (*,*) 'Reading Basal Heart Rate Fourier Coefficients...'

      read (5,50) npb,nqb
      do 40 i = 1,nqb
```

```
                read (5,60) a(i),b(i)
   40       continue
   50       format (/2(2x,i3)//)
   60       format (2(2x,D12.5))

C  Initialize arrays
     write (*,*) 'Initializing...'

     do 70 i = 1,10001,1
                f(i) = 0.0d0
  70 continue
     ksv = 0

C  Calculate function using fourier series and store in an array
C  Plot Original Proximal Flow Condition
     write (*,*) 'Calculating Function...'
     write (6,*) 'Original Proximal Flow Condition'

     do 200 i = 1,10001,1
                t = dfloat(i)*0.0001d0*p-0.0001d0
                f(i) = a(1)
                do 100 n = 2,nqb,1
                   arg = 2.0d0*dfloat(n-1)*freq*pi*t
                   f(i) = f(i)+a(n)*dcos(arg)+b(n)*dsin(arg)
  100           continue
  200       continue

C  Remove '*' comment symbols to enable

* 250       write (*,*) 'Plotting...'
*     do 300 i = 1,10001,100
*                t = dfloat(i)*0.0001d0*p-0.0001d0
*                write (6,900) t,f(i)
* 300       continue

C  Compression and re-expansion of the proximal flow pulse to proper
C  period and systolic/diastolic time ratio for the given heart
C  rate.

C  Calculate new systolic and diastolic times
```

```
C  Systolic durations interpolated from Ganong, 1989
C  Normalize compressed flow pulse

      hr = freq2*60.0d0
      rk = p/p2
      tsys = (-1.333333333333d-03 * hr + 0.370d0)*1.8966d0*rk
                tdias = p-tsys

C  Remapping of flow pulse
C  Expanding forward and backward from beginning of systole
C  (arbitrarily)

      write (*,*) 'Remapping...'

      kpts = (tsys-0.550d0)/2.0d0*10000.0d0
      k1 = (2750.0d0/dfloat(kpts)) + 1.0d0
      k2 = 2750.0d0/(dfloat(kpts)-int(2750.0d0/k1))

C  Forward

      kk1 =
      kk2 = 0
      do 330 i = 2100,7700,1
                kk1 = kk1 + 1
                kk2 = kk2 + 1
                if (kk1.gt.k1) then
                                kk1 = 0
                                do 310 j = 10000,(i+1),-1
                                   f(j+1) = f(j)
  310                           continue
                                f(i) = f(i-1)
                elseif (kk2.gt.k2) then
                                kk2 = -1
                                do 320 j = 10000,(i+1),-1
                                   f(j+1) = f(j)
  320                           continue
                                f(i) = f(i-1)
                else
                                f(i) = f(i)
                endif
```

```
  330     continue

C  Reverse
      write (*,*) 'Still Remapping...'

      kk1 = 0
      kk2 = 0
      do 360 i = 2049,2000,-1
                kk1 = kk1 + 1
                kk2 = kk2 + 1
                if (kk1.gt.k1) then
                   kk1 = 0
                   do 340 j= 2,(i-1),1
                        f(j-1) = f(j)
  340              continue
                   f(i) = f(i+1)
                else
                   if (kk2.gt.k2) then
                         kk2 = -1
                         do 350 j = 2,(i-1),1
                    f(j-1) = f(j)
  350                    continue
                            f(i) = f(i+1)
                    else
                         f(i) = f(i)
                    endif
                endif
  360     continue

C  Plot Remapped flow pulse
C  Remove '*' comment symbols to enable
*     write (*,*) 'Plotting...'
*     write (6,*) ' Remapped pulse'

*     do 362 i = 1,(10001),100
*               t = dfloat(i)*0.0001d0*p-0.0001d0
*               write (6,900) t,f(i)
* 362     continue

C  Integration of fourier coefficient integrals
```

```
      write (*,365)
  365     format (//,1x,'First Pass')

  370     write (*,*) 'Integrating...'
      write (7,510) npb,nqb

      do 500 n = 1,nqb,1
                sum1 = 0.0d0
                sum2 = 0.0d0
                do 400 i = 1,10001,1
                 t = 0.0001d0 * dfloat(i)*p-0.0001d0

                 if ((dfloat(i)/2.0d0).eq.(i/2)) cf = 4.0d0
                 if ((dfloat(i)/2.0d0).ne.(i/2)) cf = 2.0d0
                 if (i.eq.1.or.i.eq.10001) cf = 1.0d0

                 sum1=sum1+cf*f(i)*dcos(dfloat(n-1)*2.d0*pi*freq*t)
                 sum2=sum2+cf*f(i)*dsin(dfloat(n-1)*2.d0*pi*freq*t)
  400               continue
               a2(n) = 2.0d0*sum1/30003.0d0
               b2(n) = 2.0d0*sum2/30003.0d0
               if (n.eq.1) a2(1) = a2(1)/2.0d0
               write (7,1000) a2(n),b2(n)
  500     continue
  510          format (3x,'npb  nqb',/,2(2x,i3)//6x,'Q cos term'
      1        ,5x,'Q sin term')

C  Enter new stroke volume, if +Gz applications
C  Adjust amplitudes for new stroke volume.  Must re-remap and
C  reintegrate
      ksv = ksv + 1
      if (ksv.lt.2) then
sv = a2(1)*1.0e+6/freq2
         write (*,525) sv
  525    format (/,1x,'Stroke Volume is presently ',f9.4,' ml')
         write (*,*) 'Enter new Stroke Volume'
         read (*,*) sv2
         sv = sv*1.0e-6
         sv2 = sv2*1.0e-6
         write (*,540)
```

```
 540   format (//,1x,'Second Pass')
       fsv = 1.0d0 + (sv2-sv)/sv
       print*,'fsv = ',fsv
       write (*,*) 'Re-remapping...'
       do 550 i = 1,10001,1
           if (f(i).gt.10.0e-06) f(i) = f(i) * fsv
           if (f(i).lt.-10.0e-06) f(i) = f(i) * fsv
 550   continue
       goto 370
    endif

C  Plot out new Proximal Flow Condition
C  Remove '*' comment symbols to enable
*    write (*,*) 'Plotting...'
*    write (6,*) 'How pqyplot sees it'

*    do 700 i = 1,10001,100
*               t = dfloat(i)*0.0001d0*p2-0.0001d0
*               f(i) = a2(1)
*               do 600 n = 2,nqb,1
*                  arg = 2.0d0*dfloat(n-1)*freq2*pi*t
*                  f(i)=f(i)+a2(n)*dcos(arg)+b2(n)*dsin(arg)
* 600           continue
*               write (6,900) t,f(i)
* 700     continue
  900     format (1x,f5.3,4x,e12.5)
 1000     format (2(2x,e12.5e1))

    close (unit=5)
    close (unit=6)
    close (unit=7)
    stop
    end
```

CONTROL 0

CONTROL 0 is a sample input file used by PQYPLOT that contains the vascular geometry, arterial wall and blood mechanical properties, stenosis (if any), the Fourier coefficients of the proximal flow condition, and any external body forces to be modelled.

The data in this sample file is the Standard Man supine case as defined by Stergiolpulos (1990) and shown discussed in Chapter Four.

```
NUMBER OF SEGMENTS
 55
```

SEG#	BRAN	PARNT	STN	#NOD	SEGMT LENGTH	INPUT AREA	OUTPUT AREA
1	2	0	0	2	4.00000E-2	6.78866E-4	6.51440E-4
2	14	1	0	2	2.00000E-2	3.94081E-4	3.94081E-4
3	4	1	0	3	3.40000E-2	1.20763E-4	1.20763E-4
4	6	3	0	3	3.40000E-2	5.62122E-5	5.62122E-5
5	12	3	0	5	1.77000E-1	4.30084E-5	4.30084E-5
6	0	4	0	5	1.48000E-1	1.11036E-5	1.05209E-5
7	8	4	0	9	4.22000E-1	5.10222E-5	1.74974E-5
8	0	7	0	6	2.35000E-1	9.51148E-6	6.33470E-6
9	10	7	0	4	6.70000E-2	1.45220E-5	1.45220E-5
10	0	9	0	4	7.90000E-2	2.60155E-6	2.60155E-6
11	0	9	0	5	1.71000E-1	1.29462E-5	1.05209E-5
12	0	5	0	5	1.77000E-1	9.84229E-6	2.16424E-6
13	0	5	0	5	1.77000E-1	9.84229E-6	2.16424E-6
14	18	2	0	2	3.90000E-2	3.59681E-4	3.59681E-4
15	16	2	0	6	2.08000E-1	4.30084E-5	4.30084E-5
16	0	15	0	5	1.77000E-1	9.84229E-6	2.16424E-6
17	0	15	0	5	1.77000E-1	9.84229E-6	2.16424E-6
18	26	14	0	3	5.20000E-2	3.13531E-4	3.13531E-4
19	20	14	0	2	3.40000E-2	5.62122E-5	5.62122E-5
20	0	19	0	5	1.48000E-1	1.11036E-5	1.05209E-5
21	22	19	0	9	4.22000E-1	5.10222E-5	1.74974E-5
22	0	21	0	6	2.35000E-1	9.51148E-6	6.33470E-6

23	24	21	0	4	6.70000E-2	1.45220E-5	1.45220E-5
24	0	23	0	4	7.90000E-2	2.60155E-6	2.60155E-6
25	0	23	0	5	1.71000E-1	1.29462E-5	1.05209E-5
26	0	18	0	4	8.00000E-2	1.25664E-5	7.06858E-6
27	28	18	0	5	1.04000E-1	1.43139E-4	1.30698E-4
28	34	27	0	3	5.30000E-2	1.16899E-4	1.16899E-4
29	30	27	0	2	1.00000E-2	4.77836E-5	4.77836E-5
30	32	29	0	2	1.00000E-2	1.25664E-5	1.25664E-5
31	0	29	0	3	6.60000E-2	1.52053E-5	1.52053E-5
32	0	30	0	3	7.10000E-2	1.01788E-5	1.01788E-5
33	0	30	0	3	6.30000E-2	2.37583E-5	2.37583E-5
34	0	28	0	4	5.90000E-2	5.94467E-5	5.94467E-5
35	36	28	0	2	1.00000E-2	1.13097E-4	1.13097E-4
36	0	35	0	2	3.20000E-2	2.12371E-5	2.12371E-5
37	38	35	0	2	1.00000E-2	1.09359E-4	1.09359E-4
38	0	37	0	2	3.20000E-2	2.12371E-5	2.12371E-5
39	40	37	0	5	1.06000E-1	1.05683E-4	9.43432E-5
40	0	39	0	3	5.00000E-2	8.04247E-6	8.04247E-6
41	42	39	0	2	1.00000E-2	8.49486E-5	8.49486E-5
42	44	41	0	3	5.82000E-2	4.25447E-5	3.85000E-5
43	50	41	0	3	5.82000E-2	4.25447E-5	3.85000E-5
44	46	42	0	4	1.44000E-1	3.21700E-5	2.29022E-5
45	0	42	0	3	5.00000E-2	1.25660E-5	1.25660E-5
46	48	44	0	9	4.43000E-1	2.10741E-5	1.13411E-5
47	0	44	0	4	1.26000E-1	2.04282E-5	1.08686E-5
48	0	46	0	8	3.21000E-1	1.91665E-5	6.24580E-6
49	0	46	0	8	3.43000E-1	5.30929E-6	5.30929E-6
50	52	43	0	4	1.44000E-1	3.21700E-5	2.29022E-5
51	0	43	0	3	5.00000E-2	1.25660E-5	1.25660E-5
52	54	50	0	9	4.43000E-1	2.10741E-5	1.13411E-5
53	0	50	0	4	1.26000E-1	2.04282E-5	1.08686E-5
54	0	52	0	8	3.21000E-1	1.91665E-5	6.24580E-6
55	0	52	0	8	3.43000E-1	5.30929E-6	5.30929E-6

SEG#	COMPLO	COMPL1	SEEPAGE	ORIENTATION ANGLE
1	-.48530E-6	3.0794E-09	0.00000D+0	0.09000D+3
2	1.16650E-6	2.8208E-09	0.00000D+0	0.00000D+3
3	4.98820E-6	2.1620E-09	0.00000D+0	0.13500D+3
4	7.15050E-6	1.7170E-09	0.00000D+0	0.18000D+3
5	7.74630E-6	1.5746E-09	0.00000D+0	0.09000D+3

6	7.66060E-6	2.2096E-10	0.00000D+0	0.12000D+3
7	9.26730E-6	1.0976E-09	0.00000D+0	0.24000D+3
8	7.45900E-6	2.0325E-10	0.00000D+0	0.24000D+3
9	8.05040E-6	2.6030E-10	0.00000D+0	0.24000D+3
10	3.88430E-6	3.8352E-11	0.00000D+0	0.24000D+3
11	7.88450E-6	2.4264E-10	0.00000D+0	0.24000D+3
12	6.84260E-6	1.5751E-10	0.00000D+0	0.09000D+3
13	6.84260E-6	1.5751E-10	0.00000D+0	0.13500D+3
14	1.55090E-6	2.7589E-09	0.00000D+0	0.00000D+3
15	7.74680E-6	1.5745E-09	0.00000D+0	0.06000D+3
16	6.84260E-6	1.5751E-10	0.00000D+0	0.09000D+3
17	6.84260E-6	1.5751E-10	0.00000D+0	0.04500D+3
18	2.02360E-6	2.6817E-09	0.00000D+0	0.27000D+3
19	7.15050E-6	1.7170E-09	0.00000D+0	0.04500D+3
20	7.66060E-6	2.2096E-10	0.00000D+0	0.06000D+3
21	9.26730E-6	1.0976E-09	0.00000D+0	0.30000D+3
22	7.45900E-6	2.0325E-10	0.00000D+0	0.30000D+3
23	8.05040E-6	2.6030E-10	0.00000D+0	0.30000D+3
24	3.88430E-6	3.8352E-11	0.00000D+0	0.30000D+3
25	7.88450E-6	2.4264E-10	0.00000D+0	0.30000D+3
26	5.54300E-7	2.9180E-09	0.00000D+0	0.00000D+3
27	4.59810E-6	2.2348E-09	0.00000D+0	0.27000D+3
28	4.95530E-6	2.1683E-09	0.00000D+0	0.27000D+3
29	7.56190E-6	1.6201E-09	0.00000D+0	0.00000D+3
30	8.38010E-6	1.2662E-09	0.00000D+0	0.00000D+3
31	9.36680E-6	1.0505E-09	0.00000D+0	0.31500D+3
32	9.63070E-6	8.7312E-10	0.00000D+0	0.45000D+3
33	8.87870E-6	1.2487E-09	0.00000D+0	0.00000D+3
34	6.96760E-6	1.7584E-09	0.00000D+0	0.22500D+3
35	3.09500E-6	2.5017E-09	0.00000D+0	0.27000D+3
36	8.99390E-6	1.2077E-09	0.00000D+0	0.00000D+3
37	3.59640E-6	2.4148E-09	0.00000D+0	0.27000D+3
38	8.99390E-6	1.2077E-09	0.00000D+0	0.00000D+3
39	5.59580E-6	2.0450E-09	0.00000D+0	0.27000D+3
40	9.68730E-6	7.7582E-10	0.00000D+0	0.27000D+3
41	-.25920E-5	3.3951E-09	0.00000D+0	0.27000D+3
42	9.68961E-6	7.59771-10	0.00000D+0	0.31500D+3
43	9.68961E-6	7.59771-10	0.00000D+0	0.22500D+3
44	-.64348E-6	3.10359-09	0.00000D+0	0.31500D+3
45	-.18647E-4	5.51695-09	0.00000D+0	0.27000D+3

46	9.68610E-6	7.2179E-10	0.00000D+0	0.27000D+3
47	4.88360E-6	6.5690E-11	0.00000D+0	0.31500D+3
48	4.65380E-6	5.8506E-11	0.00000D+0	0.27000D+3
49	4.07200E-6	4.2755E-11	0.00000D+0	0.27000D+3
50	-.64348E-6	3.10359-09	0.00000D+0	0.22500D+3
51	-.18647E-4	5.51695-09	0.00000D+0	0.27000D+3
52	9.68610E-6	7.2179E-10	0.00000D+0	0.27000D+3
53	4.88360E-6	6.5690E-11	0.00000D+0	0.22500D+3
54	4.65380E-6	5.8506E-11	0.00000D+0	0.27000D+3
55	4.07200E-6	4.2755E-11	0.00000D+0	0.27000D+3

SEG	RES1	RES2	CT
6	.12020E+10	.48080E+10	.30955E-10
8	.10560E+10	.42240E+10	.35235E-10
10	.16860E+11	.67440E+11	.22069E-11
11	.10560E+10	.42240E+10	.35235E-10
12	.27800E+10	.11120E+11	.13384E-10
13	.27800E+10	.11120E+11	.13384E-10
16	.27800E+10	.11120E+11	.13384E-10
17	.27800E+10	.11120E+11	.13384E-10
20	.12020E+10	.48080E+10	.30955E-10
22	.10560E+10	.42240E+10	.35235E-10
24	.16860E+11	.67440E+11	.22069E-11
25	.10560E+10	.42240E+10	.35235E-10
26	.27800E+09	.11120E+10	.13384E-09
31	.72600E+09	.29040E+10	.51251E-10
32	.10820E+10	.43280E+10	.34389E-10
33	.46400E+09	.18560E+10	.80191E-10
34	.18600E+09	.74400E+09	.20005E-09
36	.22600E+09	.90400E+09	.16464E-09
38	.22600E+09	.90400E+09	.16464E-09
40	.13760E+10	.55040E+10	.27041E-10
45	.15872E+10	.63488E+10	.23443E-10
47	.95400E+09	.38160E+10	.39003E-10
48	.95400E+09	.38160E+10	.39003E-10
49	.11180E+10	.44720E+10	.33281E-10
51	.15872E+10	.63488E+10	.23443E-10
53	.95400E+09	.38160E+10	.39003E-10
54	.95400E+09	.38160E+10	.39003E-10
55	.11180E+10	.44720E+10	.33281E-10

```
    DENSITY       VISCOSITY
   0.10500D+4     0.45000D-2

CYCLES  FREQUENCY    TIME INCREMENT
   2    1.00000D00     1.00000D-3

  NPB  NQB
   0   21

   Q COS TERM      Q SIN TERM
   0.86393E-4     0.00000E+0
   -.88455E-4     0.13368E-3
   -.52515E-4     -.12280E-3
   0.86471E-4     0.22459E-4
   -.26395E-4     0.22693E-4
   -.12987E-4     0.22398E-5
   0.20133E-5     -.22315E-4
   0.70896E-5     0.10065E-4
   0.32577E-5     -.21066E-5
   -.56573E-5     0.90633E-5
   -.19302E-5     -.85422E-5
   0.22387E-5     0.14770E-5
   0.23050E-5     -.32397E-5
   0.11909E-5     0.59775E-5
   -.39818E-5     -.18464E-5
   0.58176E-6     -.14751E-5
   0.19556E-5     -.12112E-5
   0.48907E-6     0.24434E-5
   -.66338E-6     0.50967E-6
   -.21719E-5     -.23241E-6
   0.19705E-5     -.20190E-5

   ACC. GRAV.     GRAV. LOAD       ANGLE
   9.81000D00     0.00000D+0    0.27000D+3
```